ADDIS ABABA UNIVERSITY

SCHOOL OF GRADUATE STUDIES

Conducting Polymer Modified Electrodes for the Electrochemical Determination of Alkaloids and Pesticides

BY

MEAREG AMARE ABRHA

MAY 2013

Conducting Polymer Modified Electrodes for the Electrochemical Determination of Alkaloids and Pesticides

BY

MEAREG AMARE ABRHA

A Thesis Submitted to the Department of Chemistry

Presented in Fulfilment of the Requirements for the Degree of Doctor of Philosophy (Physical Chemistry)

Addis Ababa University

Addis Ababa, Ethiopia

May, 2013

Addis Ababa University

School of Graduate Studies

This is to certify that the thesis prepared by Meareg Amare Abrha entitled: Polymer Modified Electrodes for the Electrochemical Determination of Alkaloids and Pesticides and submitted in partial fulfillment of the requirement of the Doctor of Philosophy (Physical Chemistry) complies with the regulation of the University and meets the accepted standards with respect to originality and quality.

Signed by examining committee

Name	Signature	Date
1. Dr. Shimelis Admassie (Advisor)		31/05/13
2. Prof. Antonio Lopez de Lacey (External Examiner)		31/05/13
3. Dr. Merid Tessema (Internal Examiner)		31/05/13
4. Prof. Theodros Solomon (Internal Examiner)		31/05/13
5. Dr. Ahmed Mustefa (Chairman)		

Chairman, College Academic Commission

Abstract

4-Amino-3-hydroxynaphthalene sulfonic acid was electropolymerized potentiodynamically from aqueous solution at the surface of glassy carbon electrodes. Different Electrochemical and surface characterization techniques like cyclic voltammetry, impedance spectroscopy, scanning electron microscopy/energy dispersive spectroscopy, atomic force microscopy, and x-ray photoelectron spectroscopy were used to characterize the deposited electroactive polymer film at the surface of glassy carbon electrodes.

The poly(4-Amino-3-hydroxynaphthalene sulfonic acid) modified glassy carbon electrode was further studied as e lectrochemical sensor for the determination of selected alkaloids (ephedrine, theophylline, and caffeine) and organophosphorus pesticides (fenitrothion and methyl parathion) from real samples using various electroanalytical methods. The polymer modified electrode showed catalytic effect towards the studied alkaloids and organophosphorus pesticides. For the investigated alkaloids and pesticides, detection limits in the range of 4.7-79 $\times$ 10^{-8} M and 0.79-1.1 $\times$ 10^{-9} M, respectively were achieved. In contrast to most of the previous reports on similar alkaloids and pesticides, poly(4-Amino-3-hydroxynaphthalene sulfonic acid) modified glassy carbon electrode gave lower detection limits and excellent recoveries making it potentially applicable for the determination of alkaloids and pesticides in environmental samples.

The electrochemical behavior of fenitrothion at an electrochemically activated glassy carbon electrode was also investigated. The current response showed linear dependence

on the concentration of fenitrothion in the range 0.4-50 $\times$ 10^{-6} M with a detection limit of 7.8 $\times$ 10^{-8} M. The lower detection limit achieved and excellent recovery of fenitrothion from human urine samples showed the potential application of the electrode for the determination of fenitrothion in real samples.

Acknowledgements

I would like to express my deep and sincere gratitude to my advisor, Dr. Shimelis Admassie, for his expertise, sympathy, encouragement, and valuable guidance. I truly appreciate his support and guidance throughout my studies. He has been helpful in providing me with the necessary chemicals and timely advice.

My heartfelt regards and gratitude are to my family for their incessant love, unwavering support and encouragement. In particular, I would like to thank my wife Nigist Hailu, my son Fikreab Meareg, and my brother Hagos Amare for their special concern. My sincere appreciation also goes to Abrham Meareg, Bethelehem Meareg and Natnael Meareg, for the patience and optimism they showed to me throughout my studies.

I wish to thank Prof. Antonio Lopez de Lacey, Research scientist at CSIC (Spain), for giving me the opportunity to work in his lab. Besides supporting me with his profound knowledge, he has arranged for me to use all facilities in his institution. I also thank his research group members; Dr. Marcos Pita and Dr. David Olea, for their academic support and hospitality. I would also thank Prof. Isabel Diaz, without the arrangements she made, my research visit to Spain would have never been possible.

I would like to thank Prof. Theodros Solomon, Prof. Teketel Yohannes, Dr. Ahmed Mustefa and Dr. Merid Tesema for the time they spent in commenting my seminar, manuscript and thesis papers.

My lab mates have always been a source of support to me. I thank Berhanu Wondimu, Alemnew Geto, Welesamel Geremedhin, Hulugirgesh Degefu, Minaleshewa Atlabachew, Kebede Nigussie, Endale Teju, Solomon Mihretie, Negash Getachew, Wondimagegn Mamo and Nigussie Negash, for their encouragement, affection and companionship.

My special thanks go to Ato Sahlemichael Deme, Aster Tadesse, Lemlem G/egziabher, Woinshet Gebeyehu, Megabit Semu, H/gebriel Mengesha and others who have helped me a lot throughout my stay in the Department of Chemistry.

The financial help for my research from the Department of Chemistry, AAU, is gratefully acknowledged.

Finally, my thanks go to Bahir Dar University, for giving me the scholarship and additional support for my research work.

Table of contents

List of Figures

List of Schemes

List of Tables

List of abbreviations

AA	Ascorbic acid
ABS	Acetate buffer solution
AFM	Atomic force microscopy
AGCE	Activated glassy carbon electrode
AHNSA	4-amino-3-hydroxynaphthalene sulfonic acid
APF	Addis pharmaceuticals factory
CV	Cyclic voltammetry
DPV	Differential pulse voltammetry
EEC	Equivalent electrical circuit
EIS	Electrochemical impedance spectroscopy
EPF	Ethiopian pharmaceuticals factory
EPH	Ephedrine
FT	Fenitrothion
MGCE	Monomer (AHNSA) modified glassy carbon electrode
OP	Organophosphorous
PBS	Phosphate buffer solution
PGCE	Poly(AHNSA) modified glassy carbon electrode
pGCE	Electrochemically pretreated glassy carbon electrode
RBS	Britton-Robinson buffer solution
SEM/EDS	Scanning electron microscopy/electron dispersive spectroscopy
SWV	Square wave voltammetry
TP	Theophylline
UA	Uric acid
UGCE	Unmodified (bare) glassy carbon electrode
XPS	X-ray photoelectron spectroscopy

1. INTRODUCTION AND MOTIVATION

Alkaloids represent a group of natural products that have a major impact throughout history on the economic, medical, political and social affairs of humans. Many of these compounds have potent physiological effects on mammalian systems as well as other organisms, and as a consequence, some constitute important therapeutic agents [1]. Alkaloids are organic compounds known for their medicinal and, paradoxically, poisonous attributes [2-4]. The successful determination of alkaloids at their trace level concentrations in environmental samples is thus vital for the control of their hazardous effects to man.

Organophosphorus (OP) compounds are also among the most toxic substances known [5,6]. They are used as pesticides, insecticides and chemical warfare agents [7-9]. The acute toxicity of organophosphorus neurotoxins and their widespread use in modern agricultural practices has thus increased public concerns. These concerns have stimulated the development of technologies to treat effluents generated at both the producer and consumer levels effectively [10-15]. The successful use of any laboratory developed technology for the detoxification of the organophosphate neurotoxins will require analytical tools for monitoring the concentrations of these neurotoxins.

However, the common techniques used for the determination of alkaloids and organophosphorus pesticides, are time consuming, expensive and require highly trained personnel, and are available only in sophisticated laboratories [16].

A lot of efforts have been devoted to developing electroanalytical methods for the detection of these alkaloids and organophosphorus pesticides in different samples. Due to its simplicity, sensitivity and stability; the application of conducting polymer-modified electrodes as electrochemical sensors is a growing area in electrochemical analyses. Since the environment contains many compounds that need to be determined even in the presence of complex matrices, the availability of well characterized electrode modifiers is vital in electrochemical analyses. The aim of this research is thus, to contribute a conductive polymer as an alternative electrode modifier, study the conditions suitable for its electropolymerization from an aqueous system, characterize the electrodeposited polymer film using different techniques and investigate its sensor application for the electrochemical determination of selected alkaloids and organophosphorus pesticides.

In this work, we presented the potentiodynamic electropolymerization of 4-amino-3-hydroxynaphthalene sulfonic acid (AHNSA) in an aqueous medium at the surface of glassy carbon electrodes. The surface of the polymer film modified electrode was characterized using cyclic voltammetric, electrochemical impedance spectroscopic, scanning electron microscopic, atomic force microscopic, and X-ray photoelectron spectroscopic techniques.

Furthermore, the electrochemical sensor applications of the polymer modified glassy carbon electrode for the determination of selected alkaloids and organophosphorus pesticides have been studied.

General objectives

Electrosynthesis of new electrochemical sensors, characterization of the sensors using different techniques and investigate the electrochemical sensor applications of the developed sensors for the analyses of selected alkaloids and organophosphorus pesticides in environmental samples.

Specific objectives

The specific objectives of this research work include:

- Electrosynthesis of polymer-modified electrodes
- Study the kinetics of the electropolymerization process using cyclic voltammetry
- Study the stability of the polymer films
- Investigate the optimum film thickness
- Characterize the polymer film using CV, EIS, SEM, AFM, and XPS
- Study the electrocatalytic behavior of the polymer modified electrodes towards selected alkaloids and organophosphorus pesticides
- Study the kinetics of the electrochemical reactions of the alkaloids and organophosphorus pesticides at the polymer-modified electrode and propose the possible reaction mechanism for each compound.

2. LITERATURE REVIEW

2.1 Conducting Polymers

2.1.1 Introduction

Conducting polymers are polymer materials with metallic and semiconductor characteristics, a combination of properties not exhibited by any other known material. The first and most simple conducting polymer discovered was polyacetylene (-CH=CH-)n [17]. A key property of conducting polymers is the presence of conjugated double bonds along the backbone of the polymers (Fig. 1).

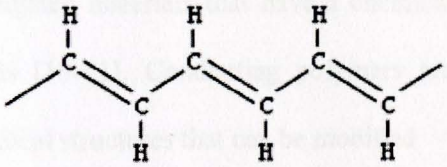

Fig. 1. Polyacetylene chain

Since the electrons in a conjugated system are only loosely bound, this enables the electrons to be delocalized over the whole system and hence shared by many atoms. However, conjugation alone is not enough to make the polymer material conductive. In addition, the polymer material needs to be doped for flow of electrons to occur. Doping is either the addition of electrons (reduction reaction) or the removal of electrons (oxidation reaction) from the polymer either by chemical or electrochemical means. Once doping has occurred, the electrons in the π-bonds are able to "jump" around the polymer chain causing current flow. For better conductivity, the molecules must be well ordered and

closely packed to limit the distance "jumped" by the electrons. The conductivity of conducting polymers can be tuned by chemical manipulation of the polymer backbone, by the nature of the dopant, by the degree of doping, and by blending with other polymers [18].

Electronic conductivity in polymers can be divided roughly into two different categories: i) polymer composites, where the conductivity is achieved by adding conducting (usually metallic) particles to an insulating polymer matrix, forming a percolative network, and ii) intrinsically conducting polymers (ICPs), where the conductivity arises from a special conjugated structure of the polymer backbone. Intrinsically conducting polymers are conjugated materials that have a chemical structure with alternating single and double bonds [19-21]. Conducting polymers are known to have considerable flexibility in chemical structures that can be modified.

The first requirement for metallic conductivity is to have energy levels near the Fermi level (i.e. the chemical potential, μ) that can be thermally populated. It has been calculated that for polyacetylene, which has ideally equal single and double bond lengths and a chain with 1000 carbon atoms, the separation between the Fermi level and the next highest level would be 0.04 eV, which is comparable to thermal energies. This fulfils the first requirement, but in practice polyacetylene is still not conducting as such due to various reasons: The first and main reason being electron mobility along the chain has to be high, i.e. scattering of electrons should be low. This is difficult to satisfy with polymers since any deviation from the planar zigzag conformation will cause scattering. A highly crystalline material can overcome these problems, but the high conductivity

level is still not achieved. Therefore, the main reason for the apparently low conductivity of polyacetylene arises from differences in the actual bond lengths: C-C and C=C bonds of the polymer are not equivalent i.e. they are alternatively shorter or longer, which is called Peierls distortion. This distortion has a conclusive effect on the electric properties of polyacetylene since it opens a gap between the HOMO (highest occupied molecular orbital) level, which is the fully occupied π-band (valence band), and the LUMO (lowest unoccupied molecular orbital) level, which corresponds to an empty π*-band (conduction band). Thus polyacetylene is an intrinsic semiconductor with a band gap of 1.5 eV and it requires doping in order to be conducting [20].

Conjugated polymers with a narrower band gap have been synthesized [22,23] but a vanishing band gap has not been reached [24,25]. Conducting polymers can be reversibly doped and undoped using electrochemical techniques accompanied by significant changes in conductivity [26].

The electrical conductivity of conducting polymers changes over several orders of magnitude in response to change in pH, applied potentials, or their environments [27]. Polymers that have π-conjugation over elements other than carbon atoms exist as well. One of the most well-known examples is polyaniline. Polyaniline differs from the other conjugated polymers due to the special chemical structure of the backbone since polyaniline exists in three different oxidation states as presented in Scheme 1. The most reduced state, leucoemeraldine, only has aminic nitrogen atoms in the chain. In the fully oxidized state, pernigraniline, all nitrogens are iminic and the ratio of phenylene rings with a benzoid or quinoid structure is 1:1. The half oxidized form, emeraldine, has an

iminic/aminic ratio of 1:1 but benzoid and quinoid structures exist in 3:1 ratio, respectively [25].

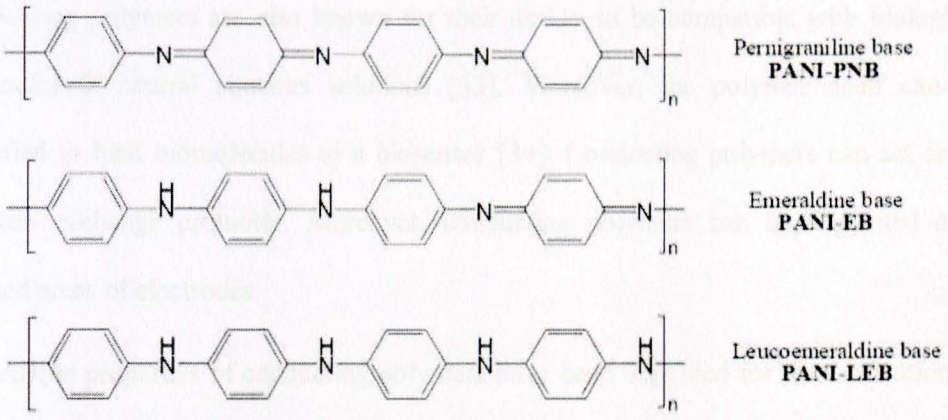

Scheme 1 Chemical structures of polyaniline under different conditions

2.1.2 Conducting polymers as Electrochemical Sensors

In 1978, Miller's and Bard's groups independently showed that chemically modified electrodes could be prepared by coating electrode surfaces with polymer films [28]. Conducting polymers have gained much attention in sensor areas [29-31] in recent years because of their unique characters [32]. A wide variety of organic molecules have been used as the monomers for the preparation of conducting polymers, such as polycyclic benzenoid, nonbenzenoid hydrocarbons, acetylene, polyaromatic and heterocyclic compounds like polyaniline and polypyrrole.

The great advantage of conducting polymer based sensors over other available techniques is that conducting polymers have the potential to exhibit improved response properties

and are sensitive to small perturbations. Conducting polymers improve the sensitivity of the sensors due to their electrical conductivity or charge transport properties [31].

Conducting polymers are also known for their ability to be compatible with biological molecules in neutral aqueous solutions [33]. Moreover, the polymer itself can be modified to bind biomolecules to a biosensor [34]. Conducting polymers can act as an electron exchange promoter. Moreover, conducting polymers can be deposited over defined areas of electrodes.

The unique properties of conducting polymers have been exploited for the fabrication of electrochemical sensors and biosensors [30,32]. Amongst many analytical techniques available, the development of chemical sensors has made significant advances in the last decades [35-42]. The rapidly growing applications of chemical sensors reflect the extent to which analytical chemists require these devices for cheap, accurate, convenient and quick analysis of various samples. Chemical sensors are miniaturized analytical devices, which can deliver real-time and on-line information about the presence of specific compounds or ions in complex samples. Usually an analyte recognition process takes place followed by the conversion of chemical information into an electrical signal (Scheme 2) [43].

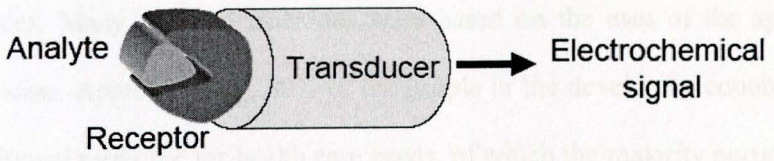

Scheme 2 Schematic representation of analyte, receptor, and transducer interaction

Polymer modified electrodes could be prepared using different methods. The common methods are: Dipping the electrode surface in to a polymer solution and allowing the solvent to evaporate [44]. In this case, film thickness is difficult to control. The other method is casting [45] which is just putting a certain volume of a polymer solution on to the surface of the electrode. The polymer film deposited is controlled by the volume of solution added and its concentration. Spin coating [44] is another method of polymer film deposition. A uniform film, whose thickness is controlled by the concentration of the polymer solution and also by the time and number of rotations, is obtained. Recently, electropolymerization method has been successfully used for the controllable preparation of polymer films from monomer solutions. Three types of electrochemical methods are commonly employed for the polymerization of different monomers at an electrode surface: (1) constant current (galvanostatic) [19-21]; (b) constant potential (potentiostatic) [20] and (3) potential scanning (potentiodynamic) [46-52].

2.2 Alkaloids

Since the beginning of human civilization, medicinal plants have been used by mankind for their therapeutic value. Nature has been a source of medicinal agents for thousands of years and an impressive number of modern drugs have been isolated from natural sources. Many of these isolations were based on the uses of the agents in traditional medicine. Approximately, 80% of the people in the developing countries rely chiefly on traditional medicine for health care needs, of which the majority portion involves the use of plant extracts. One of the criticisms on herbal medicine is lack of standardization and

quality control profiles. Of central importance with respect to quality control is correct identification of the species concerned, whether in the fresh, dried or powdered state [53,54].

Alkaloids are group of molecules with a relatively large occurrence in nature around the Globe. Most of them are plant origin, containing at least one nitrogen atom and have significant physiological effect on humans and animals. They are very diverse chemicals and biomolecules, and they are all secondary compounds derived from amino acids or from the transamination process. Alkaloids are molecules of natural origin with highly important benefits and diagnostic uses. They can be characterized as the most useful and also the most dangerous products of nature. They are known for their medicinal and, paradoxically, poisonous attributes [2-4]. The alkaloids represent a group of natural products with a major impact throughout history on the economic, medical, political and social affairs of humans. Many of these agents have potent physiological effects on mammalian systems as well as other organisms, and as a consequence, some constitute important therapeutic agents. Atropine, morphine, quinine and vincristine are representative of a host of agents used to treat a range of diseases ranging from malaria to cancer [1].

Alkaloids have provided a wealth of pharmacologically active compounds; approximately 25% of the drugs used today are of plant origin. These are administered either as pure compounds or as extracts and have often served as model structures for synthetic drugs [55]. On average, alkaloids are poisonous to extremely poisonous, but are frequently used in pharmacy, usually without a synthetic countertype. The low LD_{50} of

most of the alkaloids and their solubility in many solvents make them potential poisoning agents of choice [56]. These alkaloids can be introduced to food products innocuously (e.g., in milk, via cattle and sheep grazing on alkaloid-producing plants [20] or insidiously (e.g., intentional poisoning) [57,58].

Ephedrine is an alkaloid contained in several plants of the genus *Ephedra* [59,60]. *Ephedra*-containing supplements produce a state of wakefulness and alertness, a decreased sense of fatigue, and an elevation of mood with increased self-confidence and initiative. Unfortunately, the beneficial effects in weight management and mood alteration come at a price: high doses of ephedrine result in depletion of epinephrine (adrenaline) and norepinephrine (noradrenaline), leading to the opposite effects: depression, a sense of loneliness and suspiciousness. Also, ephedrine may elevate blood pressure, increases heart rate and comes with severe palpitations. In very serious cases, this can cause ventricular fibrillation and death. Ephedrine has been characterized as a prohibited compound by the International Olympic Committee [60,61].

Caffeine, theophylline and theobromine are purine alkaloids which are methyl derivatives of xanthine. They are widely distributed in plant products and beverages. Xanthine derivatives including caffeine and theophylline are generally known to have many physiological effects, such as gastric acid secretion, diuresis, and stimulation of the central nervous system. They have also been implicated in various disorders including heart disease, carcinogenesis, kidney malfunction, and asthma [62-65]. Therefore, it is important to develop reliable, simple and fast methodologies for the determination of alkaloids in general and the stated alkaloids (ephedrine, caffeine and theophylline) in

particular from different sources in order to find a more precise relationship between the amounts consumed and their physiological effects.

2.3 Pesticides

Pesticides in a broad sense are chemical compounds that are used to kill pests, including insects, rodents, fungi and unwanted plants (weeds) [66,67]. Pesticides are also used in public health to kill vectors of disease, such as mosquitoes. Millions of tons of pesticides are applied annually; however, less than 5% of these products are estimated to reach the target organisms, with the remainder being deposited on the soil and nontarget organisms, as well as moving into the atmosphere and water [68].

Among all the hazardous environmental compounds, pesticides are the most abundant in soil, water, the atmosphere and agricultural products. Pesticides represent a real threat not only to living organisms but also to the environment, especially to ground and surface water. Due to their widespread presence, great environmental concerns have recently emerged around this type of pollution.

Pesticides with nitro-containing structural groups are most efficient, but have very toxic properties. Within this group of pesticides, there are essentially four groups; nitrorganophosphates, nitrophenol derivatives, dinitroaniline derivatives, and nitrorgano-chlorides [66].

Organophosphorus pesticides are among the most widely used pesticides for insect control [69]. After the prohibition of organochlorine pesticides due to their bioaccumulation and persistence in the environment, organophosphorous (OP)

compounds became the most commonly-used class of insecticides for pest control [70]. Because of their efficacy, low cost, and widespread availability; organophosphorus compounds are widely applied as pesticides and insecticides in many countries [71-73]. However, most of these pesticides are known to affect animal health as a consequence of their enzyme inhibition. The significant neurotoxic properties of organophosphorus compounds are such that they have even been used as chemical warfare agents [74-76].

The widespread use of organophosphorus insecticides results in the release of their residues into natural water, thus inducing an environmental problem [77]. All organophosphorus pesticides apparently share a common mechanism of cholinesterase inhibition and can cause similar symptoms. Because they share this mechanism, exposure to the same organophosphate by multiple routes or to multiple organophosphates by multiple routes can lead to serious additive toxicity.

Acetylcholinesterase (AChE), which is essential for the central nervous system, is present in both humans and insects. This enzyme hydrolyzes the acetylcholine neurotransmitter in the synaptic membrane in order to prevent its accumulation. AChE inhibition and the subsequent acetylcholine accumulation cause a marked dysfunction of many autonomic and behavioral systems, eventually leading to respiratory paralysis and death [78-82]. The enzyme inhibition mechanism proceeds through the formation of a stable complex through reversible and irreversible reaction of OP pesticides with the active site of AChE [83,84]. As a result, acetylcholine largely accumulates in the muscular tissues and leads to severe muscular paralysis and eventually death [85,86].

Concern over the use of pesticides is primarily related to the effects they have on non-target organisms, both plants and animals, including humans. This unintended effect may be related to the method of application, the physical and chemical properties of the chemical, and the physical attributes of the environment to which it is applied (including soil type, slope and rainfall). Aquatic environments are particularly susceptible to contamination from pesticides. Many pesticides will leach through the soil into aquifers and waterways during wet periods. Other pesticides may bind to soil and be transported into waterways through erosion. Once in the water, pesticides may be more readily ingested or adsorbed by organisms leading to undesirable consequences. However, the degree to which this contamination occurs is dependent upon the intensity of pesticide use, the physical and chemical properties of the pesticides used and catchment through which it is transported [69]. As the pesticide residue is a potential hazard to the human health, the control and detection of pesticide residue plays an important role in minimizing the risk [87].

Thus, the development and continual improvement of analytical methods for the determination of this group of compounds (pesticides) in general and organophosphorous pesticides in particular, is a great challenge for analysts.

Chromatographic methods are the conventional methods most often used for the determination of alkaloids [88-93] and organophosphorus pesticides [94-103]. These methods are tedious, expensive, need trained personnel (to operate) and use organic solvents, which ultimately pollute the environment. Compared to the conventional methods, electroanalytical methods are simple, cheap, fast, suited for field analyses and

environmentally friendly [104]. However, little efforts have been made in the application of electroanalytical methods for the determination of alkaloids and organophosphorus pesticides. Many of the electroanalytical methods reported used mercury as the working electrode whose contribution to environmental pollution cannot be overlooked. Others used metal electrodes which fulfill the requirements for electroanalysis, including biocompatibility, inertness and nontoxicity. Nevertheless, these metal electrodes have not become as popular as the carbon based electrodes due to certain apparently unavoidable problems, such as metal oxide formation, resulting in electrode deactivation, which requires frequent pretreatment and other procedures to regenerate the electrodes. Compared to metal electrodes, glassy carbon electrode (GCE) has been widely used due to its biocompatibility with tissue, low residual current over a wide potential range and its minimal propensity to show deteriorated response as a result of electrode fouling [105-107].

Polymer modified electrodes (PMEs) have received attention in recent years due to their good stability, reproducibility, increased active sites, homogeneity in electrochemical deposition and strong adherence to electrode surfaces [108-110]. Potentiodynamically polymer modified electrodes have attracted much attention because the film thickness can be controlled by varying electrochemical parameters besides solution conditions [111].

The monomer used in this project, 4-Amino-3-hydroxynaphthalene sulfonic acid (AHNSA), is a derivative of aniline, whose polymer is among the most studied conducting polymers used as electrochemical sensors [112-116].

2.4 Electrochemical techniques

Electrochemical techniques are important tools in almost every chemical and biochemical research laboratory. In addition to their application in fundamental studies of oxidation and reduction processes to unravel reaction mechanisms, these techniques are also used in studying the kinetics and thermodynamics of electron and ion transfer processes [117]. Moreover, electrochemical techniques have also proven to be useful tools for the study of adsorption and crystallization phenomena at electrode surfaces [118].

Among the common electrochemical techniques, Voltammetry, Amperometry, and Impedometry are used in this dissertation.

2.4.1 Voltammetric techniques

Voltammetry is a branch of electrochemistry that was developed as the result of the discovery of polarography in 1922 by Jaroslav Heyrovsky (Nobel Prize in 1959). A major breakthrough in voltammetry was made in the early 1960s, when an expanded repertoire of analytical methods were reported, appearing in parallel with the corresponding well-developed theories [117,119]. At the same time, these developments led to enhanced sensitivities obtained with the voltammetric techniques. The excitation signal in all voltammetric techniques is the applied potential, E, on the working electrode whereas the output parameter is usually the resulting current, i, flowing through the electrochemical cell over a period of time, t. Thus, voltammetric techniques can be described as some functions of E, i, and t [120].

One of the main advantages of electrochemical techniques is the possibility of direct analysis of the sample without tedious and long preparative steps and subsequent separation. The analytical advantages of the various voltammetric techniques also include excellent sensitivity with a very large useful linear concentration range for both inorganic and organic species, a large number of useful solvents and electrolytes, a wide range of temperatures, rapid analysis times (seconds), simultaneous determination of several analytes, the ability to determine kinetic and mechanistic parameters, a well-developed theory and thus the ability to reasonably estimate the values of unknown parameters, and the ease with which different potential waveforms can be generated and small currents measured. Chemists widely use voltammetric techniques for a variety of purposes, including fundamental studies of oxidation and reduction processes in various media, adsorption processes on surfaces, electron transfer and reaction mechanisms, kinetics of electron transfer processes, and transport, speciation, and thermodynamic properties of solvated species [121].

2.4.1.1 Electrochemical cell and electrodes

An electrochemical cell is considered to be a sample holder, where the analyte dissolved in an appropriate solvent (and ionic electrolyte) and electrodes are placed (Fig. 2). The electrodes of the electrochemical system are usually all dipped in the electrochemical cell, whereas in some systems the reference electrode is placed in a separate compartment to avoid contamination, and it is connected to the cell via an electrolyte bridge.

In voltammetric techniques, three-electrode system is used, which includes the reference, counter, and working electrodes.

Reference Electrode:

The reference electrode should provide a reversible half-reaction with Nernstian behavior, be constant over time, and be easy to assemble and maintain. Its only role is to act as reference in measuring and controlling the working electrode's potential and at no point does it pass any current. A reference electrode is a nonpolarized electrode, i.e., an electrode of fixed potential. The most commonly used reference electrodes for aqueous solutions are the calomel electrode (Hg/Hg_2Cl_2), and the silver/silver chloride electrode (Ag/AgCl), which are commercially available in a variety of sizes and shapes.

Counter Electrode:

In most voltammetric techniques, the electrochemical reactions at electrode surfaces occur over very short time periods and rarely produce any appreciable changes in bulk concentrations of reduced or oxidized species. The auxiliary (counter) electrode passes all the current needed to balance the current observed at the working electrode. Thus, isolation of the counter electrode from the sample is not normally necessary. Most often the counter electrode consists of a thin Pt wire/foil, although Au and sometimes graphite have also been used.

Working Electrode:

The electrode on which the required potential is applied in a controlled way and facilitates the transfer of charge to and from the analyte is called the working electrode. It

is an ideally polarized electrode, i.e. the electrode shows a large change in potential when an infinitesimally small current passes through it. The working electrodes are of various geometries and materials, ranging from small Hg drops to flat Pt disks. Mercury is useful because it displays a wide negative potential range (difficult to reduce hydrogen ion or water at the mercury surface), its surface is readily regenerated by producing a new drop or film, and many metal ions can be reversibly reduced in it. Other commonly used electrode materials are gold, platinum, and glassy carbon.

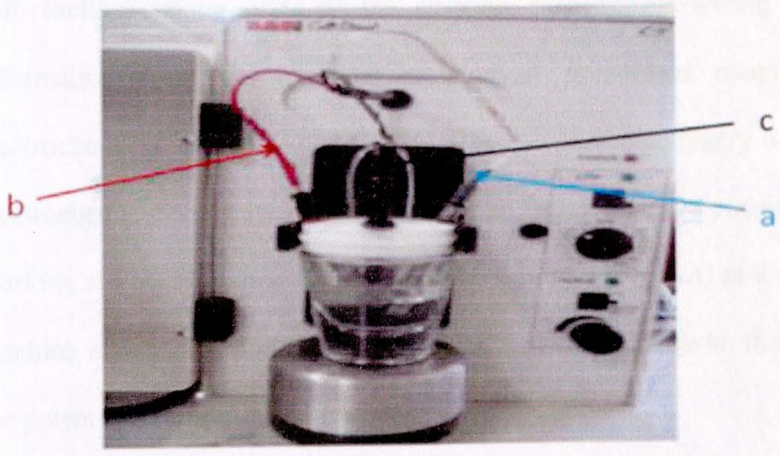

Fig. 2. A three electrode electrochemical cell: (a) reference electrode, (b) counter electrode, and (c) working electrode

The potentiostat is used to supply potential, regardless of the chemical changes taking place on the working electrode at that time [122].

The output of a potentiostat which supplies a constant potential (potentiostatic mode) or current (galvanostatic mode) to the working electrode, is a current-voltage signal, which

is called voltammogram. The commonly used voltammetric methods are cyclic, linear sweep, differential pulse, square wave, and stripping Voltammetry [117,120,123].

2.4.1.2 Cyclic voltammetry

Cyclic voltammetry is one of the most exploited techniques in electrochemical studies [120,123]. Its primary advantage comes from the fact that it gives insight into both the half-reactions taking place at the working electrode, providing at the same time information about the chemical or physical phenomena coupled to the studied electrochemical reaction [117,124,125]. Hence cyclic voltammetry is often considered as electrochemical spectroscopy [124]. In cyclic voltammetry, a potential is applied to the working electrode starting from an initial potential *a* (Fig. 3A) at a scan rate of *b*. After reaching a switching potential *c*, the sweep is reversed but with the same scan rate and the potential returns to its initial value.

The main instrumental parameter in cyclic voltammetry is the scan rate ($v = dE/dt$), since it controls the time scale of the voltammetric experiment. The useful scan rates range from 1 to 1000 mV/s. The instrumental output in cyclic voltammetric techniques is a current–potential curve, a cyclic voltammogram (Fig. 3B). The main features of a cyclic voltammogram are the cathodic and anodic peak potentials, the cathodic and anodic peak currents, and the formal potential. While the formal potential (defined simply as a median between the cathodic and the anodic peak potentials) provides mainly thermodynamics information, the magnitudes of the peak currents reveal the kinetics involved in the electrochemical reaction. The shape of the cyclic voltammogram gives information about

the type of the electrode reaction, the number of electrons involved in the elementary step of electrochemical transformation, as well as about the additional phenomena coupled to the electrochemical reaction of interest, like those for coupled chemical reactions or adsorption [117,124].

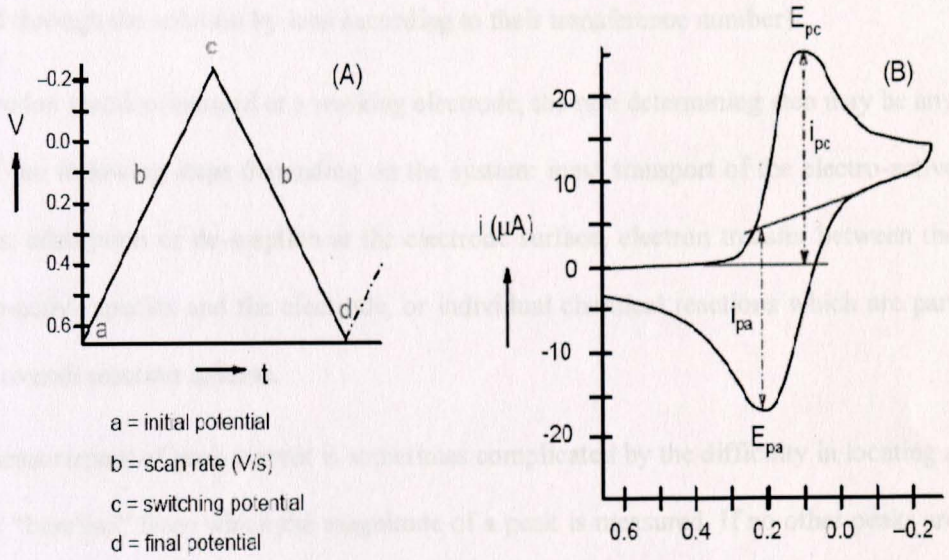

Fig. 3. (A) Potential ramp used in cyclic voltammetry, and (B) a cyclic voltammogram simulated for one-electron reversible charge transfer

Electrode processes could be limited by the rate of electron transfer or the mass transport [126]. Mass transport occurs by three different modes;

Diffusion: the spontaneous movement of electroactive species in the bulk towards the electrode surface under the influence of concentration gradient (i.e., from regions of high concentration to regions of lower concentration), aimed at minimizing concentration differences.

Convection: mass transport to the electrode by a gross physical movement; such fluid flow occurs with stirring or flow of the solution and with rotation or vibration of the electrode (i.e., forced convection).

Migration: movement of charged particles along an electric field (i.e., the charge is carried through the solution by ions according to their transference number).

For a redox reaction induced at a working electrode, the rate determining step may be any one of the following steps depending on the system: mass transport of the electro-active species, adsorption or de-sorption at the electrode surface, electron transfer between the electro-active species and the electrode, or individual chemical reactions which are part of the overall reaction scheme.

The measurement of peak current is sometimes complicated by the difficulty in locating a proper "baseline" from which the magnitude of a peak is measured. If no other peaks are present, the baseline for the forward wave can generally be defined by extrapolating the zero current portion of the scan to a position under the forward peak. The reverse peak current is more often problematic, with baselines affected by the location of the switching potential, among other things. Proper extrapolation of baselines for peak current measurement in the absence of complications is shown Fig. 4A. Many computer-controlled potentiostats have data systems that can accurately and quickly make these types of measurements. For situations where baseline assignment is more complicated, the current ratio can sometimes be conveniently calculated using the empirical method of Nicholson [127], which requires the measurement of the forward ($i_{p,f}$) and reverse peak

currents $(i_{p,r})_0$ (to differentiate it from that previously used) from the same baseline, along with a third current, i_λ, which is the current measured at the switching potential. This method is illustrated in Fig. 4B.

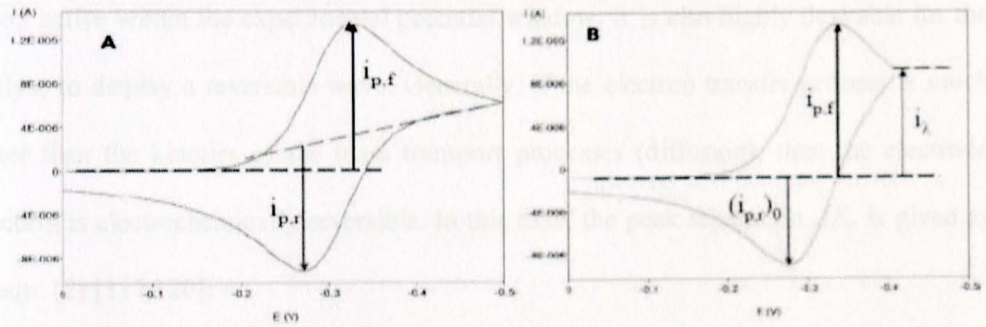

Fig. 4. Typical cyclic voltammograms for reversible processes

The currents measured using the method of Nicholson [127] can then be applied to the calculation of the peak current ratio as in eqn. (1).

$$\frac{i_{p,r}}{i_{p,f}} = \frac{(i_{p,r})_0}{i_{p,f}} + 0.48\frac{i_\lambda}{i_{p,f}} + 0.086 \quad \text{.....(1)}$$

An electrode reaction mainly consists of (i) the mass transport of electroactive reactant and product, (ii) the electron transfer at the electrode/solution interface.

Electrode reactions could be classified on different basis; as simple and complex reactions from the mechanistic standpoint. The former is a reaction which involves only process of electron transfer (E), and the latter, a reaction which involves electron transfer and other types of processes. On the other hand, electrode reactions are customarily classified as reversible and irreversible reactions based on the rate of electron transfer at the electrode/solution interface [117].

Reversible processes

A redox couple in which both species rapidly exchange electrons with the working electrode is termed as electrochemically reversible couple [117]. The analyte has to be redox active within the experimental potential window. It is also highly desirable for the analyte to display a reversible wave. Generally, if the electron transfer process is much faster than the kinetics of the mass transport processes (diffusion), then the electrode reaction is electrochemically reversible. In this case, the peak separation ΔE_p is given as in eqn. (2) [117,120]:

$$\Delta E_p = / E_{pa} - E_{pc} / = \frac{2.303RT}{nF} \text{ which at } 25\,^0C \text{ is reduced to :}$$

$$\Delta E_p = \frac{0.059}{n} V \quad \text{.....(2)}$$

The peak current (i_p) for a diffusion-controlled, reversible system is described by the Randles- Sevcik equation [117,128], which is used for quantitative analyses:

$$i_p = 2.69 \times 10^5 n^{3/2} A C_0 D^{1/2} \nu^{1/2} \quad \text{.....(3)}$$

where, i_p is peak current (A), n is number of electrons, A is electrode area (cm^2), D is diffusion coefficient (cm^2/s), C_0 is analyte initial concentration (mol/cm^3), and ν is scan rate (V/s). The potential where the current is half of the peak current is known as the half peak potential, which is related to the half wave potential $E_{½}$ (which is located at the midway between the $E_{p/2}$ and E_p) value and n by [117,120]:

$$E_{p/2} = E_{1/2} \pm \frac{0.029}{n} V \quad \text{.....(4)}$$

The ratio of reduction peak current *(i_{pc})* to oxidation peak current *(i_{pa})* for reversible couples is near unity. This ratio can be perturbed in the presence of a chemical reaction preceding or succeeding the electron exchange process. The formal potential ($E^{0'}$) for a reversible couple is centered between E_{pa} and E_{pc} [117,120,129].

$$E^{0'} = \frac{E_{pa} + E_{pc}}{2} \quad \text{.....(5)}$$

Moreover, the peak potential separation should not vary by increasing the scan rate, while both cathodic and anodic peak currents should be a linear function of the square root of the scan rate. Every breach of these criteria means deviation of the electrochemical reversibility, caused either by the slow electron transfer (quasi-reversibility or irreversibility) or by additional involvement of the electroactive species in chemical reactions or adsorption phenomena [117].

Cyclic voltammetry can also be used for evaluating the interacted behavior of electroactive compounds. Both the reactant and product can be involved in an adsorption-desorption process. A gradual increase of the cathodic and anodic peak current indicates progressive adsorptive accumulation of the species at the electrode surface. For such reversible surface-controlled system, the peak current is directly proportional to the surface coverage (Γ) and potential scan rate [117].

$$i_p = \frac{(nF)^2}{4RT} \nu A \Gamma \quad \text{.....(6)}$$

The peak area at saturation (i.e., the quantity of charge consumed during the reduction or oxidation of the adsorbed layer) can be used to calculate the surface coverage [117]:

$$Q = nFA\Gamma \quad \text{.....(7)}$$

where i_p is peak current (A), Γ is the amount adsorbed (mol/cm^2), v is scan rate (V/s), A is electrode area (cm^2), Q is amount of charge (C) consumed, and the rest have their usual meaning.

The peak potential for a reversible process is related to the half peak potential ($E_{p/2}$) and number of electrons (n) in the rate determining step as in eqn. (8) .

$$\left|E_p - E_{p/2}\right| = 2.20\frac{RT}{nF}V = \frac{56.5}{n}mV \; at \; 25\,^{\circ}C \quad \text{.....(8)}$$

Irreversible processes

For irreversible process (those with sluggish electron transfer), the individual peaks are reduced in size and widely separated. Irreversible systems are characterized by a shift of the peak potential with scan rate.

The peak current for a diffusion controlled-irreversible system is related to parameters including the transfer coefficient (α) and number of electrons involved in the charge-transfer step (n_a) by eqn. (9) [120].

$$i_p = \left(2.99\times10^5\right)n(\alpha n_a)^{1/2}AC_0D^{1/2}v^{1/2} \quad \text{.....(9)}$$

The peak current is still proportional to the bulk concentration (C_0) and to $v^{½}$.

An irreversible, adsorption-controlled electrochemical reaction is characterized by the following distinct features;

- Peak current is directly proportional to scan rate
- For the case where adsorbed O is reduced to R in a totally irreversible one step and one-electron reaction, the langmuirian-Nernstian boundary condition is replaced by a kinetic one, similar to that used for dissolved reactants. For n electron system at the rate determining step, the peak current and peak potential are given by eqns.(10-12) [117,120,130]:

$$I_{pc} = \frac{(\alpha n) n^2 F^2 A \nu \Gamma}{2.718 RT} \quad \text{.....(10)}$$

$$E_{pa} = E^{0'} + \frac{RT}{\alpha n F} \ln\left(\frac{RTk_s}{\alpha n F \nu}\right) \quad \text{.....(11)}$$

$$\left|E_p - E_{p/2}\right| = 1.85 \frac{RT}{\alpha n F} V = \frac{0.048}{\alpha n} V \; at \; 25\,^{\circ}C \quad \text{.....(12)}$$

2.4.1.3 Pulse Voltammetric Techniques

The invention of pulse voltammetric techniques was motivated by the fact that by changing the potential and measuring the current in a pulsed manner, a significant discrimination of the charging (non-faradaic) current can be achieved [117]. Applying the potential difference between the working and the reference electrodes in an electrochemical cell is a precondition for initiating an electron exchange between the working electrode and the electroactive species in the cell. However, this change in the potential difference also causes charging and discharging of the electrical double layer at

the electrode–electrolyte interface, which initiates a flow of capacitive (charging) current too [117]. This current is undesirable for kinetic and analytical purposes, and efforts are being undertaken to minimize its contribution. The basis of all pulse techniques lies in the difference in the rate of the decay of the capacitive and faradaic currents following the potential steps. While the faradaic current decays with $t^{-1/2}$ for diffusion-controlled electrode reactions, for the same reactions, the capacitive current decays exponentially with time. Accordingly, by sampling the currents at the end of the applied potential pulses, one gets negligible capacitive currents, yet significant faradaic currents [131]. In this way, the sensitivity of the voltammetric method will be significantly increased, and the measured current will refer almost exclusively to the faradaic reaction of interest. In novel electrochemical instruments, one meets various pulse voltammetric techniques, which differ in the pulse-wave form and the way by which the current is sampled. The most important parameters of all pulse voltammetric techniques are as follows: (1) pulse amplitude, which is the height of the potential pulse, (2) pulse width, which is the duration of the potential pulse, and (3) sampling period, defined as a time at the end of the potential pulse in which current is measured.

2.4.1.3.1 Differential Pulse Voltammetry

The potential form in differential pulse voltammetry (DPV) consists of small pulses of constant amplitude (10–100 mV) superimposed on a staircase-wave form. The current in this technique is measured twice in each pulse period, first at potential at the beginning of the applied pulse, and second at the ending of the same pulse (Fig. 5A) [131]. The

measured current in the instrumental output, referred to as differential pulse voltammogram (Fig. 5B), is actually the difference between the currents measured for each single pulse.

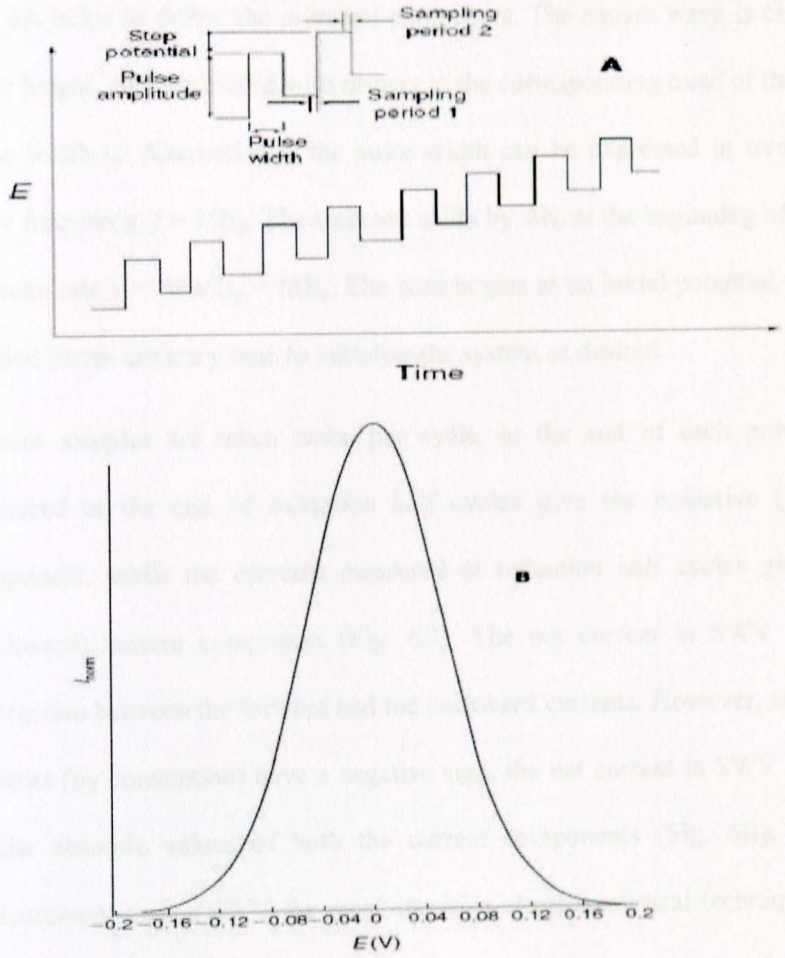

Fig. 5. (A) Potential form and (B) resulting simulated voltammogram in differential pulse voltammetry

2.4.1.3.2 Square Wave Voltammetry

Square-wave voltammetry (SWV) is the most advanced and the most sophisticated technique in the family of pulse voltammetric techniques [117, 128].

Fig. 6A helps to define the principal parameters. The square wave is characterized by a pulse height, ΔE_p, measured with respect to the corresponding tread of the staircase, and a pulse width t_p. Alternatively, the pulse width can be expressed in terms of the square wave frequency, $f = 1/2t_p$. The staircase shifts by ΔE_s at the beginning of each cycle; thus the scan rate $\nu = \Delta Es/2t_p = f\Delta E_s$. The scan begins at an initial potential, E_v which can be applied for an arbitrary time to initialize the system as desired.

Current samples are taken twice per cycle, at the end of each pulse. The currents measured at the end of oxidation half cycles give the oxidative (forward) current component, while the currents measured at reduction half cycles give the reduction (backward) current component (Fig. 6B). The net current in SWV is obtained as a subtraction between the forward and the backward currents. However, since the reductive currents (by convention) have a negative sign, the net current in SWV is actually a sum of the absolute values of both the current components (Fig. 6B). This method of measurement makes SWV the most sensitive electroanalytical technique. The net peak current in SWV, as in other pulse voltammetric techniques, is proportional to the analyte concentration, resulting often in detection limits in sub-nanomolar ranges. SWV is a very fast technique, providing insight into the kinetics of fast electron transfer reactions, and into the kinetics of rapid chemical reactions coupled to the electroactive species.

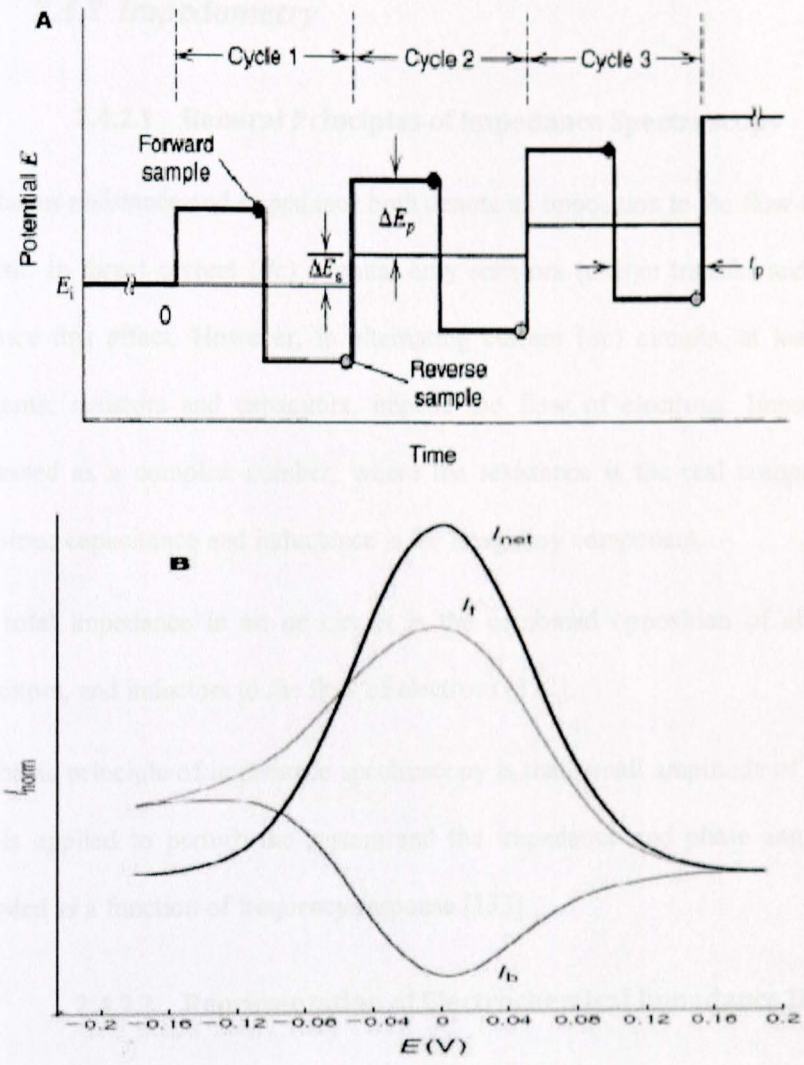

Fig. 6. (A) Potential form in square-wave voltammetry: Esw, potential amplitude; dE, potential step; t, duration of a single pulse. The current is sampled twice in each pulse, in the time period between two arrows at the inset; (B) resulting simulated voltammogram in square-wave voltammetry: If, forward current, I_b, backward current, I_{net}, net current

2.4.2 Impedometry

2.4.2.1 General Principles of Impedance Spectroscopy

The terms resistance and impedance both denote an opposition to the flow of electrons or current. In direct current (*dc*) circuits, only resistors (charge transfer and polarization) produce this effect. However, in alternating current (*ac*) circuits, at least two circuit elements; resistors and capacitors, impede the flow of electrons. Impedance can be expressed as a complex number, where the resistance is the real component and the combined capacitance and inductance is the imaginary component.

The total impedance in an *ac* circuit is the combined opposition of all its resistors, capacitors, and inductors to the flow of electrons [132].

The basic principle of impedance spectroscopy is that, small amplitude of typically 2-10 mV is applied to perturb the system and the impedance and phase angle response is recorded as a function of frequency response [133].

2.4.2.2 Representation of Electrochemical Impedance Data

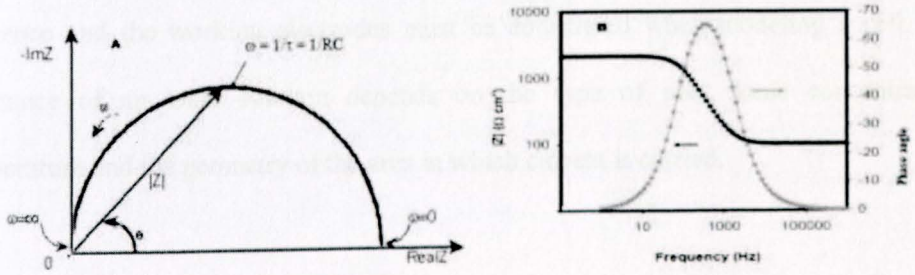

Fig. 7. (A) Typical Nyquist plot ($\omega = 2\pi f$), and (B) Bode plot of an EIS data

An electrochemical impedance data could be presented either using the ***Nyquist plot*** (Fig. 7A) which is a graph obtained usually by plotting the negative imaginary component (-Z'') against the real component (Z') at different frequencies or using the ***Bode plot*** (Fig. 7B) which is a graph obtained by plotting the complex impedance ($|Z|$) or phase angle as a function of frequency. In the case of the Bode plot, the parameters could be in logarithmic forms.

2.4.2.3 Equivalent Electrical Circuits (EECs)

A common approach for the interpretation of impedance spectra is the method of equivalent electrical circuit (EEC) [134]. The best method of quantitative analysis of impedance data is fitting the data to a theoretical model and/or equivalent electrical circuit by using softwares [135-138]. Some of the circuit elements that are commonly used in equivalent electrical circuit representations are:

Electrolyte resistance (R_s)

A modern three electrode potentiostat compensates for the solution resistance between the counter and reference electrodes. However, any solution resistance between the reference and the working electrodes must be considered when modeling a cell. The resistance of an ionic solution depends on the type of ions, ionic concentration, temperature and the geometry of the area in which current is carried.

Double layer capacitance (C_{dl})

An electrical double layer exists on the interface between an electrode and its surrounding electrolyte. This double layer is formed as ions from the solution "stick on" the electrode surface. Charges in the electrode are separated from charge of ions. The separation is very small, often on the order of angstroms. Electrode potential, temperature, ionic concentrations, types of ions, electrode roughness, impurity adsorption, etc. are factors that affect the capacitance.

Charge transfer resistance (R_{ct})

An electrode is polarized when its potential is forced away from its value at open circuit. Polarization of an electrode causes current to flow due to electrochemical reactions it induces at the electrode surface. The magnitude of the current is controlled by reaction kinetics and diffusion of reactants both towards and away from the electrode. Charge transfer resistance is a measure of the electron exchange between the electrode substrate and the electroactive probe. The simplest case is when the mass transfer impedance is negligible in the entire ω range, where it can be estimated by the diameter of the semicircle in the complex-plane diagram (Fig. 8).

This charge transfer reaction has a certain speed. The speed depends on the kind of reaction, the temperature, the concentration of the reaction products and the potential.

Charge transfer resistance is related to the current density by eqn. (13).

$$R_{ct} = \frac{RT}{nFi_0} \quad \text{.....(13)}$$

where i_0 is current density and the others have their usual meanings.

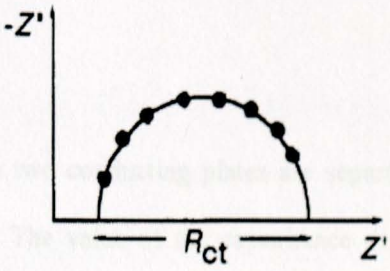

Fig. 8. Experimental determination of R_{ct} from a Nyquist plot

Diffusion (Warburg impedance)

The rate of an electrochemical reaction can be strongly influenced by diffusion of reactants towards or products away from the electrode surface. This is often the case when a solution species must diffuse through a film on the electrode surface. This situation can exist when the electrode is covered with reaction products, adsorbed solution components, or a prepared coating. Whenever diffusion effects completely dominate the electrochemical reaction mechanism, the impedance is called the Warburg Impedance, Z_W and the current is 45^0 out of phase with the imposed potential.

$$Z_W = \sigma(\omega)^{-1/2}(1-j) \quad \text{.....(14)}$$

where σ is called Warburg constant given by:

$$\sigma = \frac{RT}{n^2F^2A\sqrt{2}}\left[\frac{1}{C_0^*(D_0)^{1/2}} + \frac{1}{C_R^*(D_R)^{1/2}}\right] \quad \text{.....(15)}$$

and ω called radial frequency = $2\pi f$, D_0^* is diffusion coefficient of the oxidant, D_R^* is

diffusion coefficient of the reductant, A is surface area of the electrode and n is number of electrons involved.

Coating capacitance

A capacitor is formed when two conducting plates are separated by a non-conducting media, called the dielectric. The value of the capacitance depends on the size of the plates, the distance between the plates and the properties of the dielectric. The relationship is,

$$C_c = \frac{\varepsilon_0 \varepsilon_r A}{d} \quad \text{.....(16)}$$

where ε_o is permittivity of vacuum (physical constant), ε_r is relative permittivity (depends on the material), A is surface of one plate and d is distances between two plates.

Table 1 Typical Relative Electrical Permittivities

Material	ε_r
Vacuum	1
Organic coating	4 - 8
Water	80.1 (20 ^{0}C)

A significant increment of the capacitance of an electrode coated with an organic substance like paint and other modifiers could be an indication of the adsorption of water due to its large relative permittivity value (Table 1).

Constant phase element (CPE)

Capacitors in EIS experiments often do not behave ideally. For example, the solid electrode – solid electrolyte interface contains a large number of surface defects such as kinks, jags, and ledges, local charge inhomogeneities, adsorbed species, and variations in composition and stoichiometry. The capacitance resulted due to such defects is called constant phase element (CPE). The CPE has been used to describe the double-layer capacitance, the low-frequency pseudocapacitance, as well as the diffusion impedance [139]:

$$/Z/ = (jC\omega)^{-\alpha} \quad \text{.....(17)}$$

where α is an exponent which equals 1 for an ideal capacitance, 0.5 for an ideal resistor and less than 1 for a CPE [140].

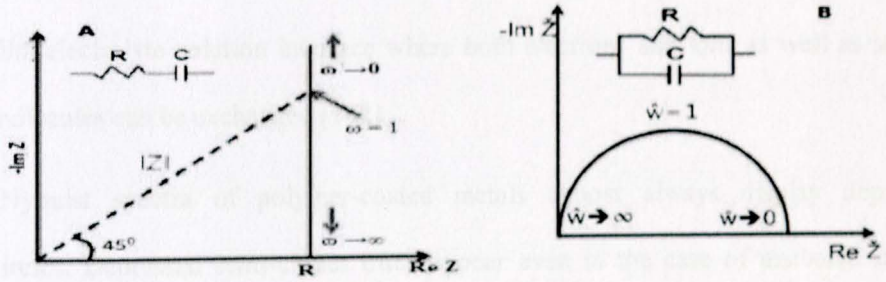

Fig. 9. Nyquist plot and EEC for (A) series and (B) parallel RC connections

To express the total impedance of a circuit, it is important to separate the circuit into parallel part and series part (Fig. 9). Calculation of the resultant impedance of an equivalent electrical circuit in both connections obeys Kirchhoff's law [141].

2.4.2.4 Polymer-Coated Surfaces and Equivalent Circuits

Among the possible polymer film arrangements, the two most common arrangements are [137]:

1. The polymer film is supported on a metal or other electronic conductor and dipped in an electrolyte solution containing only electrochemically "inert" species. The solution only contains ions that do not possess a redox activity. In this electrode arrangement, two different interfaces exist: a metal/film interface where only electrons may be exchanged and a film/electrolyte solution interface, which is permeable only for counterions that are able to cross the film/solution boundary to retain the bulk film electroneutrality, and for neutral (e.g., solvent) molecules.
2. The polymer film is supported on a metal or other electronic conductor and dipped in an electrolyte solution containing a redox couple. In this case also two interfaces exist: a metal/film interface where only electrons may be exchanged and a film/electrolyte solution interface where both electrons and ions as well as solvent molecules can be exchanged [142].

The Nyquist spectra of polymer-coated metals almost always display depressed semicircles. Depressed semi-circles often appear even in the case of uncoated metals. This phenomenon, referred to as impedance dispersion, is explained by the distribution of the time constants of the electrode process around a central value due to the roughness of the electrode surface [143] and/or the non-uniform distribution of the current density of the surface [144]. The depression of semi-circles in the Nyquist plots of polymer-coated

metals is probably due to surface heterogeneity [145] or solid corrosion products of the metal substrate developing in the defects in the organic coating [146]. The latter explanation is supported by the observation that an intact (protective) coating shows no depression at all and the depression increases with the increasing deterioration of the coating. Depressed Nyquist semi-circles are better represented by substituting CPE in place of capacitance [147].

If the spectrum displays more than one semi-circle, usually it is the high-frequency semi-circle which contains coating information while the low-frequency semi-circle contains information about the processes related to reactions on the electrode surface [148]. When only one semi-circle is observed in the Nyquist plot of a polymer coated metal (electrode), a simple method to identify whether it is due to the coating (polymer/metal) or due to the electrode reactions (polymer/electrolyte), is by varying the applied ***ac*** voltage [149]. A higher voltage should decrease the time constant due to the electrode reaction but should not normally affect the time constant due to the coating unless the pores are plugged by the higher voltage in which case it would increase.

For a redox-active polymer coating, Randles model (Fig. 10b) that includes semi-infinite linear diffusion element (Warburg) is usually recommended. The capacitive current is separated from the faradaic current, which is justified only when different ions take part in the double-layer charging and the charge transfer processes, that is, a supporting electrolyte is present in high concentration. The semi-circle region at high frequencies is related to the parallel combination of C_{dl} and R_{ct}, where as the straight line at about an angle of 45^0 to the real axis at low frequencies is related to the Warburg diffusion

parameter (W). In other words, at high frequencies (short time scales), the impedance is determined by electron transfer kinetics, whereas at low frequencies (long time scales), the impedance is diffusion-controlled.

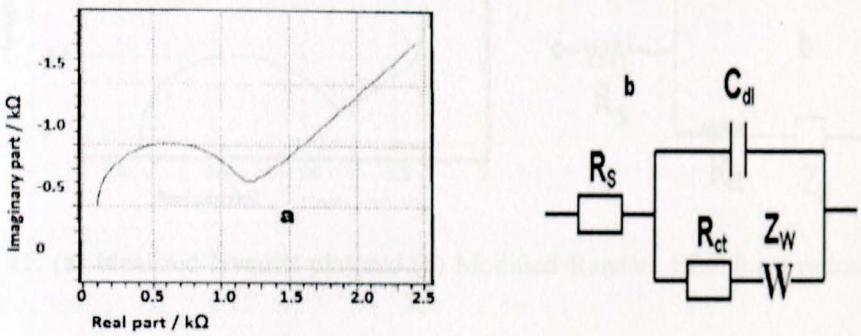

Fig. 10. (a) Nyquist plot (b) Randles EEC for a redox-active species

Under ideal conditions, an impedance spectrum of the type in Fig. 9a is obtained for a redox polymer film which consists of three regions; a semi-circle at high frequency, a line at an angle of 45^0 in the mid-frequency, and a line with a slope of about 1 at low frequency regions. Such a spectrum can be modeled using a modified Randles circuit (Fig. 11b). The Warburg element for semi-infinite diffusion has been replaced by the diffusion element Z_D, which is defined by eqns. (18-20) [150]:

$$Z_D = \frac{A}{(j\omega)^{1/2}} \coth\left[B(j\omega)^{1/2}\right] \quad \text{.....(18)}$$

At large x, coth x = 1, hence $Z_D = \frac{A}{(j\omega)^{1/2}} = Z_W = \sigma(\omega)^{-1/2}(1-j)$ which is a mathematical representation of the Warburg impedance (semi-infinite diffusion) [117].

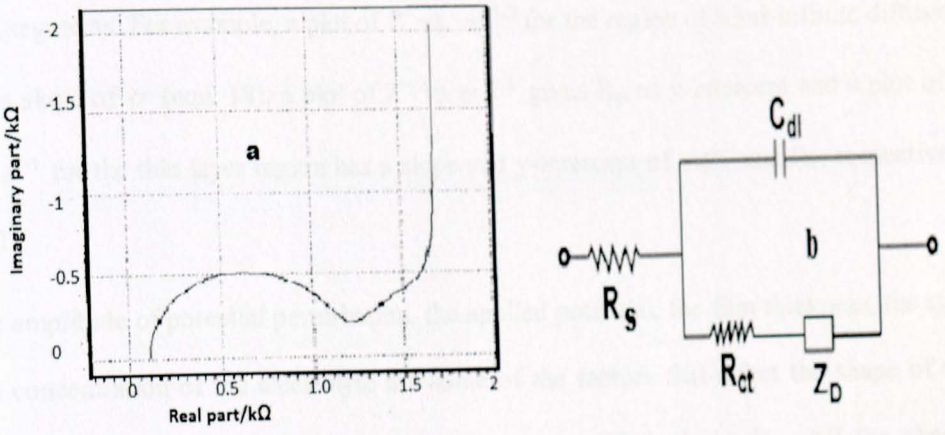

Fig. 11. (a) Idealized Nyquist plot and (b) Modified Randles EEC for a redox polymer film

At small x, coth $x = \frac{1}{x} + \frac{x}{3}$, and hence;

$$Z_D = \frac{AB}{3} + \frac{A}{j\omega B} \quad \text{.....(19)}$$

which corresponds to a series combination of *resistance (AB/3)* and *capacitance (B/A)* [150].

For a polymer film, this resistance is the film resistance R_F, and the capacitance is the psedo-capacitance ΔC. Thus, eqn.(19) can be rewritten as;

$$Z_D = R_F + \frac{1}{j\omega\Delta C} \quad \text{.....(20)}$$

Therefore the important parameters that can be extracted from the impedance spectrum of a redox-polymer are the charge transfer resistance (R_{ct}), the Warburg coefficient (σ), the film resistance (R_F) and the film pseudo-capacitance (ΔC). For an ideal system, these parameters can be derived from equivalent circuit, or from specific analysis of certain

data segments. For example, a plot of Z' vs. $\omega^{-1/2}$ for the region of semi-infinite diffusion has a slope of σ (eqn. 18), a plot of Z'' vs $\omega^{-1/2}$ gives R_{ct} as y-intercept and a plot of Z vs. ω^{-1} for the thin layer region has a slope and y-intercept of ΔC^{-1} and R_F, respectively [151].

The amplitude of potential perturbation, the applied potential, the film thickness, the type and concentration of the electrolyte are some of the factors that affect the shape of the electrochemical impedance spectra of a polymer-modified electrode. All the charge transfer resistance, low-frequency (redox) capacitance, and the Warburg coefficient change with the potential; more exactly, they depend on the redox state of the polymer. Ohmic resistance which is the sum of the solution resistance and the film resistance; may also depend on the potential due to the potential-dependent electron conductivity, sorption of ions, and the swelling of the polymer film [152].

EIS has found widespread applications in the field of characterization of materials. It is routinely used in the characterization of coatings, corrosion phenomena, batteries and fuel cells.

2.5 Surface Characterization Techniques

As was discussed under the previous sections, electrochemical techniques such as the cyclic voltammetry and electrochemical impedance spectroscopy are commonly used for the characterization of electrode surfaces. There are also other techniques such as the Scanning Electron Microscopy (SEM), Atomic Force Microscopy (AFM), and X-ray

Photoelectron Spectroscopy (XPS) which entirely are used for the surface characterization and surface composition analyses.

2.5.1 X-ray photoelectron spectroscopy (XPS)

XPS is a surface sensitive technique used to determine atomic compositions and learn information about the types of bonding that occurs within various compounds. Using an x-ray source, photons are created which have the ability to transfer their entire energy to electrons within atoms when struke [153]. If the energy transfer is sufficient, the receiving electron is jettisoned out of its energy level and away from the atom becoming a photoelectron (Fig. 12A). XPS works by sending massive amounts of photons toward the sample to produce large numbers of photoelectrons and comparing the kinetic energy with the initial energy of the photon. The difference is accounted for by the amount of attraction the electron has with the nucleus to remove it (binding energy) and the amount of energy the particle loses in transit from the sample to the analyzer (work function). While the work function is consistent for each sample on a specific XPS analyzer, the binding energy is dependent on the type of atom the electron came from as well as the environment it came from. The electrons of atoms that are photoemitted remain within a range of binding energies to help identify the specific element within the sample.

When the core electron leaves a vacancy, an electron of higher energy will move down to occupy the vacancy while releasing energy (Fig. 12B). This energy, which is weaker than the applied X-ray, may be released either in the form of photons to its surrounding or may cause a photoelectron called Auger electron that appears at a lower binding energy

than the core electron. Thus, the auger electron which appears at a characteristic energy is sometimes used for qualitative analyses purpose.

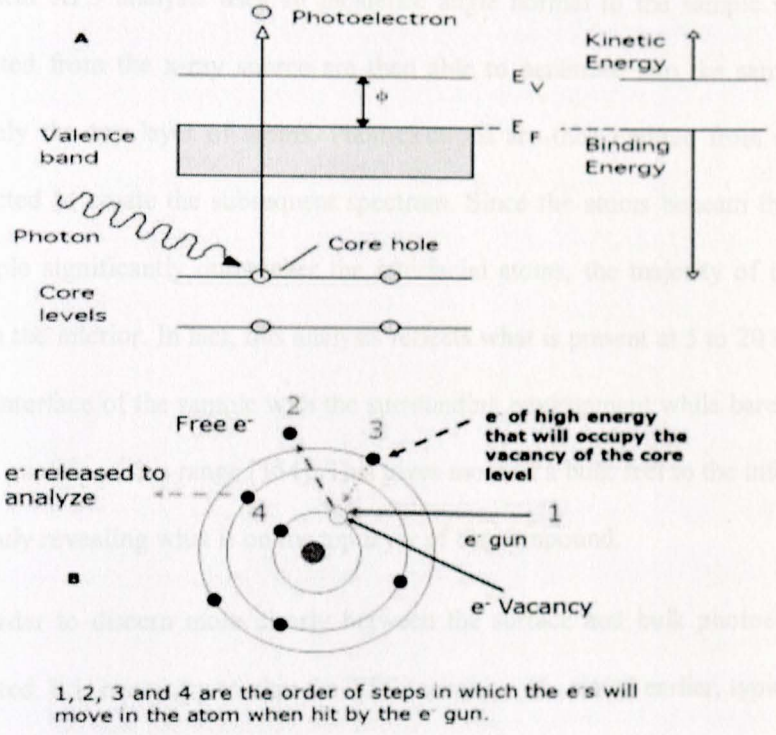

Fig. 12. Schematic representation of (A) overall photoelectron process and (B) Auger electron formation during XPS

Different types of bonds affect where in the range these binding energies fall creating a "chemical shift" which acts as another part of the compound's fingerprint [153]. Chemical shift is mainly a function of oxidation state and chemical environment. For instance, a carbon of a carboxyl group will behave slightly different than that of a carbon in a methyl group for the core electrons are under different chemical environments.

Comparing results of an unknown sample to those of other known standards leads to the identification of the compound or at least an idea of what sort of structure is present. Typical XPS analysis uses an incidence angle normal to the sample surface. Photons emitted from the x-ray source are then able to penetrate into the sample further than merely the top layer of atoms. Photoelectrons are then emitted from all of the atoms affected to create the subsequent spectrum. Since the atoms beneath the surface of the sample significantly outnumber the interfacial atoms, the majority of the signal comes from the interior. In fact, this analysis reflects what is present at 5 to 20 angstroms below the interface of the sample with the surrounding environment while barely noticing what falls outside of this range [154]. This gives more of a bulk feel to the information instead of truly revealing what is on the top layer of the compound.

In order to discern more clearly between the surface and bulk photoelectrons that are emitted, it is necessary to alter the XPS technique. As stated earlier, typical XPS analysis is done from an incidence angle normal to the sample surface which allows for too much photon penetration and subsequently, too many photoelectrons from the bulk. By altering the angle of incidence, it is possible to change the sampling depth to a level that includes almost exclusively the surface atoms. While the bulk contribution to the signal is still present, the surface portion shows a significant boost in signal strength. The increase in surface resolution leads to analysis that can show a difference between binding energies of the surface atoms and the bulk atoms. This difference is known as a surface core-level shift (SCLS) and can be used to gain more information about the atoms at the interface.

2.5.2 Scanning Electron Microscopy (SEM)

The method of scanning electron microscopy with energy dispersive spectroscopy analysis (SEM/EDS) has been extensively used in the past to characterize the morphology and elemental composition of different samples [155].

In SEM imaging, a voltage is applied between a conductive sample and a filament in a vacuum environment ranging between 10^{-4} to 10^{-10} torr, resulting in the emission of beam of electrons from the filament to the sample. The electrons interact with the sample within a few nanometers to several microns of the surface, depending on beam parameters and sample type. Electrons are emitted from the sample primarily as either backscattered electrons or secondary electrons. Secondary electrons are the most common signal used for investigations of surface morphology. They are produced as a result of interactions between the beam electrons and weakly bound electrons in the conduction band of the sample. Some energy from the beam electrons is transferred to the conduction band electrons in the sample, providing enough energy for their escape from the sample surface as secondary electrons. Secondary electrons are low energy electrons (<50 eV), so only those formed within the first few nanometers of the sample surface have enough energy to escape and be detected. High energy beam electrons which are scattered back out of the sample (back scattered electrons) can also form secondary electrons when they leave the surface. Since these electrons travel farther into the sample than the secondary electrons, they can emerge from the sample at a much larger distance away from the impact of the incident beam which makes their spatial distribution larger.

Once these electrons escape from the sample surface, they are typically detected by the detector. The SEM image formed is the result of the intensity of the secondary electron emission from the sample at each x,y data point during the rastering of the electron beam across the surface. The brightness of the image is a function of the intensity of secondary electrons reaching the detector.

Along with the secondary electron emission which is used to form a morphological image of the surface, it provides elemental analysis by the attachment of an Energy-Dispersive Spectrometer (EDS) to the SEM system [156,157]. Interaction of the primary beam with atoms in the sample causes shell transitions which result in the emission of an X-ray. The emitted X-ray has an energy characteristic of the parent element. Detection and measurement of the energy permits elemental analysis (Energy Dispersive X-ray Spectroscopy or EDS). EDS can provide rapid qualitative, or with adequate standards, quantitative analysis of elemental composition with a sampling depth of 1-2 microns. X-rays may also be used to form maps or line profiles, showing the elemental distribution in a sample surface.

2.5.3 Atomic Force Microscopy (AFM)

AFM imaging consists of sharp scanning tip at the end of a flexible cantilever across a sample surface while maintaining a small, constant force. The tips typically have an end radius of 2-20 nm, depending on tip type. The scanning motion is conducted by a piezoelectric scanner which scans the tip in a raster pattern with respect to the sample (or scans the sample with respect to the tip). The tip-sample interaction is monitored by

reflecting a laser beam off the back of the cantilever into a split photodiode detector. By detecting the difference in the photodetector output voltages, changes in the cantilever deflection or oscillation amplitude are determined.

The two most commonly used modes of AFM operation are contact mode and tapping mode. Contact mode AFM consists of raster-scanning the probe (or sample) while monitoring the change in cantilever deflection with the split photodiode detector.

The distance the scanner moves vertically at each x,y data point is stored by the computer to form the topographic image of the sample surface. This feedback loop maintains a constant force during imaging.

Tapping mode AFM consists of oscillating the cantilever at its resonance frequency (typically ~300 kHz) and lightly "tapping" the tip on the surface during scanning. The laser deflection method is used to detect the root-mean-square (RMS) amplitude of antilever oscillation. The advantage of tapping mode over contact mode is that, it eliminates the lateral, shear forces present in contact mode. This enables tapping mode to image soft, fragile, and adhesive surfaces without damaging them, which can be a drawback of contact mode AFM.

The work presented in this thesis encompasses electrosynthesis of a new polymer (poly(4-amino-3-hydroxynaphthalene sulfonic acid)) at glassy carbon electrodes, characterization of the polymer modified electrodes using different techniques, study the application of the polymer-modified electrodes for the electrochemical determination of selected alkaloids and organophosphorus pesticides in environmental samples. Moreover,

the application of electrochemically pretreated glassy carbon for the electrochemical determination of fenitrothion, which is one of the organophosphorus pesticides considered, is included.

3. EXPERIMENTAL

3.1 Chemicals

4-amino-3-hydroxynaphthalene sulfonic acid (AHNSA), Methyl parathion, Fenitrothion (FT) and Ascorbic acid (AA) were purchased from Sigma-Aldrich while Uric acid (UA) from Fluka Chemika, Switzerland. Ephedrine hydrochloride (EPH), Theophylline anhydrous (TP), and Caffeine were supplied by Emmellen Biotech Pharmaceuticals Limited, the China associate limited supplier and Fischer Scientific Limited, respectively. Potassium ferricyanide and potassium ferrocyanide were supplied by BDH, England.

Britton-Robinson buffer solutions (RBS) were prepared using equi-volume mixtures of 0.04 M H_3BO_3, 0.04 M H_3PO_4 and 0.04 M CH_3COOH (all from Sigma-Aldrich). Phosphate buffer solutions (PBS) were prepared from 0.1 M KH_2PO_4 or K_2HPO_4 (Fluka Chemika, Switzerland) whilst the Acetate buffer solutions (ABS) by mixing appropriate amounts of 0.1 M CH_3COOH and CH_3COONa (Sigma-Aldrich). The pH of each buffer solution was adjusted to the required pH with 0.1M HCl or 2.0 M NaOH using Jenway 3345 ion meter. All chemicals used were of analytical grade and were used without further purification.

3.2 Apparatus

Voltammetric measurements were performed using BAS-50W electrochemical analyzer, CHI760D Electrochemical Workstation, CH Instruments (Austin, Texas, USA) and Autolab PGSTAT30 analyzer controlled by GPES 4.9 software (Eco Chemie, The

Netherlands). Similarly, the electrochemical impedance spectra were recorded using FRA 4.9 software (EcoChemie, The Netherlands).

Scanning electron microscopic (SEM) images, Atomic force microscopic (AFM) images and the X-ray photoelectron spectroscopic (XPS) spectra of the electrodes used were recorded using TM 1000 tabletop microscope from HITASHI, an Agilent 5500 microscope, and SPECS GmbH spectrometer, respectively. SpecsLab Version 4.1 software was used for spectrometer control and data handling of XPS results.

All electrochemical experiments were performed employing a conventional three-electrode system with unmodified glassy carbon electrode (UGCE), electroactivated glassy carbon electrode (AGCE), poly(AHNSA) modified glassy carbon electrode (PGCE), or electrochemically pretreated glassy carbon electrode (pGCE) as working electrode, platinum wire as an auxiliary electrode and Ag/AgCl or SCE as a reference electrode.

3.3 Procedure

3.3.1 Electrode preparation

3.3.1.1 Electrochemical measurements

For the electrochemical (CV and EIS) experiments, three glassy carbon electrodes were first rinsed with distilled water, polished carefully with alumina powder having different particle size (1.0, 0.3 and 0.05 μm) to mirror finish surfaces. Residual polishing materials were removed from the surface by repetitive rinsing of the surface with distilled water or

sonicating the electrodes in ethanol for 30 seconds. One of the three polished GCEs was used unmodified (UGCE). The surface of the second polished GCEs was polymer-modified by scanning the electrode between -0.8 and +2.0 V in a 0.1 mol L^{-1} HNO_3 solution containing 2.0×10^{-3} mol L^{-1} AHNSA for 15 cycles. The polymer-modified electrode (PGCE) was then rinsed with distilled water to remove physically adsorbed and unreacted species from the electrode surface. Subsequently, the modified electrode was electroactivated in a 0.5 mol L^{-1} H_2SO_4 potentiodynamically between -0.8 and +0.8 V until a steady voltammogram was obtained. Finally, the modified electrode was dried in air and made ready for use. The third electrode was modified following the same procedure as for the polymer modification except that the 0.1 M HNO_3 was monomer free. This electrode was named as electroactivated glassy carbon electrode (AGCE). A fourth working electrode (pGCE) was prepared by adapting the procedure reported [158]. Briefly: a constant oxidative potential of +1.75 V was applied to the polished electrode in pH 5 ABS for 200 s. The pretreated electrode was then scanned between -0.4 and -1.0 V in pH 5 ABS until a stable voltammogram was obtained. Prior to each measurement, the electrode surface was cleaned by running a linear sweep in the reverse direction.

The electrochemical impedance spectroscopic spectra for the above four electrodes (UGCE, AGCE, PGCE, and pGCE) were recorded by applying 0.23 V bias potential and 10 mV alternative voltage in the frequency range 0.01-100,000 Hz. As an electrochemical probe, 10 mM $K_4[Fe(CN)_6]/K_3[Fe(CN)_6]$ in pH 7 PBS containing 0.1 M KCl was used. The experimental impedance spectra were fitted using electronic equivalent circuits employing the Randles EEC.

3.3.1.2 Surface characterization

For SEM, AFM, and XPS analyses, three glassy carbon electrodes, each 1 cm long were prepared. The electrodes were polished first with a sand paper and then with alumina slurry of 1.0, 0.3, and 0.05 μm size. The polished electrodes were rinsed with distilled water to remove polishing materials and further sonicated in ethanol for 30 seconds.

The PGCE, UGCE and AGE electrodes for SEM, AFM and XPS analyses were prepared following the procedure discussed above. Furthermore, monomer modified GCE (MGCE) was prepared by casting 20 μL of 2.0×10^{-3} mol L^{-1} AHNSA (in 0.1 M HNO_3) at the surface of a polished GCE.

Finally, the SEM images, AFM images, and XPS spectra for the electrodes were recorded after fixing the electrodes erected on a small metal sheet using an epoxy resin and allowing them to dry in air.

3.3.2 Sample preparation

3.3.2.1 Standard samples

50 mM ephedrine hydrochloride (EPH) in pH 11.0 RBS, 25 mM theophylline in distilled water, 10 mM caffeine in pH 5 ABS, 0.534 mM fenitrothion (FT) in ethanol, and 10 mg/100 mL methyl parathion in ethanol were prepared as stock solutions and were kept in the dark under refrigeration. 100 mL of 2.0×10^{-3} mol L^{-1} monomer (AHNSA) in 0.1 M HNO_3 was prepared. The dissolution of the monomer was facilitated by sonication or continuous hand shaking.

Standard samples of the selected alkaloids and organophosphorus pesticides were prepared from their respective stock solutions by dilution with the buffer solutions of the required pHs. Buffer type for the analysis of each analyte was chosen based on the matching between the buffering capacity of the specific buffer and the pH range used for the analyte in literature.

3.3.2.2 Urine samples

Human urine collected from a volunteer was divided in to two portions. One portion was suction filtered using a 0.45 µm pore size filter paper. The filtrate was then diluted with pH 10.5 RBS in a 1:5 volume ratio. Then, 80, 100, and 200 µM EPH solutions were prepared from the stock solution using the diluted filtered urine as a solvent. The same procedure was used to prepare 80, 100, and 200 µM EPH solutions with the unfiltered urine portion.

Filtrate of the human urine used for fenitrothion analyses was first diluted with pH 5.4 ABS in a 1:20 (urine: buffer) volume ratio. The diluted urine was then used to prepare three samples with 20, 10, and 5 µM FT, respectively.

Human urine sample collected from a volunteer was also filtered and diluted with pH 5.4 ABS using which, three FT solutions of 20, 10, and 5 µM were prepared.

3.3.2.3 Theophylline tablet samples

Theophylline tablets (labeled as 120 mg per tablet) were collected from two local pharmaceuticals manufacturing factories: Addis pharmaceuticals factory (APF) and

Ethiopian pharmaceuticals factory (EPF). Stock solutions of the tablets from each factory were prepared by dissolving 3 randomly selected tablets in 500 mL of distilled water. 10 and 20 μM TP tablet solutions were prepared from each stock solution by dilution with PBS (pH 3.0). Triplicate measurements were taken for each sample solution. The recovery of spiked standard TP in tablet sample solutions using the developed method was investigated. For this purpose, two solutions were prepared from 10 mL of 10 μM drug samples (EPF) spiked with 10 μM and 20 μM standard TP solutions, respectively.

3.3.2.4 Coffee extract samples

Ethiopian coffee purchased from a supermarket was roasted, ground, boiled in water and then extracted by decantation. The filtrate of the coffee extract was made ready for caffeine measurement after diluting it with pH 5.0 ABS in a volume ratio of 1:200. The amount of caffeine contained in the coffee extract was determined employing the developed method. Furthermore, the application of the method was evaluated based on the recovery of spiked standard caffeine in coffee extracts.

3.3.2.5 Tap water samples

Instead of distilled water, tap/drinking water was used to prepare the buffer solutions of the optimized pH for the recovery studies of fenitrothion (sections 4.2.4.8 and 4.2.6.10.1) and methyl parathion (4.2.5.4). Standard FT and methyl parathion from their stocks (3.3.2.1) were spiked in to the buffer solutions of the required pH prepared from tap/drinking water. The recoveries were calculated by comparing the experimental

current response with the expected current according to the respective linear regression equations formulated.

4. Results and Discussion

4.1 Electrosynthesis and Characterization of poly(AHNSA) modified glassy carbon electrodes

One of the critical problems during the potentiodynamic electropolymerization of 4-amino-3-hydroxynaphthalene sulfonic acid (AHNSA) (Scheme 3) at a glassy carbon electrode from an aqueous solution was optimizing the potential window within which it polymerizes. CV, EIS, SEM, AFM, and XPS techniques were used to characterize the polymer film deposition (electrode surface modification) at the electrode surface.

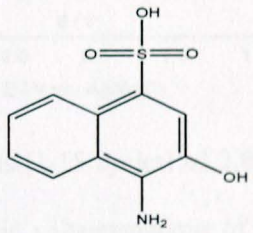

Scheme 3 Structural formula of 4-amino-3-hydroxynaphthalene sulfonic acid (AHNSA)

4.1.1 Cyclic voltammetry

4.1.1.1 Electropolymerization of AHNSA at the surface of GCE

Cyclic voltammetry was used to deposit the polymer film at the electrode surface. The most important thing was the potential scan range within which the monomer (AHNSA) forms a polymer film at the electrode surface. No polymer formation was observed when the anodic potential is below +2.0 V and the cathodic potential is above -0.8 V.

Therefore, the optimum potential window for the cyclic voltammetric electropolymerization of AHNSA at GCE was between -0.8 and +2.0 V. Fig. 13 depicts the repetitive cyclic voltammograms of 2.0×10^{-3} mol L^{-1} of AHNSA in 0.1 M HNO_3 at a polished GCE between -0.8 and +2.0 V.

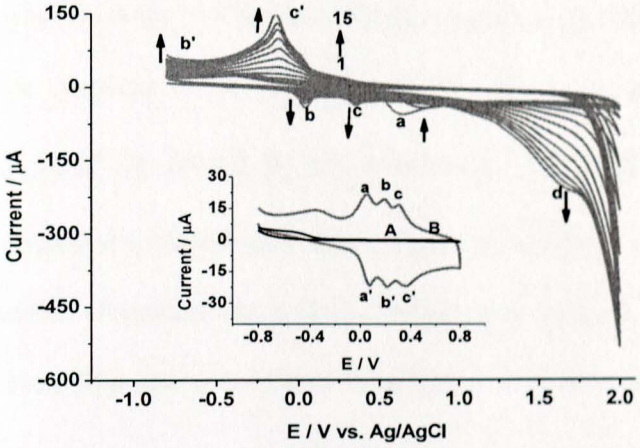

Fig. 13. Cyclic voltammograms (1-15 cycles) of 2.0×10^{-3} mol L^{-1} AHNSA in 0.1M HNO_3 at GCE. Inset: the cyclic voltammograms of UGCE (A) and PGCE (B) in a monomer free 0.5 M H_2SO_4 scanned between -0.8 and +0.8 V. Scan rate: 0.1 V s^{-1}

In the first cycle, weak anodic peaks (*b*), strong anodic peak (*a*) and cathodic peak (*b'*) were observed at about -15, +650 and –300 mV, respectively. In the consecutive scans, additional peaks; anodic peaks *(c)* and (d) and a cathodic peak *(c')* appeared at about +250, +1650 and +200 mV, respectively. Upon continuous scanning, the peak current growth for all peaks (except peak (*a*)) was accompanied by potential shifts. The anodic and cathodic peaks showed potential shift in the direction of higher positive and negative values, respectively. Contrasting the other peaks, the peak current for peak (*a*) decreased

with increasing scanning cycles which could be ascribed to the presence of a species being irreversibly oxidized.

Inset of Fig. 13 represents the cyclic voltammograms of unmodified GCE (A) and polymer modified GCE (B) in a monomer free 0.5 M H_2SO_4. In contrast to the voltammogram at the UGCE (curve A), three redox couples designated as: a-a', b-b', and c-c' were observed at the PGCE (curve B) with peak-to-peak separations ($\Delta E_p = |E_{pc} - E_{pa}|$) of 30, 30 and 60 mV, respectively. The observed peak separations are characteristics of quasireversible redox couples governed by $\Delta E_p = (59\ m/n)$ mV; where m is number of protons and n number of electrons involved in the reaction. Thus, the results suggested that an electroactive poly(AHNSA) film is deposited at the electrode surface.

The effect of scan rate on the peak currents and peak potentials of the redox couples of the polymer film was also investigated. Fig. 14 depicts the cyclic voltammograms of PGCE in a monomer free 0.5 M H_2SO_4 at various scan rates. In the scan rate range studied, the anodic and cathodic peak currents (I_{pa} and I_{pc}, respectively) for the redox couple with the highest peak currents (a-a') increased linearly with scan rate with a linear regression equation and correlation coefficient (R^2) of I_{pa} (μA) = -1.944 – 0.194 ν (mV s^{-1}), I_{pc} = 1.967 + 0.196ν (mV s^{-1}), 0.9979 and 0.9985, respectively (Inset of Fig. 14). Linear dependence of peak current on the scan rate is an indication of a redox process involving surface-confined species [159] confirming the deposition of a polymer film at the electrode surface. Besides, variation of scan rate showed no potential shift in the

redox peaks of the polymer modified electrode confirming the reversibility of the couples.

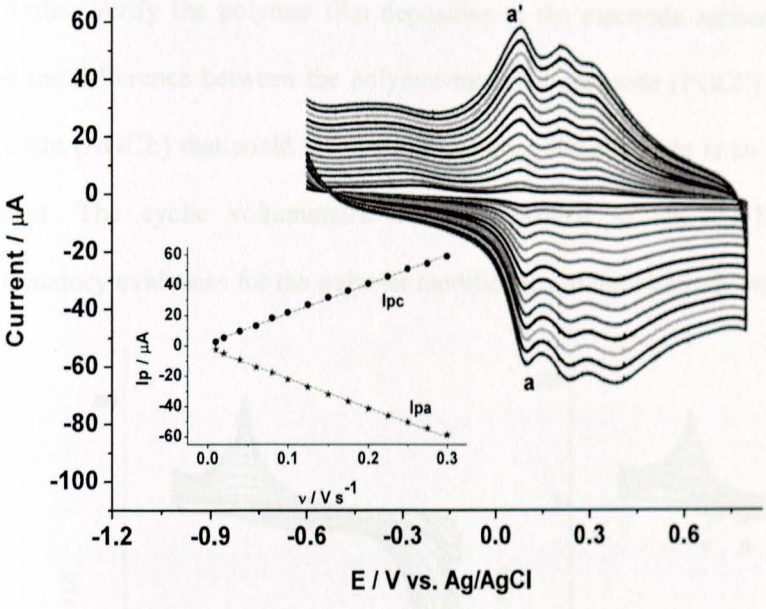

Fig. 14. Cyclic voltammograms of PGCE in 0.5 M H_2SO_4 at various scan rates (a-l: 10, 20, 40, 60, 80, 100, 125, 150, 175, 200, 225, 250, 275 and, 300 mV s^{-1}, respectively)

In the case of a surface-confined reversible redox processes, the peak current and charge consumed during the electrolysis are given by eqns. (6 and 7), respectively [117,160]. Integrating the reductive peak *a'* at scan rate of 100 mV s^{-1} in Fig. 12, *n* and Γ were calculated to be 2.2 and 1.32×10^{-9} mol cm^{-2}, respectively. Thus, the calculated surface coverage along with the appearance of distinct redox peaks (Inset of Fig. 13) at the modified GCE confirmed the deposition of polymer film at the electrode surface.

4.1.1.2 Cyclic voltammetric Characterization of the polymer-modified electrode

To further verify the polymer film deposition at the electrode surface, an approach to show the difference between the polymer-modified electrode (PGCE) and the activated electrode (AGCE) that could result while scanning the electrode in an acid medium was pursued. The cyclic voltammetric results presented in Fig. 15-18 were used as confirmatory evidences for the polymer modification of the electrode surface.

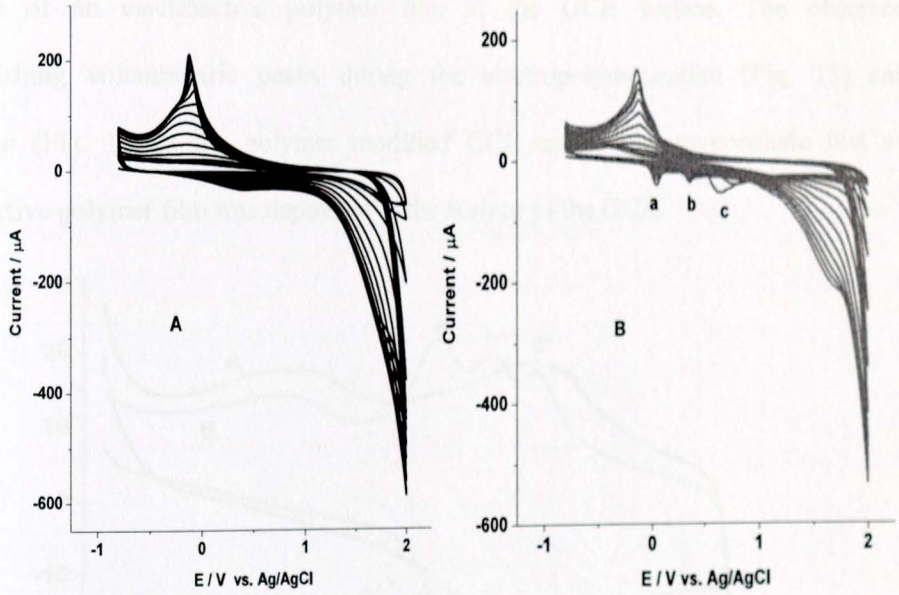

Fig. 15. Cyclic voltammograms of polished GCE in 0.1 M HNO_3 containing (A) no AHNSA and (B) 2×10^{-3} M AHNSA. Scanning cycles: 15; scan rate: 0.1 V s^{-1}.

Fig. 15 presents the cyclic voltammograms of two polished GCEs; one in a monomer free 0.1 M HNO_3 (A), and the other in a 0.1 M HNO_3 containing 2.0×10^{-3} mol L^{-1} HNSA

(B). The cyclic voltammograms of the electrode in the presence of monomer (PGCE) showed at least three distinct oxidative peaks (*a, b* and *c*). On the contrary, the same electrode in a monomer free solution showed no observable oxidative peaks confirming the deposition of a polymer film at the electrode surface.

Fig. 16 depicts the cyclic voltammograms of the two electrodes; AGCE and PGCE in 0.5 M H_2SO_4 after steady state wave formation. Still, three distinct redox couples appeared at the polymer modified GCE (B) which are absent at the activated GCE (A) signifying the presence of an electroactive polymer film at the GCE surface. The observed distinguishing voltammetric peaks during the electropolymerization (Fig. 15) and activation (Fig. 16) at the polymer modified GCE enabled us to conclude that an electroactive polymer film was deposited at the surface of the GCE.

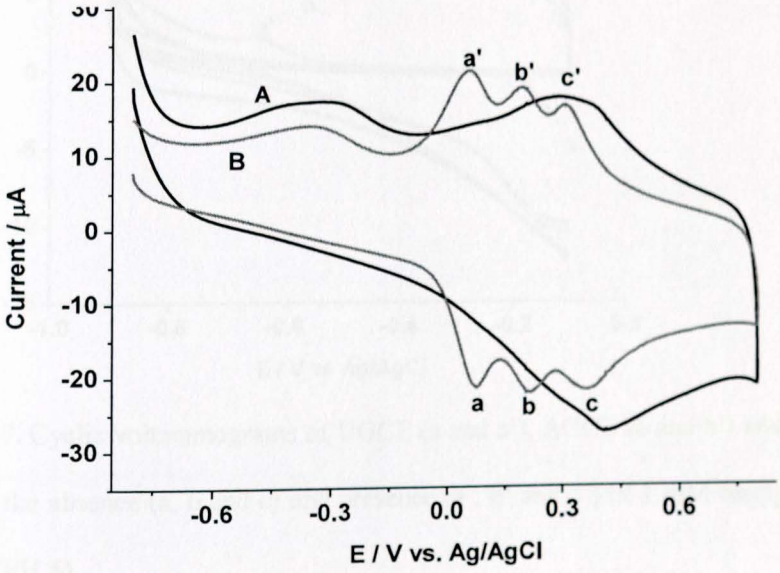

Fig. 16. Steady state voltammograms of AGCE (A) and PGCE (B) in 0.5 M H_2SO_4

The electrocatalytic activities of UGCE, AGCE and PGCE towards methyl parathion was also used as an alternative means to confirm the polymer film deposition.

As can be observed from Fig. 17, a significantly enhanced reduction peak for methyl parathion was recorded at the polymer-modified (*c'*) than at the activated electrode (*b'*). Hence the catalytic activity of the polymer-modified GCE towards the studied alkaloids and organophosphorus pesticides (section 4.2) is attributed to the presence of a polymer film and not to the activation of the electrode surface which could result from scanning the electrode in acids during electropolymerization.

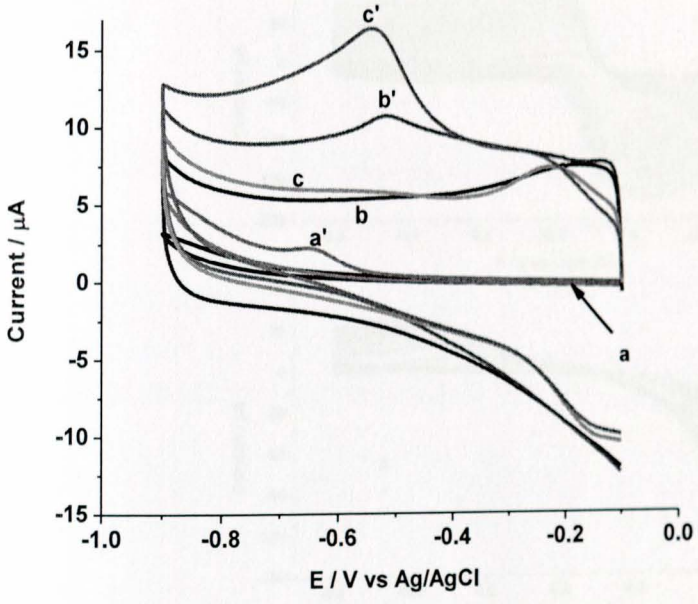

Fig. 17. Cyclic voltammograms of UGCE (a and a'), AGCE (b and b') and PGCE (c and c') in the absence (a, b and c) and presence (a', b' and c') of 1 mM methyl parathion in ABS (PH 5)

Another means of exploring the difference between the polymer-modified and electroactivated electrodes is, comparing the response of the PGCE and AGCE for a well studied analyte. For this purpose, $Fe(CN)_6^{3-/4-}$ was taken as a probe whose number of electrons and diffusion constant are known.

The cyclic voltammograms of both the PGCE and AGCE in pH 7 PBS containing 0.1 M KCl and a mixture of 10 mM of potassium ferrocyanide and potassium ferricyanide are shown in Fig. 16.

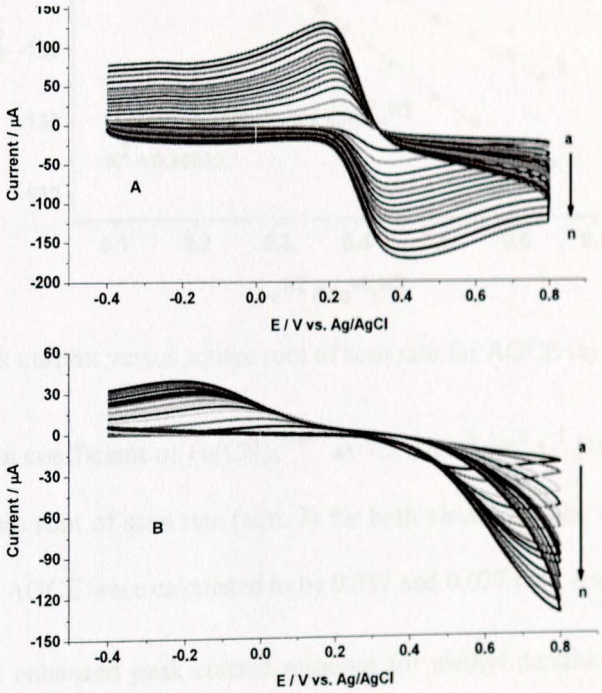

Fig. 18. Cyclic voltammograms of PGCE (A) and AGCE (B) in pH 7 PBS containing 0.1 M KCl, and a mixture of 10 mM of potassium ferrocyanide and potassium ferricyanide at various scan rates (a-n: 10, 20, 40, 60, 80, 100, 125, 150, 175, 200, 250, 300, 350, and 400 mV s^{-1}, respectively)

In contrast to the AGCE (Fig. 18B), an improved reversibility of $Fe(CN)_6^{3-/4-}$ was observed at the PGCE (Fig. 18A). This signified the presence of a polymer film at the electrode surface that improved the electron exchange process between the electrode and the redox species.

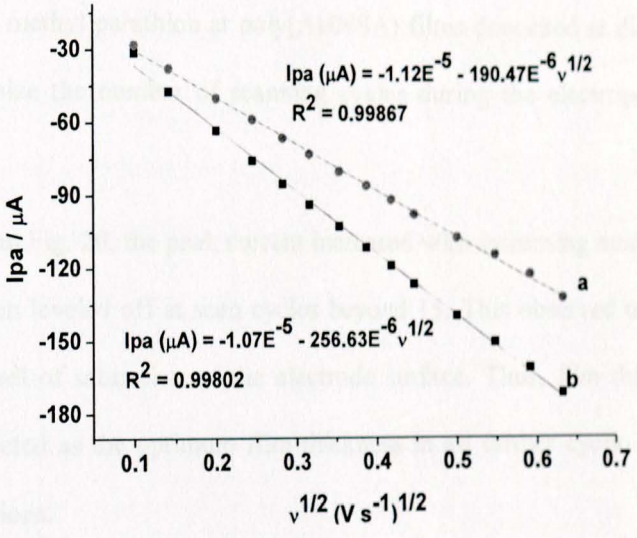

Fig. 19. Plot of peak current versus square root of scan rate for AGCE (a) and (b) PGCE

Taking the diffusion coefficient of $Fe(CN)_6^{3-/4-}$ as 7.5×10^{-6} cm^2 s^{-1} [161] and slope of current versus square root of scan rate (eqn. 3) for both electrodes, the effective surface areas of PGCE and AGCE were calculated to be 0.037 and 0.027 cm^2, respectively.

Thus, the observed enhanced peak current response for methyl parathion (Fig. 17c') at the polymer-modified GCE could partly be ascribed to the increased effective surface area of the electrode. On the other hand, the worest reversibility of $Fe(CN)_6^{3-/4-}$ at the activated GCE could be ascribed to the electrostatic repulsive force between the negatively charged ferric/ferrocyanide ions and the surface of the electrode.

4.1.1.3 Optimization of polymer film thickness

One of the advantages of potentiodynamic electropolymerization over the other techniques such as potentiostatic and galvanostatic electropolymerization is controlling the film thickness of the polymer film using the number of scanning cycles. The current response of 1 mM methyl parathion at poly(AHNSA) films deposited at different cycles was used to optimize the number of scanning cycles during the electropolymerization process.

As can be seen from Fig. 20, the peak current increased with increasing number of cycles up to 15 which then leveled off at scan cycles beyond 15. This observed trend could be ascribed to the level of saturation of the electrode surface. Thus, film thickness of 30 segments was selected as the optimum film thickness in all further cyclic voltammetric electropolymerizations.

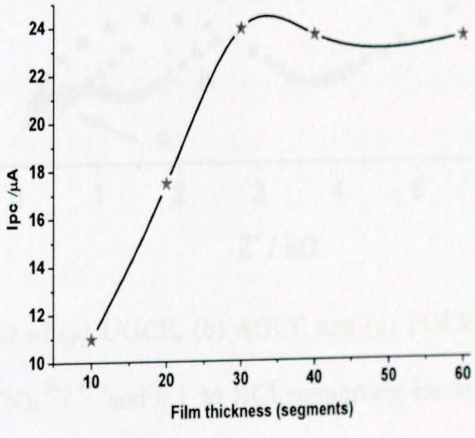

Fig. 20. Effect of film thickness of poly(AHNSA) on the cathodic peak current response for 10×10^{-6} mol L^{-1} of methyl parathion in pH 5.0 ABS

4.1.2 Electrochemical impedance spectroscopy (EIS)

From the Nyquist plots (curves *a, b,* and *c*) in Fig. 21, two characteristic parts of the spectra can be marked out: a semi-circle located in the range of high frequencies whose diameter varied with the type of electrode used, and a linear curve at low frequency region which could be assigned to the Warburg impedance showing the diffusion of the electroactive species through the electrode surface [139]. Randles electrical equivalent circuit (EEC) comprising solution resistance, double layer capacitance, charge transfer resistance and Warburg resistance described in Fig. 10b was proposed.

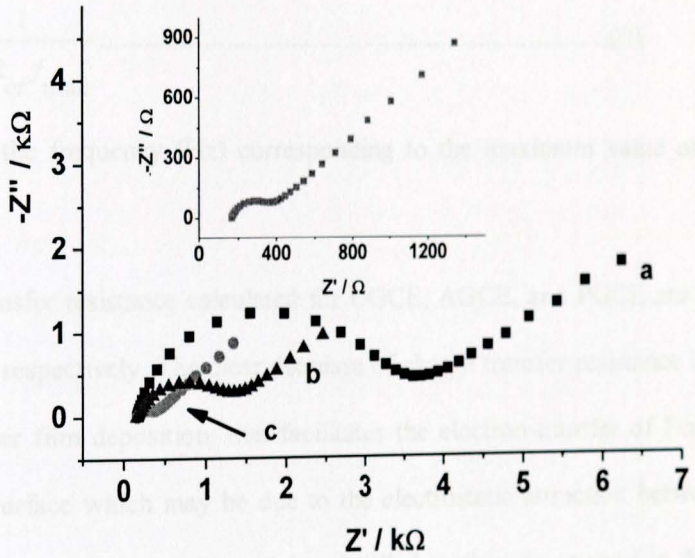

Fig. 21. EIS Nyquist plot of (a) UGCE, (b) AGCE and (c) PGCE in 0.1 M PBS (pH 7) containing 10 mM $Fe(CN)_6^{3-/4-}$ and 0.1 M KCl supporting electrolyte. Inset: magnified Nyquist plot of PGCE. Frequency range: 0.01-100,000 Hz, applied potential: +0.23 V; amplitude: 0.01 V

As it is well known, a semi-circle at high *ac* frequencies in Nyquist plots corresponds to a parallel $R_{ct}C_{dl}$ element in the relevant equivalent circuit. The presence of such an element is attributed to a dominant contribution of charge transfer resistance R_{ct} at either the substrate/film or film/solution interface and hence the necessity to charge double layer capacitance C_{dl} of the corresponding interface.

The parameters R_{ct} and C_{dl} of the presumed RC-elements for the studied electrodes were obtained (Table 2) from the respective semi-circles by taking into account the facts that R_{ct} is the semi-circular diameter, and C_{dl} satisfies the equation;

$$C_{dl} = \frac{1}{2\pi R_{ct} f_{\max}} \quad \text{.....(21)}$$

where f_{max}, is the frequency (Hz) corresponding to the maximum value of $-Z''$ at the semi-circle.

The charge transfer resistance calculated for UGCE, AGCE, and PGCE are 3.65, 1.241, and 0.257 kΩ, respectively. The clear decrease of charge transfer resistance at the PGCE implied polymer film deposition, that facilitates the electron-transfer of $Fe(CN)_6^{3-/4-}$ at the electrode surface which may be due to the electrostatic attraction between polymer and probe or increased conductivity of the modified surface. In contrast to AGCE, lower charge transfer resistance value for PGCE is in agreement with the CV result in Fig. 16, which showed reversible redox couples at PGCE confirming fast electron exchange process at the polymer modified electrode.

Table 2 Summary of the calculated values of the EEC parameters

Electrode Type	R_s (Ω)	R_{ct} (kΩ)	C_{dl} (F)	W
UGCE	97	3.65	1.7E-6	0.1303E-2
AGCE	97	1.241	2.3E-8	0.2818E-2
PGCE	97	0.257	1.6E-5	0.3079E-2

4.1.3 Scanning Electron Microscopy (SEM)

To further justify the poly(AHNSA) film deposition at the GCE, SEM/EDS, which is Scanning Electron Microscopy (SEM) equipped with an Energy Dispersive Spectrometer (EDS) chemical analyzer was used. Three GCEs, each with 1.0 cm length were prepared following the procedure discussed in 3.3. The SEM image for each electrode was recorded followed by the EDS elemental analysis. The EDS instrument used does not detect elements lighter than sodium. Among the elements in the monomer of the polymer (oxygen, carbon, sulfur, nitrogen and hydrogen), only sulfur was detected whose amount was expressed relative to an arbitrarily chosen element.

As can be seen from the SEM images in Fig. 22, the morphology of the three electrodes is undistinguishable. So, it was not possible to visualize the morphology difference between the three electrodes, which might be due to the smooth and very thin film thickness of the polymer film deposited. Nevertheless, it was possible to extract important information from the EDS spectra for the SEM images of the three electrodes above.

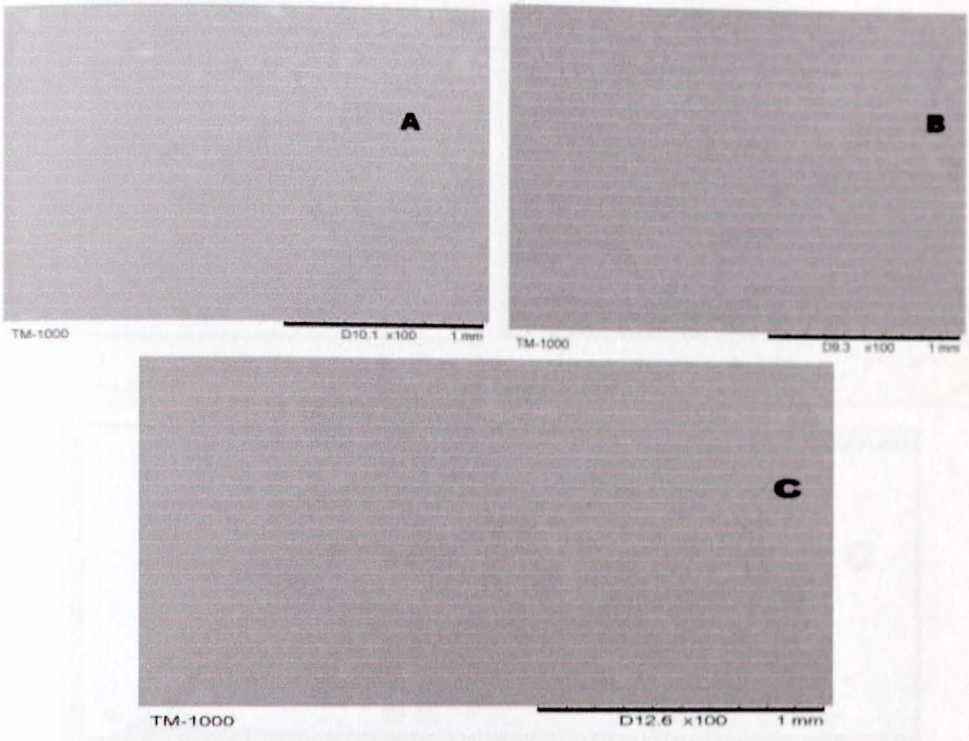

Fig. 22. SEM images of (A) UGCE, (B) AGCE, and (C) PGCE at 100X magnification

Table 3 presents summary of the percentage (%wt/wt) of sulfur detected at each electrode (Fig. 23) relative to nickel which was selected arbitrarily. The weight percentages of sulfur detected relative to nickel at the UGCE, AGCE, and PGCE were 0.0, 1.7, and 68.6%, respectively. The presence of trace amount of sulfur (1.7 %) at the AGCE could be attributed to the contamination of the electrode surface during the activation step of the electrode in 0.5 M H_2SO_4 as discussed in the procedure. On the contrary, sulfur amount to the extent of 68.6 % on the PGCE signified the presence of large amount of sulfur containing polymer film confirming the polymer film modification of the electrode surface.

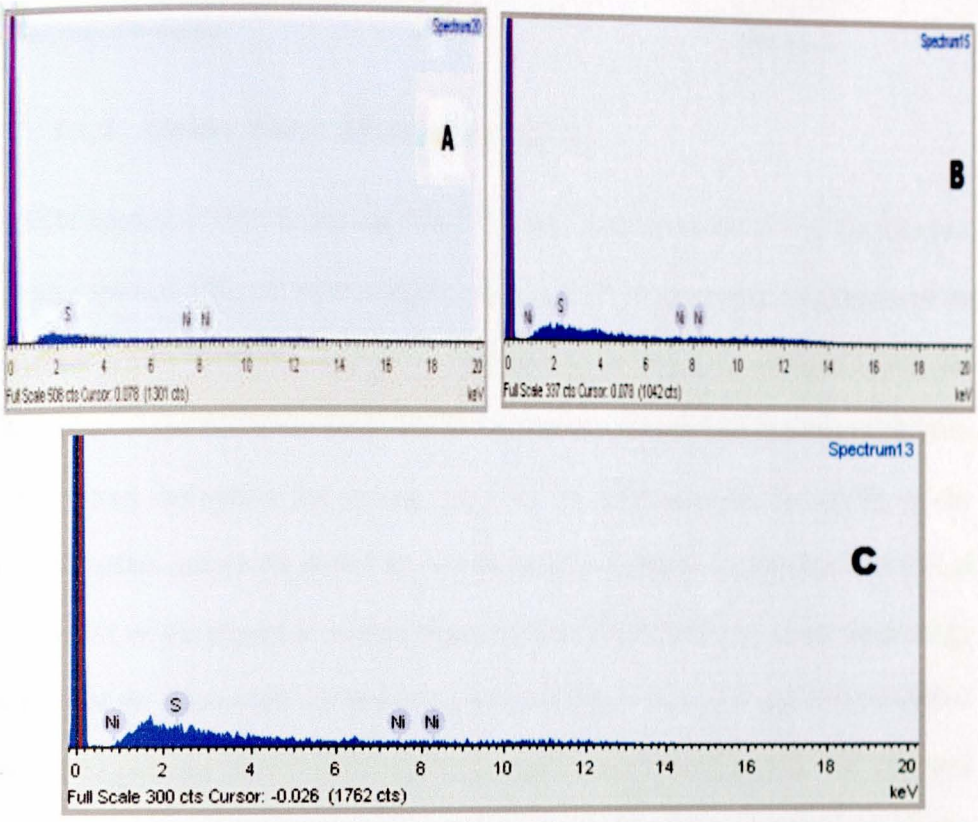

Fig. 23. EDS spectra of (A) UGCE, (B) AGCE, and (C) PGCE for selected elements under all elements normalized. Acquisition time: 90 s; Accelerating voltage: 15 kV

Table 3 Summary of EDS results on the weight % of Sulfur relative to Nickel

Electrode type	Element	Weight %
UGCE	Sulfur	0.0
	Nickel	100.0
AGCE	Sulfur	1.7
	Nickel	98.3
PGCE	Sulfur	68.6
	Nickel	31.4

4.1.4 Atomic Force Microscopy (AFM)

The AFM images of UGCE (A) and PGCE (B and C) are presented in Fig. 24. The two electrodes showed different morphologies. At the UGCE image, certain lines appeared on the surface which could be assigned to the polishing directions. In contrast to this, the AFM images of the PGCE (B and C) showed a different morphology over which platelets are distributed throughout the surface. Inset of Fig. 24B describes the profile of the electrode surface across the dotted line on the image. Existence of platelets of tenths of nm in height at the electrode surface suggested that the surface has rough morphology which could be responsible for the increased effective surface area and hence catalytic effect of the polymer modified GCE towards methyl parathion (Fig. 18). The thickness of the polymer film deposited at the electrode surface was also estimated by measuring the hole (scratch) on the electrode surface obtained by applying a high load force on the polymer modified electrode surface. Inset of Fig. 24C shows the profile across the scratched portion of the film. A film thickness in the range 40-50 nm was measured across the scratch. From these observations, it was possible to conclude that the surface of glassy carbon electrode was modified by a thin polymer film of about 40-50 nm thickness.

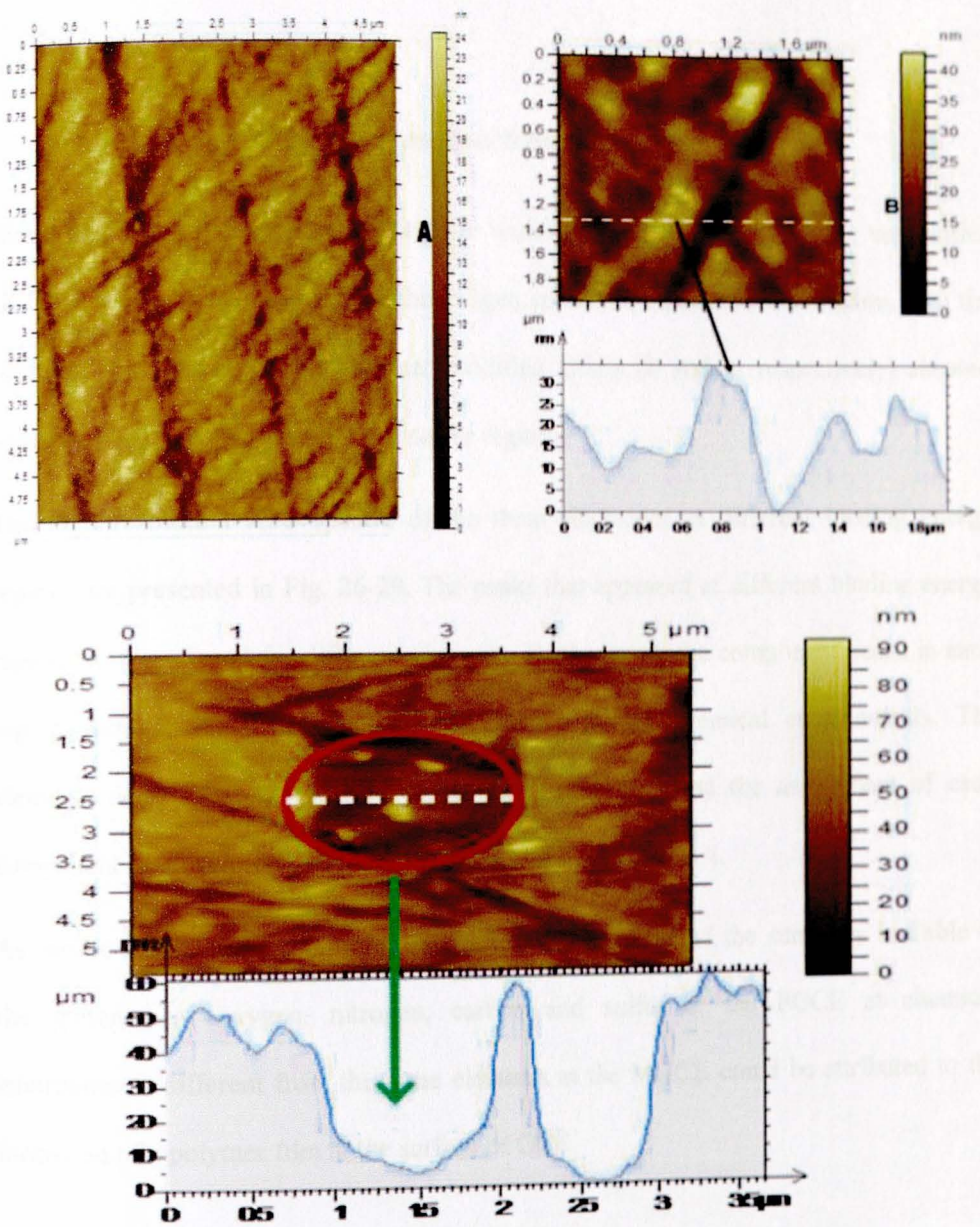

Fig. 24. AFM images of UGCE (A) and PGCE (B and C) with the corresponding cross sectional analysis along the dotted lines

4.1.5 X-ray photoelectron spectroscopy (XPS)

From the XPS survey spectra of the three working electrodes (Fig. 25), the unmodified GCE (a) showed response only in the oxygen and carbon characteristic regions. On the contrary, the monomer and polymer modified GCEs (b and c, respectively) showed additional peaks in the nitrogen and sulfur regions.

The high resolution XPS spectra of the three electrodes in different binding energy regions are presented in Fig. 26-29. The peaks that appeared at different binding energy regions were assigned for different elements. Furthermore, the component peaks in each region were assigned for the element under different chemical environments. The elements detected at the surface of each electrode type and the assignment of each component spectrum (peak) [162,163] is summarized in Table 4.

As can be observed from the high resolution XPS spectra and the summary in Table 4, the presence of oxygen, nitrogen, carbon and sulfur at the PGCE at chemical environments different from the same elements at the MGCE could be attributed to the formation of a polymer film at the surface of GCE.

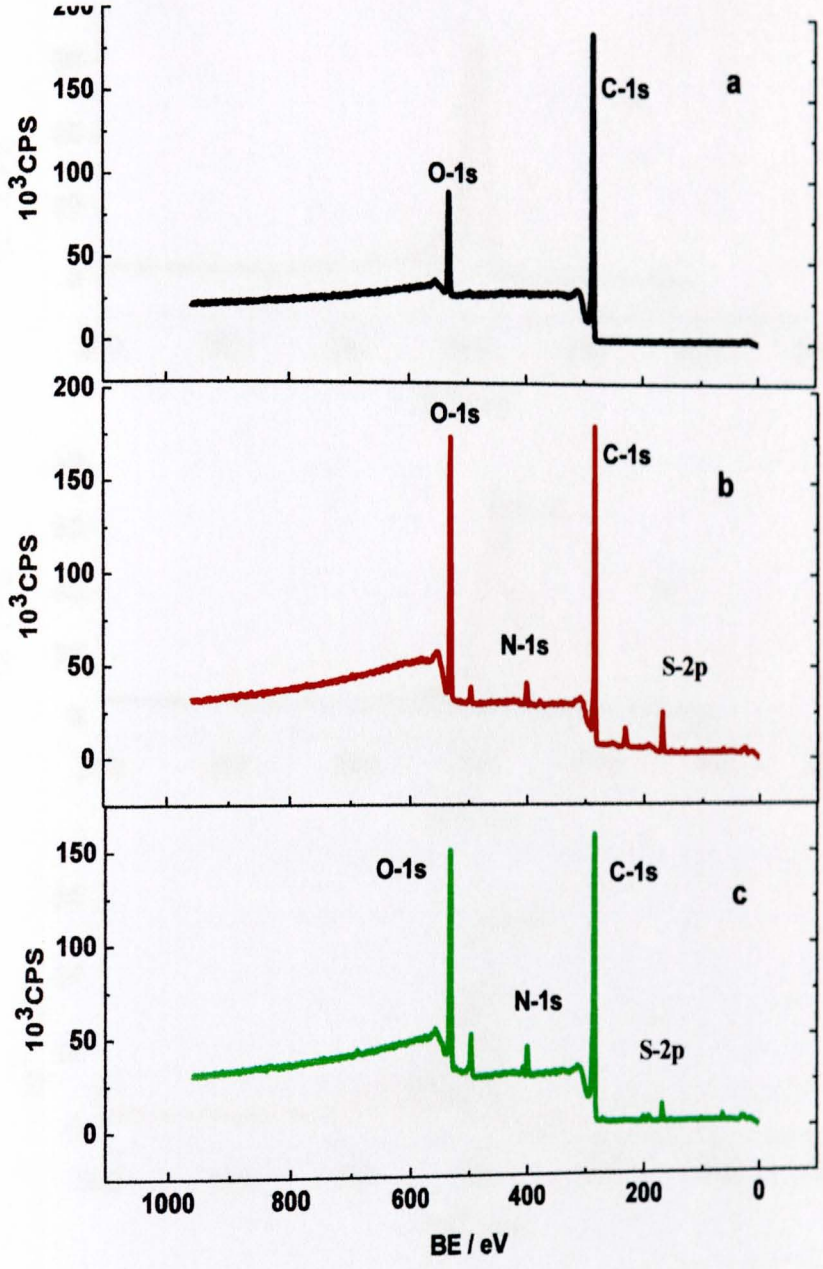

Fig. 25. Survey XPS spectra in the binding energy range 0 and 960 eV for (a) UGCE, (b) MGCE, and (c) PGCE at 75 eV Al radiation

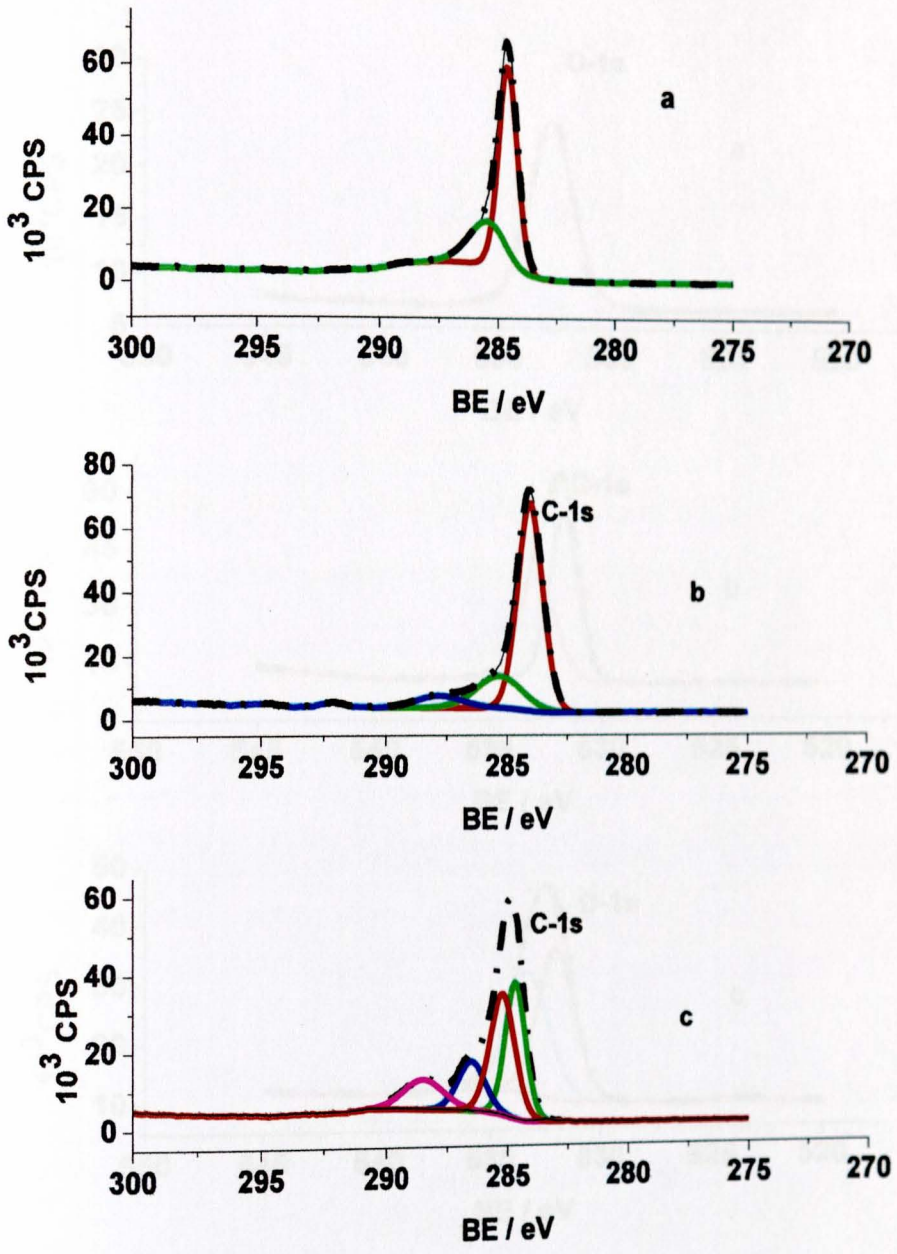

Fig. 26. XPS core spectra for (a) UGCE, (b) MGCE, and (c) PGCE in the carbon binding energy region (300-275 eV) (dash dot line: experimental and solid lines: least squares fit)

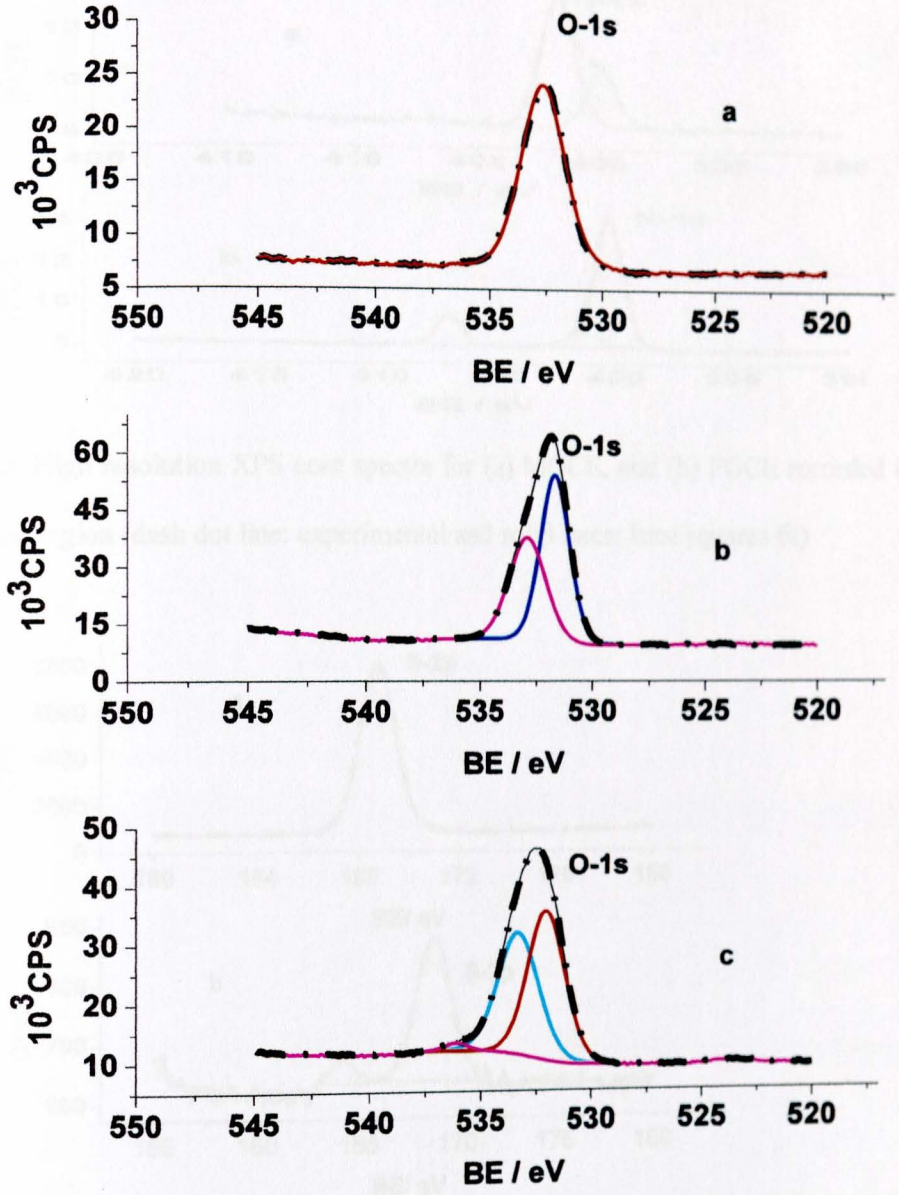

Fig. 27. High resolution XPS core spectra for (a) UGCE, (b) MGCE, and (c) PGCE recorded in the oxygen region (dash dot line: experimental and solid lines: least squares fit)

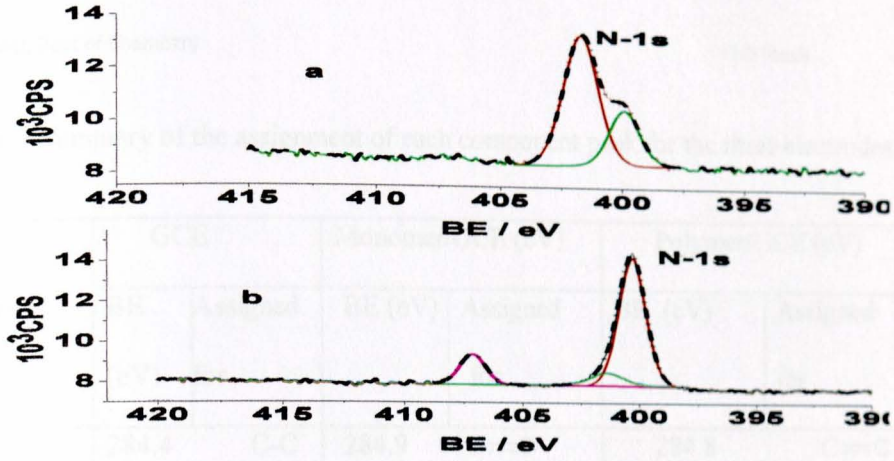

Fig. 28. High resolution XPS core spectra for (a) MGCE, and (b) PGCE recorded in the nitrogen region (dash dot line: experimental and solid lines: least squares fit)

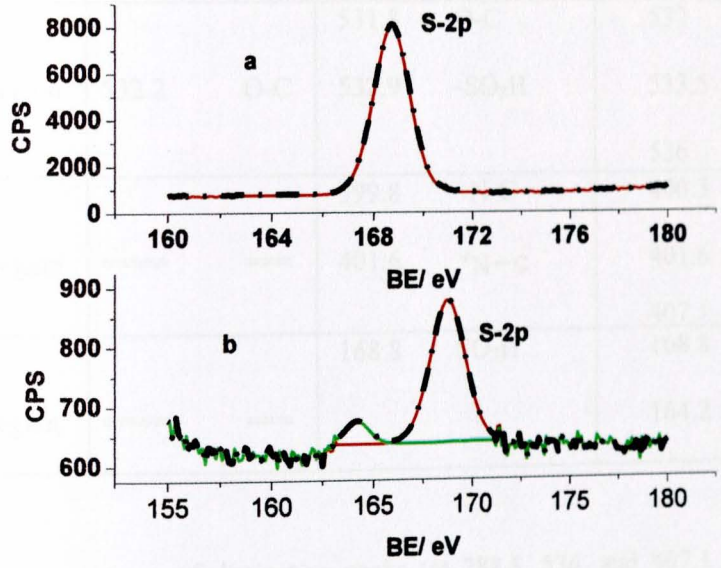

Fig. 29. High resolution XPS core spectra for (a) MGCE, and (b) PGCE recorded in the sulfur region (dash dot line: experimental and solid lines: least squares fit)

Table 4 Summary of the assignment of each component peak for the three electrodes

Region	GCE		Monomer/GCE (eV)		Polymer/GCE (eV)	
	BE (eV)	Assigned for	BE (eV)	Assigned for	BE (eV)	Assigned for
C-region	284.4 286.7	C-C C-O	284.9 285.5 286.7	C=C C-SO_3H C-N, C-O	284.8 285.4 286.3 288.5	C=C C-SO_3H C-N, C-O C=N, C=O
O-region	532.2	O-C	531.8 532.9	O-C -SO_3H	532 533.5 536	O-C SO_3H O=C
N-region	====	===	399.8 401.6	N-C $^{+}$N−C	400.3 401.6 407.1	N-C $^{+}$N−C N=C
S-region	====	===	168.8	SO_3H	168.8 164.2	SO_3H S-Auger

Hence, appearance of distinctive peaks (at 288.5, 536, and 407.1 eV) at the polymer modified GCE which are absent at the monomer modified GCE indicated the electropolymerization of AHNSA.

4.1.6 Conclusion

Potentiodynamic electropolymerization of AHNSA from aqueous solution of the monomer by scanning the potential between -0.8 and +2.0 V was evident. The observed dependence of peak current and peak potential of the polymer-modified electrode on scan rate showed the presence of an adsorbed substance possessing reversible redox couples. The EIS, SEM/DES, AFM, and XPS results are in agreement with the CV results, confirming the polymer modification of the electrode surface. The improved catalytic effect of the polymer-modified electrode towards methyl parathion also indicated the potential of the polymer modified glassy carbon electrode for its electrochemical sensor application.

4.2 Poly(AHNSA) modified glassy carbon electrodes for the electrochemical determination of selected alkaloids and pesticides

4.2.1 Ephedrine in human urine

4.2.1.1 Background

Ephedrine (scheme 4) has been used at therapeutic doses of 15–60 mg in the treatment of bronchial asthma, allergic states, catalepsy and myasthenia gravis, as a nasal decongestive, as an antidote for poisoning by central nervous system (CNS) depressants and in spinal anaesthesia [59,164]. It is a sympathomimetic drug that stimulates both α- and β-adrenergic receptors in the central nervous system [58,59]. It causes a rise of systolic and diastolic pressure, bronchodilation and mild stimulation of the CNS [164,165].

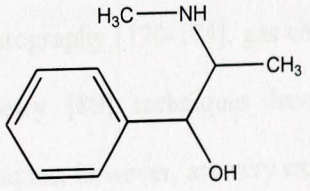

Scheme 4 Structural formula of ephedrine

The stimulant properties of ephedrine are well established and the alkaloid has been exploited in numerous over the counter (OTC) medicines [166]. Another problem that has arisen in recent years has been its potential of drug to impair driving ability [166-

168]. This concern is compounded by the exploitation of ephedrine's stimulant properties by transport workers, especially those involved in long distance routes, where they can be used to alleviate the effects of fatigue [167]. Ephedrine, which is characterized as a prohibited compound by the International Olympic Committee, is not only an ingredient of common anti-cold preparations but also of various nutritional supplements, athletes tested positive for ephedrine often claim to have received it while using products without indication[164]. The extensive use of this chemical is of great concern for the international athlete associations and has generated significant interest for development of methods for its rapid detection in health foods, pharmaceutical products and human fluids of athletes. The international Olympic committee and most international sports federations have put ephedrine on the list of prohibited substances and have adopted urinary threshold concentrations above which an athlete is regarded as positive. The threshold amount is 10 μg/ml of ephedrine in urine [169]. Therefore, fast, simple and reliable method for the quantitative determination of ephedrine in human urine is needed.

High performance liquid chromatography [170-174], gas chromatography [175] and gas chromatography-mass spectrometry [89] techniques have been used to determine ephedrine samples. These techniques, however, are very expensive, highly sophisticated and tedious which also need organic solvents for separation aggravating environmental pollution. Therefore, the determination of ephedrine in biological fluids and pharmaceutical preparations *via* a simple and reliable method is of great interest. Electrochemical methods have been of great interest due to several advantages, including high sensitivity, simplicity, rapid response and low cost [104]. However, there are few

reports on the application of electrochemical methods for the determination of ephedrine using modified electrodes [59,61,164,165].

Compared to metal electrodes, glassy carbon electrode (GCE) has been widely used due to its biocompatibility with tissue, low residual current over a wide potential range and minimal propensity to show deteriorated response as a result of electrode fouling [105-107]. Hence, in this work we report the use of poly-(4-amino-3-hydroxynaphthalene sulfonic acid) modified glassy carbon electrode for quantitative determination of ephedrine in human urine samples, which to our knowledge have not been communicated previously.

4.2.1.2 Electrocatalytic oxidation of EPH at the PGCE

Fig. 30a shows cyclic voltammograms of 1.0 mM EPH in pH 11.0 RBS at bare GCE. At UGCE, EPH is observed to undergo an irreversible oxidation reaction at 1.08 V vs. Ag/AgCl, which was consistent with reported references [59,164,168]. At the PGCE however, the same irreversible oxidative peak appeared at a potential of 0.83 V with an enhanced peak current (Fig. 30b) and lower peak potential. The peak current enhancement and peak potential shift to a lower oxidative potential observed indicated the electrocatalytic activity of the modified electrode surface towards oxidation of ephedrine.

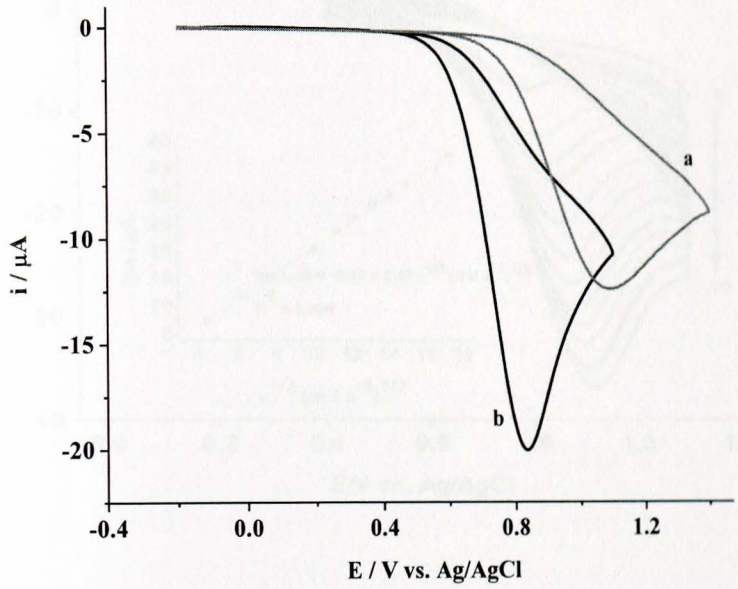

Fig. 30. Cyclic voltammograms of UGCE (a) and PGCE (b) in 1.0×10^{-3} mol L^{-1} ephedrine in pH 11.0 RBS. Scan rate: 0.1 V s^{-1}

4.2.1.3 Effect of scan rate

Fig. 31 depicts the cyclic voltammograms of the modified electrode in pH 11 RBS containing EPH at various scan rates. Linear dependence of the oxidative peak current on the square root of scan rate in the studied range indicated that the oxidation of EPH at the surface of polymer modified electrode is diffusion-controlled process (Inset of Fig. 31). The observed peak potential shift with scan rate also confirmed the irreversibility of the oxidation of EPH at PGCE.

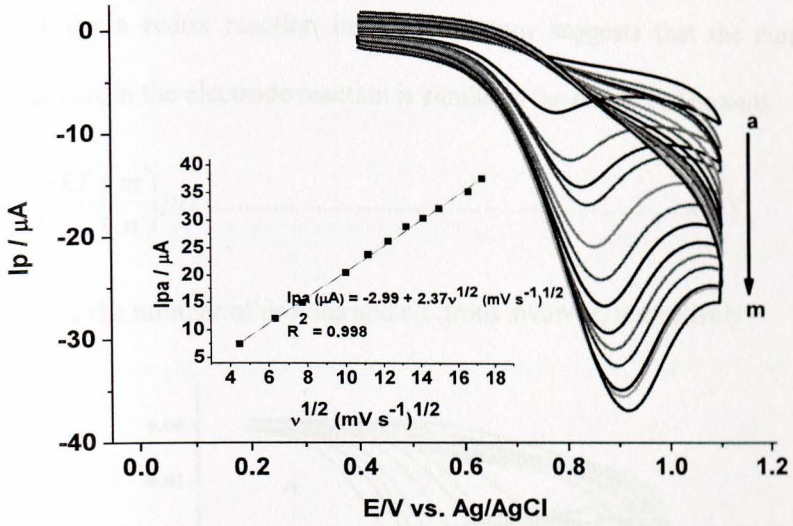

Fig. 31. Cyclic voltammograms of PGCE in 1.0×10^{-3} mol L^{-1} EPH (pH 11.0 RBS) at different scan rates (a-m: 20, 40, 60, 80, 100, 125, 150, 175, 200, 225, 250, 275 and 300 mV s^{-1}, respectively). Inset: Plot of anodic peak current vs. square root of scan rate

4.2.1.4 Effect of solution pH

Cyclic voltammograms of 1.0×10^{-3} M EPH in RBS of different pHs at poly(AHNSA) - modified GCE are shown in Fig. 32A. An increase in the pH of the solution (in the range of 7.5–11.5) caused peak potential shift in the negative direction indicating the involvement of protons in the reaction of EPH at the surface of the modified electrode. A linear correlation between the peak potential and solution pH was obtained (curve *a* of Fig. 32B) with a linear equation and correlation coefficient of Epa (V) = 1.526 – 0.068pH and $R^2 = 0.9942$, respectively. According to the Nernst equation (eqn. 22) [117], a slope

of 0.068 V/pH for a redox reaction involving protons suggests that the number of electrons taking part in the electrode reaction is similar to the number of protons.

$$E = E^{0'} + \frac{2.303RT}{F}\left(\frac{m}{n}\right)pH \quad \text{.....(22)}$$

where m and n are the number of protons and electrons involved, respectively.

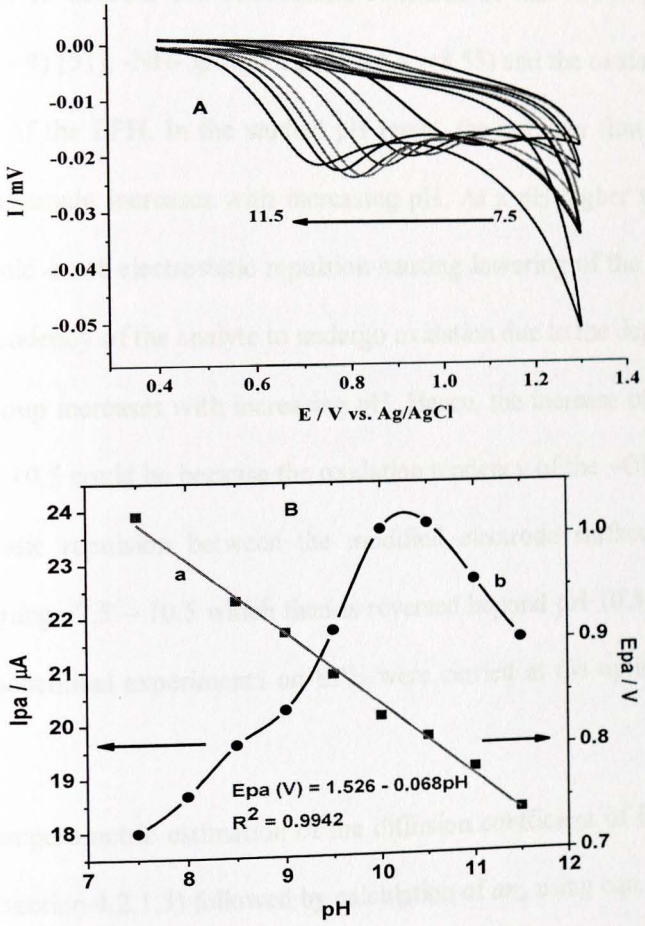

Fig. 32. (A) CVs of 1.0 × 10^{-3} M EPH at PGCE in different pHs (7.5 – 11.5) of RBS at a scan rate of 0.1 V s^{-1}. (B) Plot of peak current (a) and peak potential (b) versus the pH

Curve b of Fig. 32B depicts the dependence of peak current on the pH in the range 7.5 – 11.5. The anodic peak current increased sharply from pH 7.5 to 10.0 and then gradually to 10.5. At a pH higher that 10.5, it sharply decreased showing that pH 10.5 is the optimum pH of the buffer solution which has been used as the solution pH in the subsequent experiments. This dependence of peak current on pH could partly be explained taking in to account the dissociation constants of the $-SO_3H$ group of the modifier (pKa $\approx$ 3 – 4) [51], -NH- group of EPH (pKa $\approx$ 8.55) and the oxidative tendency of the –OH group of the EPH. In the studied pH range, the polymer film is negatively charged whose magnitude increases with increasing pH. At a pH higher than 8.55, the analyte species could exert electrostatic repulsion causing lowering of the peak current. Furthermore, the tendency of the analyte to undergo oxidation due to the deprotonation of –OH functional group increases with increasing pH. Hence, the increase of peak current in the range 7.5 to 10.5 could be because the oxidation tendency of the –OH is dominant over the electrostatic repulsion between the modified electrode surface and analyte species in the pH range 7.5 – 10.5 which then is reversed beyond pH 10.5. Thus, all the subsequent electrochemical experiments on EPH were carried at the optimum pH 10.5 unless stated.

After the Chronoamperometric estimation of the diffusion coefficient of EPH using the Cottrell equation (section 4.2.1.5) followed by calculation of αn_a using eqn. (12), the total number of electrons participated (n) was calculated from eqn. (9) to be 2. Thus, a reaction mechanism (scheme 5) that involves two electrons and two protons was thus proposed which is in agreement with previous reports.

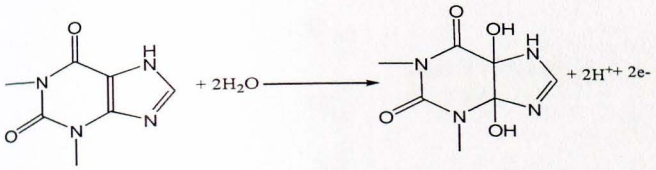

Scheme 5 Proposed reaction mechanism of EPH at PGCE

4.2.1.5 Chronoamperometric studies of EPH at PGCE

Amperometric method was also employed to study the catalytic oxidation of EPH at poly (AHNSA)-modified GCE. Amperometric experiments were carried out at an applied potential of +0.9 V (sufficient to oxidize EPH) for 20 s on different concentrations (100.0, 200.0 and 400.0 μM) of EPH in pH 10.5 RBS. Fig. 33 shows the experimental plots of current against time for different concentrations of EPH. The slopes of the best fits of the plots of I_{pa} vs. $(\text{time})^{-1/2}$ (Inset of Fig. 33) for each concentration were used to estimate the diffusion coefficient for EPH in the polymer film using the Cottrell equation: $I_{pa} = nFAD^{1/2}C^{*}/(\pi t)^{1/2}$ [176], where I_{pa}, n, F, A, D, C^{*} and t represent the anodic peak current (A), number of electrons transfer, Faraday's constant (C mol^{-1}), area of the electrode (cm^2), diffusion coefficient (cm^2 s^{-1}), initial concentration of EPH (mol cm^{-3}) and time (s), respectively. By taking the value of n as 2 and A as 0.0707 cm^2, we calculated the diffusion coefficient of EPH to be $7.011 \times 10^{-8} \pm 3.15 \times 10^{-11}$ cm^2 s^{-1}. As can be seen from the curves, the time needed to reach the minimum concentration is too short which indicated that the response of the polymer to EPH is rapid and hence the polymer can be used as an amperometric sensor of EPH.

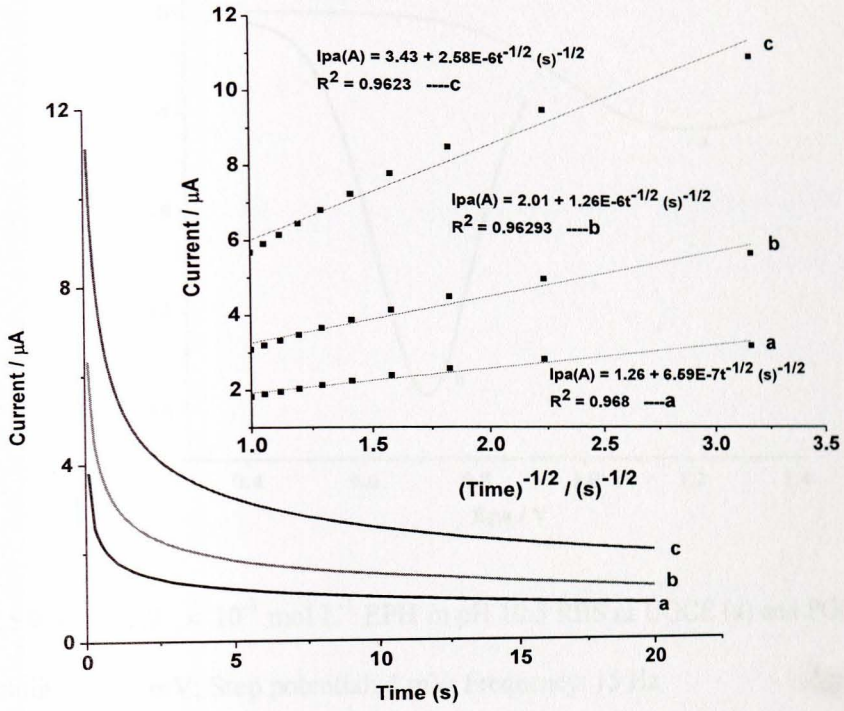

Fig. 33. i–t curves of PGCE in EPH (pH 10.5 RBS) of different concentrations (a-c: 100, 200 and 400 µM, respectively). Insets: I (A) vs. $(t)^{-1/2}$. Applied potential: 0.9 V; time: 20 s

4.2.1.6 Square wave voltammetry for quantitative analyses

Square wave voltammetry (SWV) has been used to study the applicability of poly(AHNSA)-modified GCE for the determination of EPH in human urine samples.

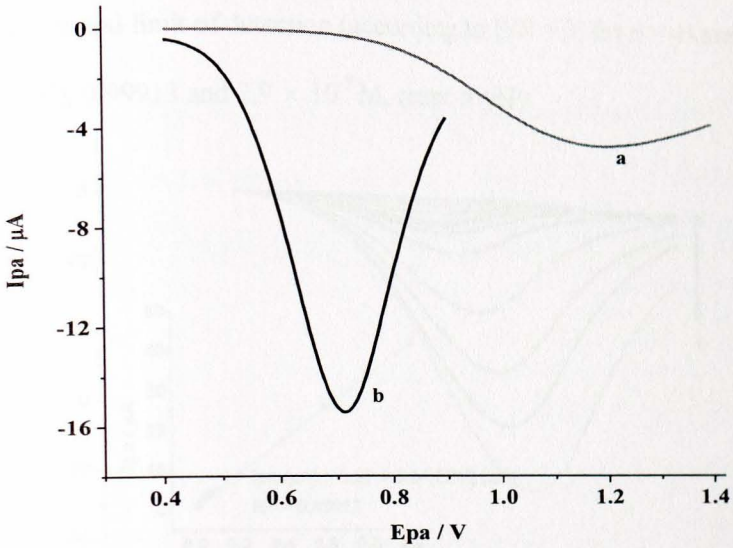

Fig. 34. SWVs of 1.0 × 10^{-3} mol L^{-1} EPH in pH 10.5 RBS at UGCE (a) and PGCE (b). Pulse amplitude: 50 mV; Step potential: 4 mV; Frequency: 15 Hz

Fig. 34 shows the SWVs of EPH at the UGCE (a) and PGCE (b). It can be observed that, the peak current response at the polymer-modified electrode is much more enhanced than at the unmodified GCE. The peak potential shift towards lower oxidative potential also verifies the electrocatalytic oxidation of EPH at the surface of the PGCE.

4.2.1.7 Linear range and Detection limit

Under the optimized pH (pH 10.5 RBS) and SWV parameters (potential step, pulse amplitude and frequency of 12 mV, 75 mV and 15 Hz, respectively), the square wave voltammograms for different concentrations of ephedrine are illustrated in Fig. 33. Inset of Fig. 35 depicts the linear dependence of anodic peak current on the concentration of EPH in a range of 8.0 × 10^{-6} to 1.0 × 10^{-3} mol L^{-1}. The linear regression equation, linear

regression coefficient and limit of detection (according to S/N = 3; for n = 4) are Ipa (μA) = 0.97 + 0.04C (μM), 0.99913 and 7.9×10^{-7} M, respectively.

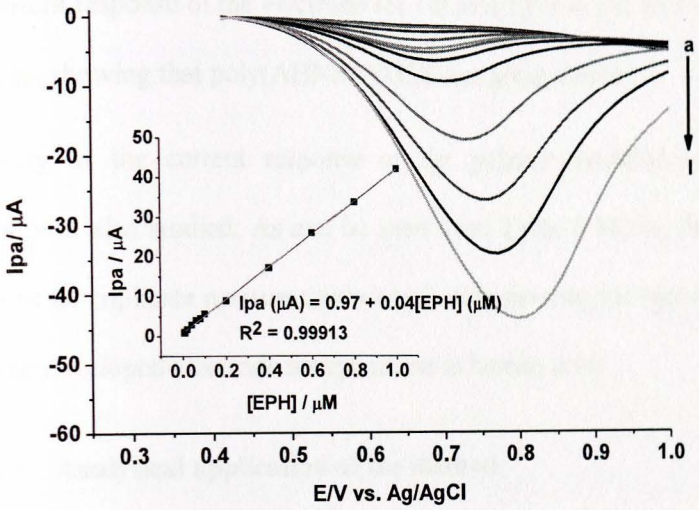

Fig. 35. SWVs of PGCE in pH 10.5 RBS with different concentrations of EPH (a-l: 8, 10, 20, 40, 60, 80, 100, 200, 400, 600, 800 and 1000 μM, respectively). Inset: Plot of oxidative peak current versus concentration of EPH. Step potential: 12 mV; pulse amplitude: 75 mV; frequency: 15 Hz

The peak potential shift towards higher oxidation potentials observed with increasing concentration (Fig. 35) could be attributed to the increased overpotential due to the adsorbed oxidation products of the reaction.

4.2.1.8 Stability and reproducibility studies

The stability of poly(AHNSA)/GCE was examined. After keeping it in refrigerator for one week, the current response of the electrode for 1.0 mM EPH in pH 10.5 RBS did not remarkably change, showing that poly(AHNSA)/GCE has good stability.

The reproducibility of the current response of the polymer-modified electrode for ephedrine sample was also studied. As can be seen from Table 5 below, the maximum R.S.D(%) recorded for triplicate measurements was 2.11% showing the reproducibility of the response of the developed electrode for ephedrine in human urine

4.2.1.9 Analytical application of the method

The utility of the proposed square wave voltammetric method using the polymer modified electrode for the determination of ephedrine in human urine was investigated. Known concentrations (80, 100 and 200 μM) of ephedrine in urine samples were prepared using the filtered and unfiltered human urine (1:5 diluted with pH 10.5 RBS). Square wave voltammetry under the optimized parameters was employed to determine the anodic current response for the urine samples at poly(AHNSA)/GCE and the results are summarized in Table 5. As can be seen from the Table, recoveries in the range 92.06-93.15% from the filtered and 81.15-86.3% from the unfiltered human urine showing the applicability of the proposed method for the determination of EPH in human urine samples. Lower recoveries from the unfiltered human urine may be ascribed to the fouling effect of the urine matrices. The significantly low R.S.D (%) values indicated the reproducibility of the developed modifier.

Table 5 Percentage recovery of EPH from human urine samples

[EPH] (μM)	Filtered urine sample				Unfiltered urine sample			
	Added (mg)	Detected* (mg)	Recovery (%)	R.S.D (%)	Added (mg)	Detected* (mg)	Recovery (%)	R.S.D (%)
80	16	14.73	92.06	1.49	16	13.20	82.50	2.11
100	20	18.63	93.15	1.07	20	16.23	81.15	1.87
200	40	37.12	92.8	1.90	40	34.52	86.30	1.98

* Average of triplicate measurements using one modified electrode

4.2.1.10 Conclusion

The approach taken in this work provides a simple method to detect ephedrine using an environmentally friendly electrode-modifier. Using the developed method, a wide linear response up to 8.0 μM and a low limit of detection of 7.9×10^{-7} M, which is well below the current acceptable threshold limit by the International Olympic Committee for this alkaloid in athlete urine, was achieved. Good recoveries of EPH in human urine prior to filtration showed the potential applicability of the developed method for the direct determination of EPH in environmental samples.

4.2.2 Theophylline in pharmaceutical formulations

4.2.2.1 Background

The N-methyl derivatives of xanthine (Table 6), including theophylline (3,7-dihydro-1,3-dimethyl-1H-purine- 2,6-dione), theobromine (3,7-dihydro-3,7-dimethyl- 1H-purine-2,6-dione), and caffeine (3,7-dihydro-1,3,7-trimethyl- 1H-purine-2,6-dione), are alkaloids that are widely distributed in plant products and beverages and are known to have many physiological effects, such as gastric acid secretion, diuresis, and stimulation of the central nervous system. They have also been implicated in various disorders including heart disease, carcinogenesis, kidney malfunction, and asthma [62,65,177].

Table 6 Structure of xanthine and its naturally occurring N-methyl derivatives

Structure	R_1	R_2	R_3	Compound
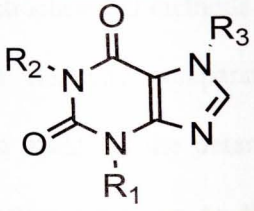	H	H	H	Xanthine
	CH_3	CH_3	H	Theophylline
	CH_3	H	CH_3	Theobromine
	CH_3	CH_3	CH_3	Caffeine

Theophylline (3,7-dihydro-1,3-dimethyl-1H-purine-2,6-dione) as one of the xanthine-based alkaloids, has a stimulating effect on respiration and is widely used as a bronchodilator for the treatment of bronchial asthma and neonatal apnea [178-180]. Owing to the toxicity of theophylline and the variations in metabolism between individuals, the most accepted range of effective plasma theophylline concentrations in

adults is between 5 and 20 μg mL^{-1} [180-182]. Levels below this range are usually non-therapeutic, while higher levels may cause serious toxicity. Excessive administration of theophylline occasionally produces serious toxicity, including vomiting, tachycardia, seizures and central nervous system excitation [62,179,180].

The interest in monitoring the levels of TP in plasma has led to the development of a variety of methods, such as high performance liquid chromatography (HPLC) [183-186], electrokinetic capillary chromatography [62,187], capillary electrophoresis [188], liquid chromatography [178], liquid chromatography–mass spectrometry [180], gas chromatography [185], spectrophotometry [182,186,189] and differential-derivative spectroscopy [190]. Many of the above methods often require tedious extraction procedures employing organic solvents which pollute the environment and some requiring derivatization procedure before determination.

Electrochemical methods have been of great interest due to several advantages, including high sensitivity, comparative simplicity, rapid response and low cost [104]. Efforts have been made on the determination of theophylline using electrochemical methods and detection limits up to the order of 10^{-8} mol L^{-1} have been reported [179,191-194]. However, the fabrication processes of most of the above listed electrodes are rather complicated and the surface renewing is not convenient.

Compared to metal electrodes, the glassy carbon electrode (GCE) has been widely used, due to its biocompatibility with tissue, low residual current over a wide potential range and minimal propensity to show deteriorated response as a result of electrode fouling

[105-107]. Hence, the purpose of this work is to develop an alternative; selective, sensitive, simple, environmentally friendly and easily fabricated modified electrode for the electrochemical determination of TP. Here we report an electrochemical method for the determination of TP at poly(AHNSA)-modified glassy carbon electrode.

4.2.2.2 Electrochemical behavior of TP at PGCE

Fig. 36 shows the cyclic voltammograms of 1.0×10^{-3} M TP in pH 5.0 PBS, at UGCE (a) and PGCE (b). The electrochemical oxidation process revealed one broad and poor anodic peak centered at about +1.37 V vs. SCE at the bare GCE. Under similar conditions, a sharp peak at +1.22 V has been observed at the poly(AHNSA) modified GCE. The oxidation process of TP both at the bare and modified electrodes is irreversible. The potential shift towards negative direction accompanied by the remarkable peak current enhancement at the polymer-modified GCE are clear evidences for the catalytic effect of the poly(AHNSA) modified GCE towards TP oxidation. The catalytic effect of the polymer modified surface may be attributed partly to the increased effective surface area of the poly(AHNSA) modified GCE and partly to the pH dependent affinity of TPH^+ (protonated TP in acidic medium) for the negatively charged sulfonic group in the modifier structure.

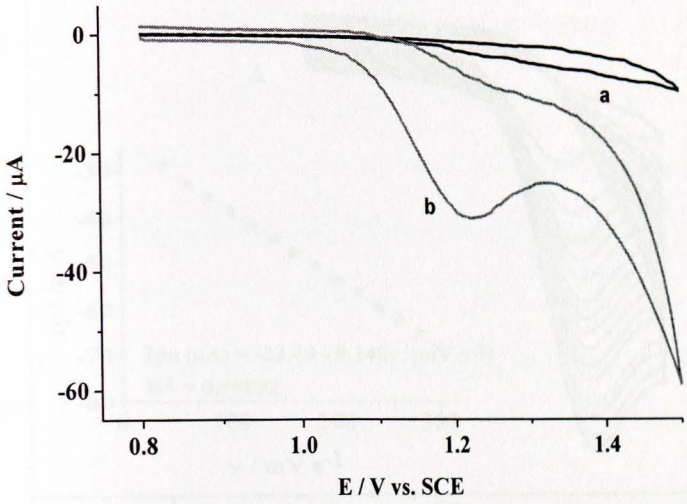

Fig. 36. CVs of UGCE (a) and PGCE (b) for 1.0 mM TP in PBS (pH 5.0) at 100 mV s^{-1}

The effect of scan rate on the oxidation peak potential (E_{pa}) and, current (I_{pa}) of TP at poly(AHNSA) modified GCE was studied using cyclic voltammetry. Fig. 37A reveals the CVs of 1 × 10^{-3} mol L^{-1} of TP in pH 5.0 PBS at scan rates ranging between 20 and 300 mV s^{-1}. The peak current (I_{pa}) of TP showed linear dependence on the scan rate (ν) in the studied range (Inset of Fig. 37A) with a correlation coefficient of 0.99892 indicating an adsorption-controlled behavior during the electrode reaction [195]. The electrode reaction was irreversible as depicted from the lack of a reduction peak in the cyclic voltammograms (Fig. 37). This was also further confirmed by the potential (E_{pa}) shift to more positive values with increasing ν (Fig. 37A). Since the reaction is surface-adsorbed irreversible, the number of electrons participated (n) and transfer coefficient (α) values were calculated using eqns. 7, 10 and 11) to be 2 and 0.43, respectively [196].

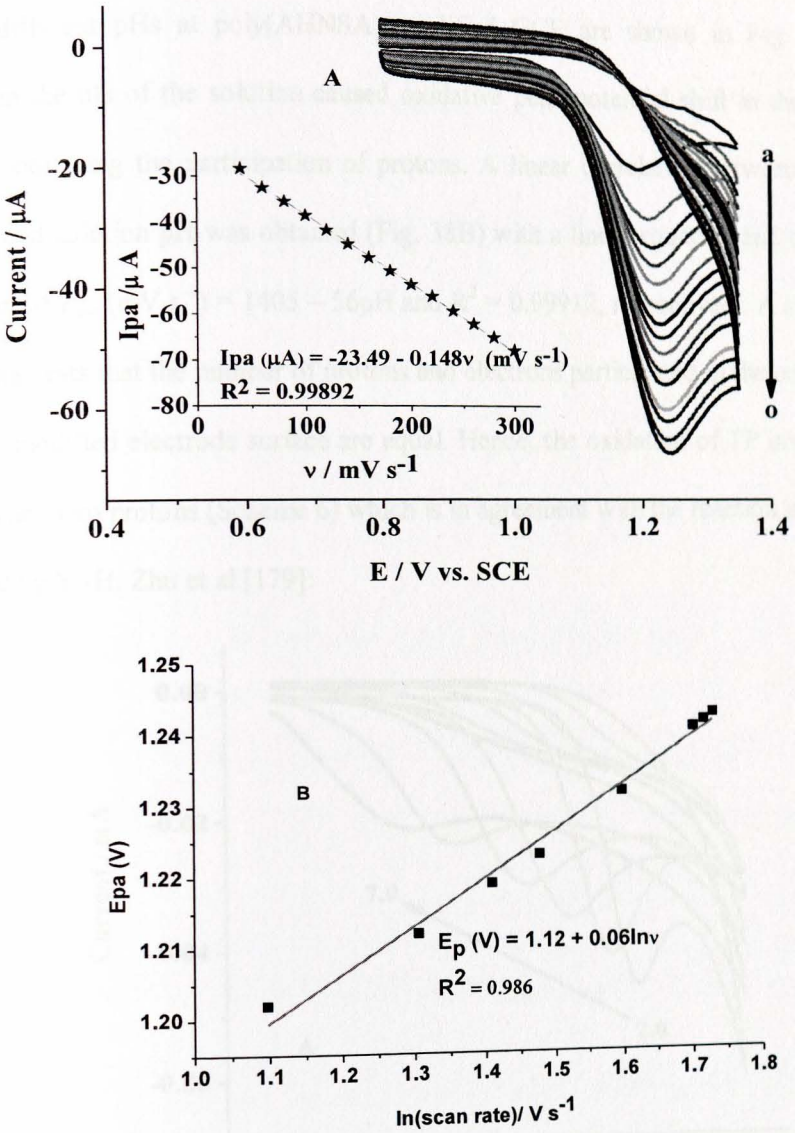

Fig. 37. (A) CVs of the PGCE in PBS (pH 5.0) containing 1.0×10^{-3} M of TP at various scan rates (a-o: 20, 40, 60, 80, 100, 120, 140, 160, 180, 200, 220, 240, 260, 280, and 300 mV s^{-1}, respectively). Inset: plot of peak current vs. scan rates. (B) plot of E_{pa} vs. lnv

The effect of solution pH on peak potential and peak current of TP at the polymer-modified electrode was also investigated. Cyclic voltammograms of 1.0×10^{-3} M TP in

PBS of different pHs at poly(AHNSA) modified GCE are shown in Fig. 38A. An increase in the pH of the solution caused oxidative peak potential shift in the negative direction indicating the participation of protons. A linear correlation between the peak potential and solution pH was obtained (Fig. 38B) with a linear equation and correlation coefficient of E_{pa} (mV s^{-1}) = 1405 – 56pH and R^2 = 0.99912, respectively. A slope of 56 mV/pH suggests that the number of protons and electrons participated in the oxidation of TP at the modified electrode surface are equal. Hence, the oxidation of TP involves two electrons and two protons (Scheme 6) which is in agreement with the reaction mechanism suggested by Y.-H. Zhu et al [179]:

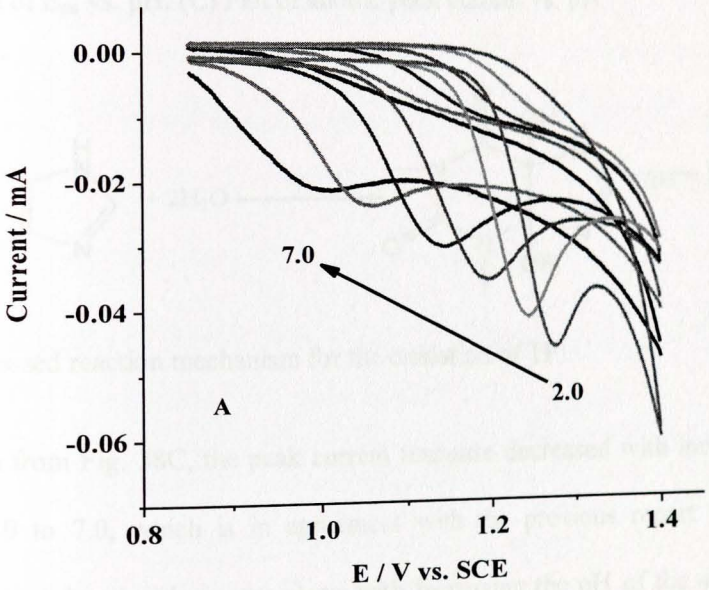

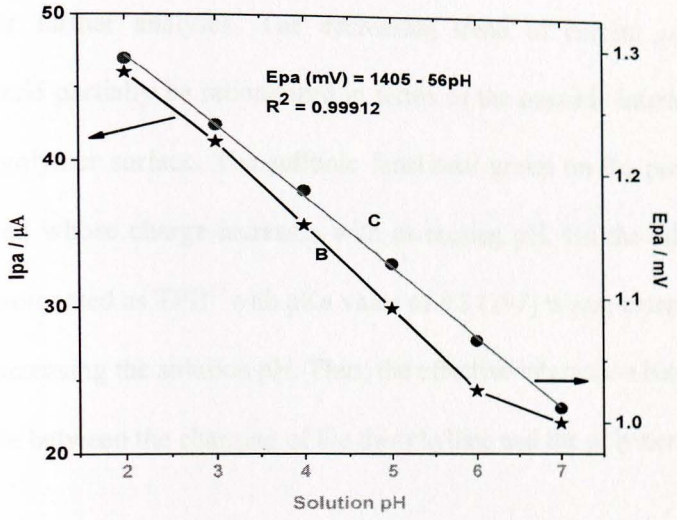

Fig. 38. (A) CVs of 1.0×10^{-3} M TP at PGCE in different pHs (2.0 - 7.0) of PBS at 100 mV s^{-1}. (B) plot of E_{pa} vs. pH. (C) Plot of anodic peak current vs. pH

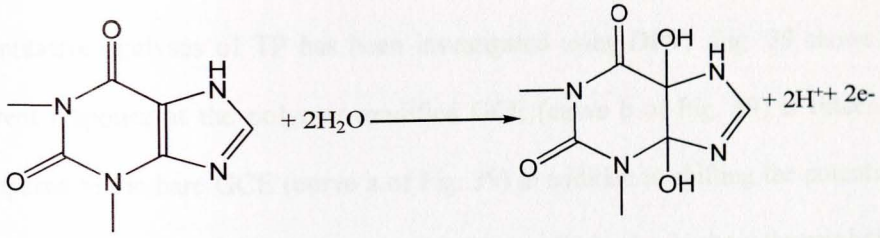

Scheme 6 Proposed reaction mechanism for the oxidation of TP

As can be seen from Fig. 38C, the peak current response decreased with increasing pH values from 2.0 to 7.0, which is in agreement with the previous report [191]. The sharpness of the peaks also decreases along with increasing the pH of the solution. As seen in Fig. 38A, it is at pH 2.0 where maximum current is obtained. However, this voltammogram suffers from poor back ground current. The one at pH 3.0 showed the next maximum current with lower back ground current effect and hence was taken as the

preferred pH for further analyses. The decreasing trend of current response with increasing pH could partially be rationalized in terms of the possible interactions of the analyte and the polymer surface. The sulfonic functional group on the polymer film is negatively charged whose charge increases with increasing pH. On the other hand, the theophylline is protonated as TPH^+ with pKa value of 8.8 [197] whose extent of charging decreases with increasing the solution pH. Thus, the effective interaction between the two is the compromise between the charging of the theophylline and the polymer.

4.2.2.3 Optimization of Technique parameters

For DPV has a much higher current sensitivity and better resolution than cyclic voltammetry [186], the application of the poly(AHNSA) modified GCE for the quantitative analyses of TP has been investigated using DPV. Fig. 39 shows that the current response at the polymer modified GCE (curve b of Fig. 39) is fifteen fold as compared to the bare GCE (curve a of Fig. 39) in addition to shifting the potential to the negative direction from 1370 to 1160 mV. These effects clearly show the catalytic roll of the polymer film modified electrode towards oxidation of TP.

Since the oxidation of TP at the modified electrode was found to be adsorption-controlled, the effects of accumulation potential (E_{acc}) and accumulation time (t_{acc}) on the current response of the modified electrode for 1×10^{-3} mol L^{-1} TP (pH 3.0 PBS) were also investigated. Fig. 40A shows the influence of the accumulation potential on the peak current. The current increases as the potential is varied in the positive direction and reaches maximum at a potential of +50 mV beyond which, the current response

decreases. Thus, +50 mV was selected as the optimum preconcentration potential for accumulating TP on poly(AHNSA) modified GCE. The optimized accumulation potential is too low relative to the oxidation potential of PT at the polymer modified electrode. This could happen because the potential is strong enough to cause the adsorption of the analyte without causing its oxidation.

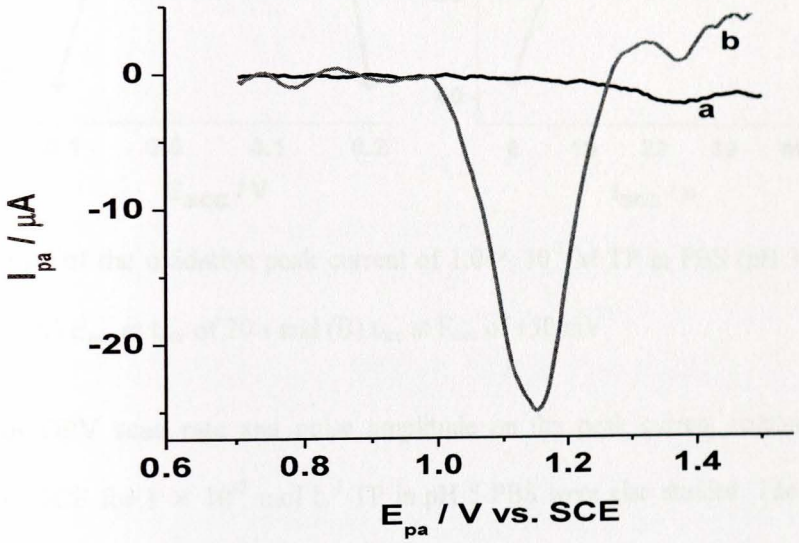

Fig. 39. DPVs of 1.0 mM TP in pH 3 PBS at UGCE (a) and PGCE (b)

Moreover, the peak current increases as the pre-concentration time increase up to 30 s and then begin to decline (Fig. 40B). Thus, 30 s was taken as the optimum pre-concentration time.

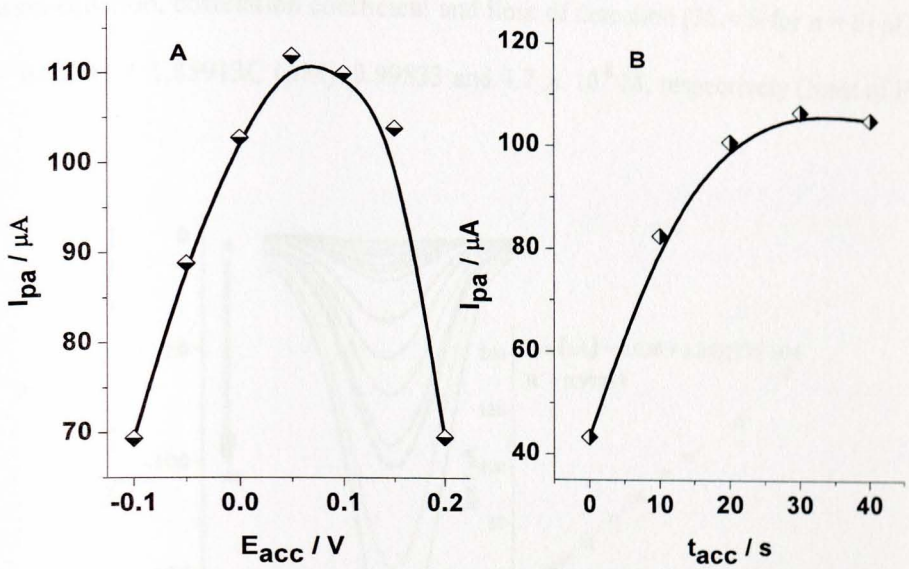

Fig. 40. (A) Plot of the oxidative peak current of 1.0×10^{-3} M TP in PBS (pH 3.0) at PGCE versus: (A) E_{acc} at t_{acc} of 20 s and (B) t_{acc} at E_{acc} of +50 mV

The effects of DPV scan rate and pulse amplitude on the peak current response of poly(AHNSA)/GCE for 1×10^{-3} mol L^{-1} TP in pH 5 PBS were also studied. The DPV scan rate and pulse amplitude that give maximum peak current response were 60 mV s^{-1} and 100 mV, respectively.

4.2.2.4 Linear range and detection limit

In order to evaluate the feasibility of the explored method for the quantitative analyses of TP, the relationship between the oxidative peak current and the concentration of TP was studied using DPV. Under the optimized solution and method parameters, the DPVs of variable concentrations of TP are presented in Fig. 41. The current response was linearly related to concentration in the range 1.0×10^{-6}–1.0×10^{-4} mol L^{-1} with a linear

regression equation, correlation coefficient and limit of detection (3δ = S for n = 6) of I_{pa} (μA) = 0.03043 + 1.85913C (μM), 0.99833 and 4.7×10^{-8} M, respectively (Inset of Fig. 39).

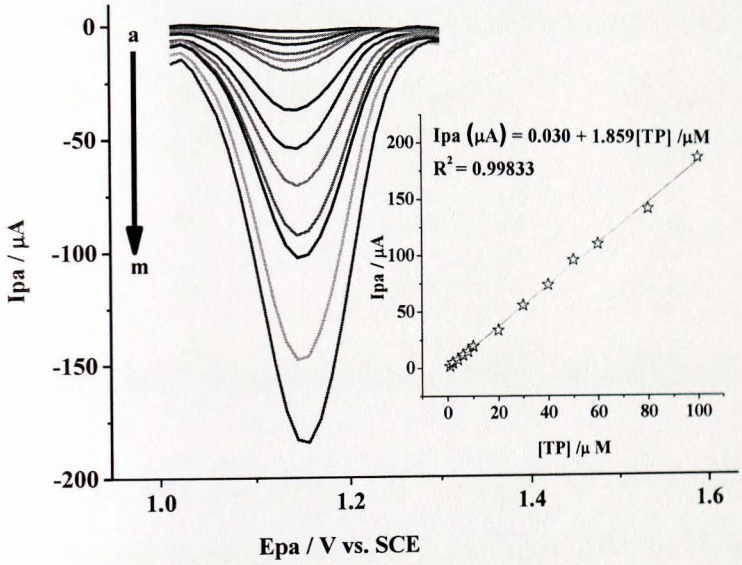

Fig. 41. DPVs of PGCE in PBS (pH 3.0) for different concentrations of TP (a-m: 1, 2, 4, 6, 8, 10, 20, 30, 40, 50, 60, 80 and 100 μM, respectively) at the optimized parameters. Inset: Plot of peak currents (I_{pa}) versus concentration of TP

4.2.2.5 Analytical Application

The applicability of the developed method for the determination of theophylline in real samples was investigated. The developed modified electrode was also used for the determination of TP in tablet formulations collected from two local pharmaceuticals manufacturing factories: Addis pharmaceuticals factory (APF) and Ethiopian pharmaceuticals factory (EPF). The differential pulse voltammograms for 10 and 20 μM

samples from both factories were recorded and the results are summarized in Table 7. As can be seen from the Table, the results for the sample collected from the EPF are in good agreement with the marked content (120 mg per tablet).

Table 7 Determination of TP in drug samples from two local pharmaceutical factories

Tablet sample	TP added **[a]** (μM)	TP found **[b]** (μM)	Recovery (%)
APF	10	6.29 ± 0.059	62.90
	20	15.56 ± 0.265	77.80
EPF	10	9.15 ± 0.271	91.49
	20	18.36 ± 0.262	91.78

[a] Concentration as per the drug label (120 mg per tablet), **[b]** Mean of triplicate

Recovery experiments were also carried out to evaluate the matrix effect on the determination of TP at our electrode. The recoveries for 0.018 and 0.036 mg standard TP from spiked theophylline drug samples are summarized in Table 8. Excellent recoveries in the range 96.11–97.78% indicate that the poly(AHNSA) modified GCE has a great potential for the determination of TP in pharmaceutical samples.

Table 8 Recovery of TP from pharmaceutical (EPF) tablet solutions

Sample code	TP in drug sample (mg)	Spiked TP(mg)	Found**[a]** (mg)	Recovery**[b]** (%)	R.S.D.**[c]** (%)
A	0.018	0.018	0.0356	97.78	3.2
B	0.018	0.036	0.0526	96.11	1.4

Mean of triplicate [a]measurements, [b] recoveries and [c] RSD of recoveries

4.2.2.6 Comparison with other methods

Finally, the voltammetric determination of TP in this study is compared with other methods and is summarized in Table 9. It can be seen that the electrochemical sensor based on poly(AHNSA) modified GCE provides a comparable analytical performance and lower detection limit than most of the reported modified electrode. Furthermore, the poly(AHNSA) modified GCE offers easy modification with controlled film thickness and rapid electrode preparation compared to the other modified electrodes reported.

Table 9 Comparison between previously reported methods and this work

Electrode	Linear range (mol L^{-1})	LoD (mol L^{-1})	Method	Ref.
MWNT/GCE	3×10^{-7} to 1×10^{-5}	5×10^{-8}	CV	178
Boron-doped diamond	1 to 400×10^{-6}	----------	LSV	190
Nafion®/lead–ruthenium oxide pyrochlore/GCE	0 to 100×10^{-6}	1×10^{-7}	SWV	192
Phthalocyanine Particles Modified CPE	4×10^{-7} to 1.0×10^{-4}	1.4×10^{-7}	DPV	193
Poly (AHNSA)/GCE	1×10^{-6} to 1×10^{-4}	4.7×10^{-8}	DPV	This work

4.2.2.7 Conclusion

The modified electrode showed notable electrocatalytic activity towards the oxidation of TP. The anodic peak current of TP at the polymer modified electrode was directly proportional to its concentration in the range 1.0×10^{-6} mol L^{-1} to 100×10^{-6} mol L^{-1}. A lower detection limit for TP in our work signified the potential applicability of our method for the determination of TP in real samples.

4.2.3 Caffeine in coffee extract

4.2.3.1 Background

Caffeine (1,3,7-trimethylxanthine) (scheme 7) is a naturally occurring alkaloid that is widely found in plant products and beverages. It is a natural stimulant contained in coffee, tea, chocolate, soft drinks and can also be purchased in capsules or tablets for the treatment of asthma, nasal congestion, headache or to improve athletic endurance and facilitate weight loss [198]. Almost half of the caffeine consumers ingest caffeine from multiple sources [199,200], the caffeine content of which varies with the type of source [201-203].

In human and animal studies, caffeine produces mental and behavioral effects that are similar to those of typical psychomotor stimulant drugs (e.g., amphetamine and cocaine) [204]. Stimulation of the central nervous system, diuresis and gastric acid secretion are the most studied physiological effects caused by caffeine [198]. Habitual coffee and tea drinkers also experience increase in blood pressure when consuming caffeine at the doses found in the commonly consumed beverages; tea, coffee, cola soft-drinks and energy drinks as well as in many pharmaceuticals [205]. Since the caffeine content in coffee is the highest of the common sources [202], a sensitive, fast, selective and inexpensive analytical method for determining caffeine in coffee is highly needed.

Many methods, including high performance liquid chromatography [206], capillary chromatography [207], capillary electrophoresis [208], spectroscopy [209,210] and liquid chromatography-tandem mass spectroscopy [211] have been reported for the

determination of caffeine in coffee, tea and cola beverages. Usually, these methods demand expensive apparatus, highly skilled technicians, complicated and time-consuming procedures. Compared to these conventional analytical methods, electroanalytical methods are rapid, convenient, of low-cost and environmental-friendly [212].

Among the electroanalytical methods recently reported for the determination of caffeine [213-221], a single work using poly(safranine)/GCE was published based on electropolymerized polymer-modified electrode [221] which could be because of the high interfering back ground current at its oxidative potential [214].

Hence, we planned to develop a polymer-modified electrode that lowers the oxidation potential of caffeine for its determination without a significant influence from background current. To the best of our knowledge, the use of poly(AHNSA) modified GCE for the electroanalytical detection of caffeine is not reported. Hence, we report the application of poly(AHNSA) modified GCE for the determination of caffeine in coffee.

Scheme 7 The chemical structure of caffeine

4.2.3.2 Electrochemical behavior of caffeine

The electrochemical behavior of caffeine at the polymer modified electrode was investigated using cyclic voltammetry. Fig. 42 shows the CVs of bare GCE (curve a) and

poly(AHNSA) modified GCE (curve b) in pH 5.0 ABS containing 1×10^{-3} mol L^{-1} of caffeine recorded under similar conditions. At the bare GCE, caffeine exhibited a poor and irreversible oxidative peak centered at about +1.60 V (curve a). But at the polymer modified electrode (curve b), a well-defined, irreversible anodic peak with an enhanced peak current was observed at +1.45 V. This could be ascribed to the selective preferential accumulation of caffeine on surface bound functionalities of the polymer modified electrode [222]. The potential shift to a lower positive potential along with current enhancement at the modified electrode relative to the unmodified electrode indicate the catalytic oxidation of caffeine at the polymer modified electrode.

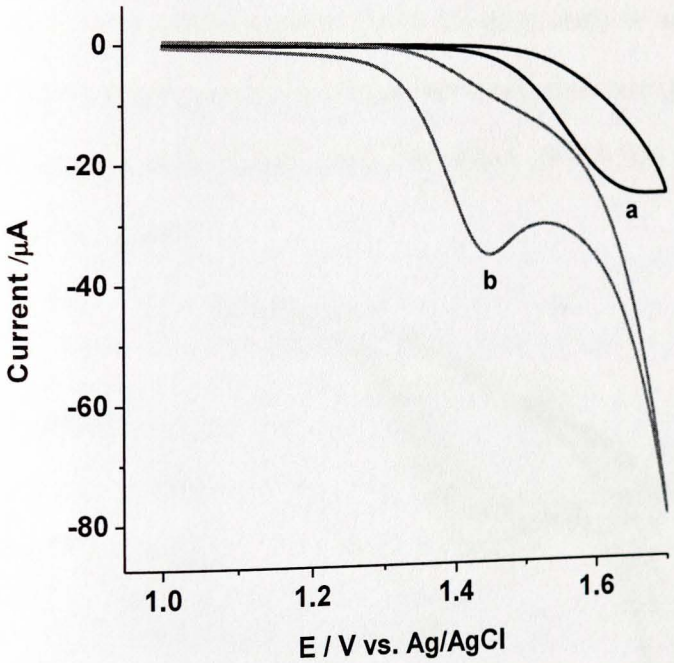

Fig. 42. Cyclic voltammograms of UGCE (a) and PGCE (b) in pH 5 ABS containing 1.0 $\times 10^{-3}$ mol L^{-1} caffeine at 0.1 V s^{-1}

4.2.3.3 Effect of pH and scan rate

The effect of pH on the peak current and peak potential of caffeine was investigated in the pH range 3.0 to 6.0 ABS (Fig. 43A). The peak potential shifted negatively with increasing pH indicating the participation of protons in the reaction. Plot of peak potentials *versus* pH was found to be linear over the pH range 3.0-5.0 with a slope of 48.4/pH and correlation coefficient of $R^2 = 0.99809$ (Inset of Fig. 43A), corresponding to a mechanism involving protons and electrons in a 1:1 ratio [223]. It was also observed that the peak current of caffeine at the poly(AHNSA)/GCE increased with increase in pH from 3.0 to 5.0 and then started to decrease for pH values higher than 5.0 (Inset of Fig. 43B). The increase in peak current from pH 3.0 to 5.0 could partly be ascribed to the increasing electrostatic attraction between the polymer modified surface ($pKa \approx 4$) [51] and the positively charged caffeine (pKa 10.4) [93]. Hence, pH 5.0 was chosen as the optimum pH for further analyses.

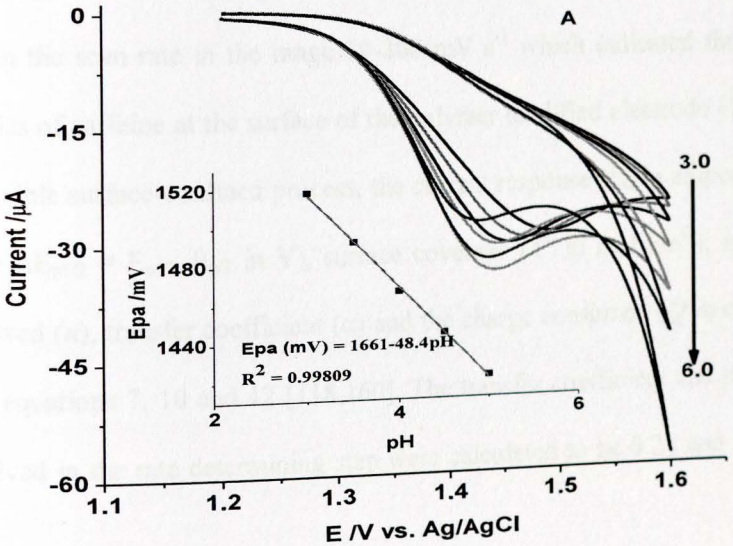

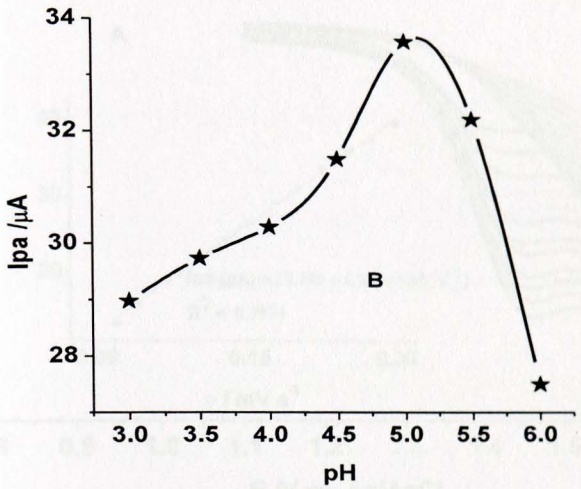

Fig. 43. (A) CVs of PGCE in ABS of different pHs (3.0 to 6.0) containing 1.0×10^{-3} mol L^{-1} of caffeine. Inset: plot of anodic peak potential versus pH of buffer solution. (B) Plot of Ipa versus pH in pH range 3.0 to 6.0 at 0.1 V s^{-1}

The effect of scan rate on the oxidative peak current of 1×10^{-3} mol L^{-1} caffeine at PGCE in pH 5 ABS was also studied. Fig. 44A shows the CVs at different scan rates in the range 20 to 300 mV s^{-1}. Inset of Fig. 44A depicts the linear dependence of the anodic peak current on the scan rate in the range 20-300 mV s^{-1} which indicated the surface-confined kinetics of caffeine at the surface of the polymer modified electrode [159]. For such an irreversible surface-confined process, the current response (I_{pa} in amperes), peak current (where $\Delta E_{p1/2} = E_p - E_{p/2}$ in V), surface coverage (Γ in mol cm^{-2}), number of electrons involved (n), transfer coefficient (α) and the charge consumed (Q in coulombs) are related by equations 7, 10 and 12 [118,160]. The transfer coefficient and number of electrons involved in the rate determining step were calculated to be 0.23 and 3.8 (≈ 4), respectively.

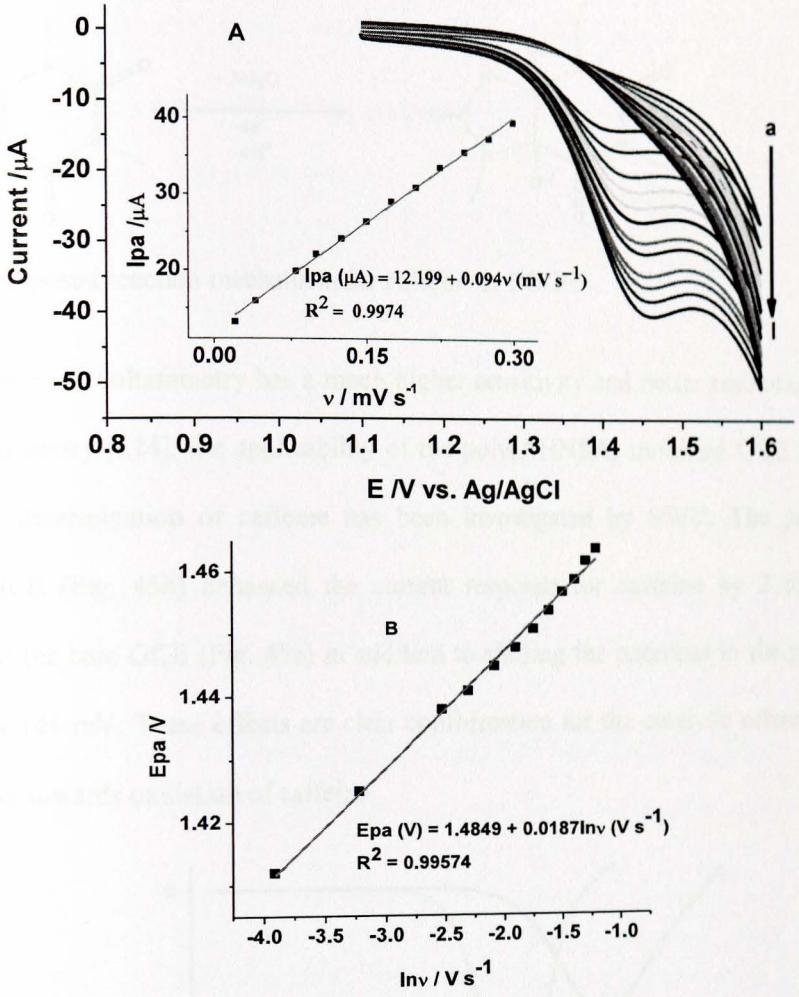

Fig. 44. (A) CVs of PGCE in pH 5.0 ABS containing 1.0×10^{-3} mol L^{-1} caffeine at different scan rates (a-l: 20, 40, 80, 100, 125, 150, 175, 200, 225, 250, 275 and 300 mV s^{-1}, respectively). Inset: plot of I_{pa} vs. scan rate. (B) Plot of E_{pa} vs. ln(v)

From the CV response of the polymer modified electrode for caffeine (Fig. 42), the effect of pH on the peak potential (Inset of Fig. 43A) and calculated value of *n*, the proposed reaction mechanism is shown in Scheme 8 which is in agreement with the mechanism reported elsewhere [70].

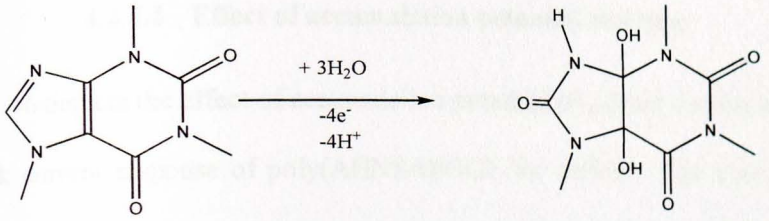

Scheme 8 Proposed reaction mechanism for caffeine at PGCE

Since square wave voltammetry has a much higher sensitivity and better resolution than cyclic voltammetry [224], the applicability of the poly(AHNSA) modified GCE for the quantitative determination of caffeine has been investigated by SWV. The polymer modified GCE (Fig. 45b) enhanced the current response for caffeine by 2 folds as compared to the bare GCE (Fig. 45a) in addition to shifting the potential in the positive direction by 144 mV. These effects are clear conformation for the catalytic effect of the polymer film towards oxidation of caffeine.

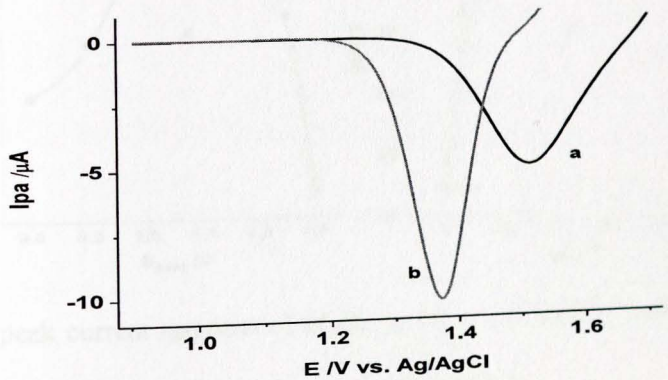

Fig. 45. SWVs of (a) UGCE and (b) PGCE in 1.0×10^{-3} mol L^{-1} caffeine (pH 5.0 ABS). Amplitude: 50 mV; potential step: 4 mV; frequency: 15 Hz; scanning potential: +0.9 to +1.7 V

4.2.3.4 Effect of accumulation potential and time

Fig. 46 depicts the effect of accumulation potential (E_{acc}) and accumulation time (t_{acc}) on peak current response of poly(AHNSA)/GCE for caffeine. The peak current increased with increasing E_{acc} from +0.8 to +1.1 and then dropped at higher potentials (Fig. 46A). The observed decrease in the current response at potentials higher than +1.1 could be because; the applied potential is high enough to cause the oxidation of caffeine than to accumulate it at the surface of the electrode. Fig. 46 shows the effect of t_{acc} recorded at E_{acc} of +1.1 V. The current response increased gradually up to 80 s and then leveled off which could probably be due to saturation of the electrode surface. Thus, E_{acc} of +1.1 V and t_{acc} of 80 s were taken as the optimum accumulation potential and time, respectively.

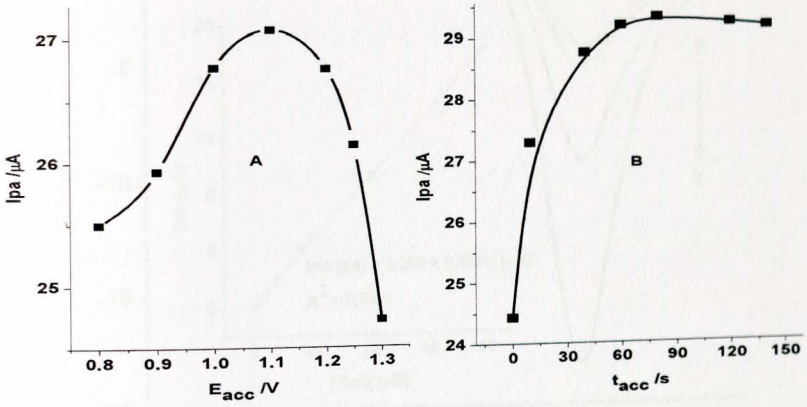

Fig. 46. Anodic peak current response of PGCE in 1.0×10^{-3} mol L^{-1} caffeine (pH 5.0 ABS) at different (A): E_{acc} and t_{acc} 30 s (B): t_{acc} and E_{acc} +1.1 V

After the optimization of the solution pH and preconcentration conditions, the SWV parameters (pulse amplitude, potential step and frequency) were optimized to be 70 mV, 14 mV and 30 Hz, respectively and were used in the subsequent analyses.

4.2.3.5 Calibration curve and detection limit

Using the optimized solution and method parameters described, the anodic peak currents at +1.340 V were found to be proportional to caffeine concentration in the range 6.0×10^{-8} to 4.0×10^{-5} mol L^{-1} (Fig. 47) with a linear regression equation, correlation coefficient and detection limit of Ipa (μA) = 0.289 + 0.503C (10^{-6} mol L^{-1}), R^2 = 0.99872 (Inset of Fig. 47) and 6.7×10^{-8} mol L^{-1} (S/N = 3), respectively. When the concentration of caffeine was more than 4.0×10^{-5} mol L^{-1}, the current response decreased gradually which could be ascribed to the saturation of the active sites of the polymer film.

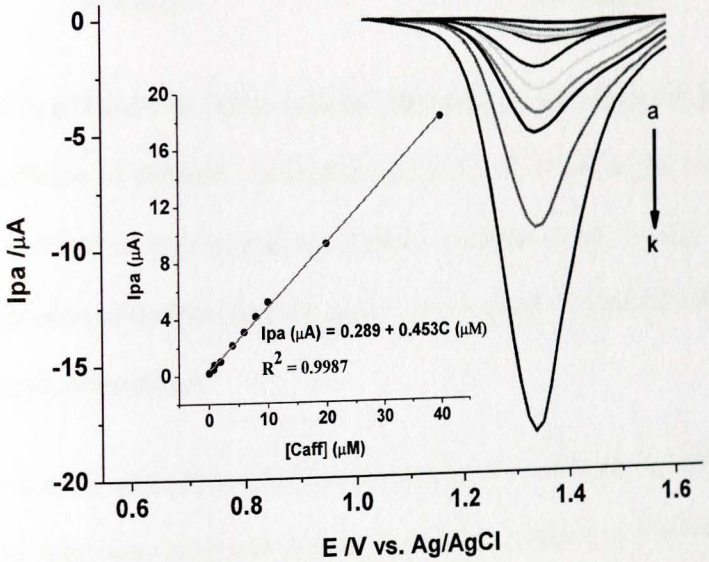

Fig. 47. SWVs of PGCE in pH 5.0 ABS containing caffeine of different concentrations (a–k: 0.06, 0.08, 0.8, 1.0, 2.0, 4.0, 6.0, 8.0, 10.0, 20.0 and 40.0 μM, respectively). Inset: plot of anodic peak current versus concentration of caffeine

4.2.3.6 Application of the method for the determination of caffeine in coffee

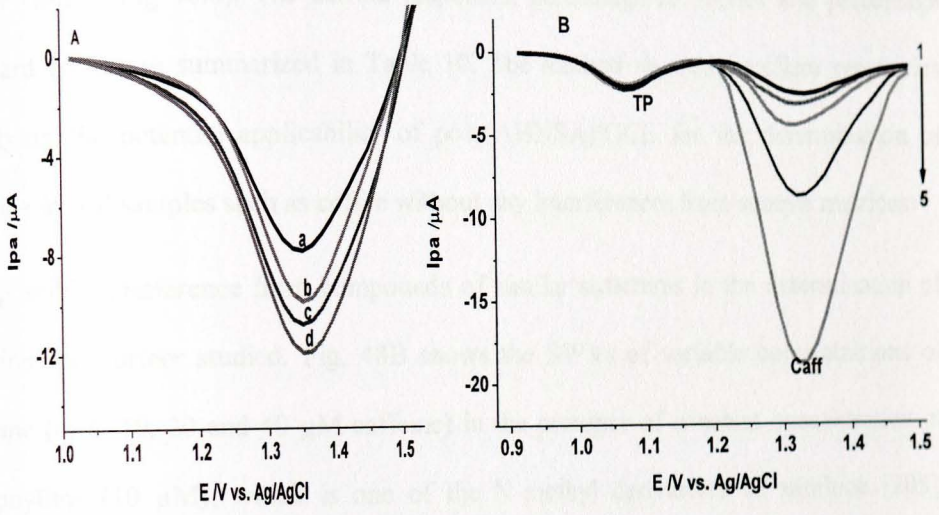

Fig. 48. (A) SWVs of PGCE in coffee extracts (200 times diluted with pH 5 ABS) spiked with standard caffeine of different concentrations (a-d: 0, 4, 6 and 8 µM, respectively). (B) SWVs of variable concentrations of standard caffeine in pH 5 ABS containing constant concentration of theophylline (10 µM). Concentration of standard caffeine (1-5): 4, 6, 10, 20, 40 µM, respectively

The method developed was applied for the determination of caffeine in coffee extracts. Coffee extract samples were prepared as described in the procedure. Using the optimized conditions, square wave voltammograms of caffeine in coffee extract were recorded (*curve a* of Fig. 48A). The average result of three separate determinations of caffeine in coffee extract samples at 95% confidence level, was 67.2 ± 0.095 mg/100 mL which is in the range reported in the literature [203,204]. Furthermore, three equal volumes of coffee

extract samples in pH 5.0 ABS (1:200 diluted) were spiked with different concentrations of standard caffeine (4, 6 and 8 μM) and the square wave voltammograms were recorded (curves *b-d* in Fig 48A). The current responses, percentage recoveries and percentage standard errors are summarized in Table 10. The method showed excellent recoveries signifying the potential applicability of poly(AHNSA)/GCE for the determination of caffeine in real samples such as coffee without any interferences from sample matrices.

The possible interference from compounds of similar structures in the determination of caffeine was further studied. Fig. 48B shows the SWVs of variable concentrations of caffeine (4, 6, 10, 20 and 40 μM caffeine) in the presence of constant concentration of theophylline (10 μM); which is one of the N-methyl derivatives of xanthine [208]. Clearly, there is an increase in the voltammetric peak current corresponding to oxidation of caffeine with the increase of the concentration whiles the peak current response for theophylline almost remaining constant. This confirms that analysis of caffeine in coffee extract using the polymer modified electrode is not affected not only by the sample matrices but also by structurally similar compounds like theophylline.

Table 10 Percentage recoveries of spiked standard caffeine in coffee extract

Sample	Initial	Spiked (μM)	Detected[a] (μM)	Recovery[a] (%)
Coffee extract	17.35	4.0	21.10 ± 0.115	93.75 ± 2.32
Coffee extract	17.35	6.0	23.00 ± 0.127	94.17 ± 2.11
Coffee extract	17.35	8.0	25.41 ± 0.386	100.75 ± 3.32

[a] Mean of triplicate measurements

4.2.3.7 Stability and comparison of the method developed with other similar methods

The stability of poly(AHNSA)/GC electrode towards caffeine oxidation was tested via the retention of the electrocatalytic currents (i/i_0, where i_0 represents the current recorded during the first cycle and i during successive cycles) [225] as a function of the number of cycles. The modified electrode was first scanned repetitively in the supporting electrolyte until a steady current was attained.

Then, the stabilized electrode was put in pH 5 ABS containing 1×10^{-3} mol L^{-1} caffeine. Two SWV measurements were recorded daily at an interval of 8 hours for ten consecutive days. To secure the cleanness of the electrode, each measurement was preceded by linear scanning of the electrode in pH 5.0 ABS in the negative direction of the same potential window. The calculated mean current ratio (i/i_0) for twenty measurements in ten days duration was 0.99958±0.00437 demonstrating the stability of the electrode.

The method developed is compared with other similar electroanalytical methods (Table 11). Apart from the stability and simplicity in the preparation of the modified electrode, the present method gives a reasonably lower detection limit and wider linear range.

Table 11 Comparison between the newly developed method and other reported methods

Electrode	method	Linear range (mol L^{-1})	LoD (mol L^{-1})	Ref.
Surfactant/MWCNTs	AdSDPV	$2.91 \times 10^{-7} - 6.27 \times 10^{-5}$	8.83×10^{-8}	212
Nafion/GCE	DPV	$9.95 \times 10^{-7} - 1.06 \times 10^{-5}$	7.98×10^{-7}	214
Nafion/MWCNTs/GCE	DPV	$6 \times 10^{-7} - 4 \times 10^{-4}$	2.3×10^{-7}	215
MWCNTs/Nafion/GCE	DPSV	$2.9 \times 10^{-6} - 3.77 \times 10^{-4}$	5.13×10^{-7}	216
MIP	SWV	$6 \times 10^{-8} - 2.5 \times 10^{-5}$	1.5×10^{-8}	217
Nafion/boron-doped diamond	DPV	$2 \times 10^{-7} - 1.2 \times 10^{-5}$	1.0×10^{-7}	218
Boron-doped diamond	DPV	9.7×10^{-6} - 1.1×10^{-4}	7.0×10^{-6}	219
Poly(safranine)/GCE	LSV	$3 \times 10^{-7} - 1 \times 10^{-4}$	1.0×10^{-7}	220
Poly(AHNSA)/GCE	SWV	$6 \times 10^{-8} - 4 \times 10^{-5}$	6.7×10^{-8}	This work

4.2.3.8 Conclusion

The approach taken in this work provides a simple method for the determination of caffeine in coffee samples. The modifier is relatively cheaper than other modifiers reported and easily deposited at the electrode surface. A wide linear range with a lower limit 6.0×10^{-8} mol L^{-1} and a limit of detection as low as 6.7×10^{-8} mol L^{-1} was observed. Excellent recoveries with acceptable errors were achieved for the determination of spiked standard caffeine samples in coffee extracts. Therefore, the method developed can be used for the direct analysis of caffeine content in real samples.

4.2.4 Fenitrothion in tap water samples

4.2.4.1 Background

Fenitrothion, O,O-dimethyl O-(3-methyl-4-nitrophenyl) phosphorothioate (scheme 9), which is one of the OP pesticides, is a contact and stomach poison [226,227]. It is widely used to control penetrating, chewing, and sucking insect pests (coffee leafminers, locusts, rice stem borers, wheat bugs, flours beetles, grain beetles, and grain weevils) on cereals, cotton, rice, and vegetables [227-229]. It is also used on farms and in public health programs as a residual contact spray for flies, mosquitoes, and cockroaches [94,227].

Occupational exposure to FT causes many adverse health effects [95,230-233]. It is known to be one of the neurotoxic compounds which can irreversibly inhibit acetylcholinesterase and lead to excessive cholinergic neurotransmission and subsequent signs of toxicity including autonomic dysfunction, involuntary movements, and even death at higher and prolonged exposure [234-236]. Because its extensive usage constitutes an important risk for nontarget species, including humans, and has already caused serious environmental problems [231], there is a growing concern about the toxicological and environmental risks associated with FT residues [231,235].

Therefore, there is a considerable interest for the development of rapid, selective, sensitive, cost-effective and environmentally friendly analytical methods for the determination of trace level of FT in environmental samples. Chromatographic methods with different detectors [234,237,238], and biosensors [239-241] are the common analytical methods reported for the determination of FT. Although these methods are

sensitive and specific, most of them demand complicated and time-consuming procedures, expensive apparatus, highly skilled technicians and large amount of organic solvents which eventually pollute the environment.

Electroanalytical techniques have been of great interest due to their advantages, including high sensitivity, comparative simplicity, rapid response and low cost [104]. Although reports have been made on the application of electroanalytical methods for the determination of FT [160,227-229,233,242,243], most of them used mercury as working electrode whose toxicity cannot be overlooked.

We recently reported the fabrication, characterization and application of poly(AHNSA)/GCE for the electrochemical determination of some selected alkaloids [244-247].

To the best of our knowledge, no conducting polymer-based electroanalytical method is reported for the determination of FT. In this regard, the aim of this study is to illustrate the applicability of a sensitive, selective and environmentally-friendly poly(AHNSA)/GCE working electrode for the trace level determination of FT in environmental samples.

In this work, square wave adsorptive stripping voltammetric (SWAdSV) technique based on poly(AHNSA)/GCE is presented. Cyclic voltammetry was used to investigate the electrochemical behavior of FT at the polymer-modified electrode. Furthermore, SWAdSV was employed for the determination of trace level concentrations of FT in tap water samples.

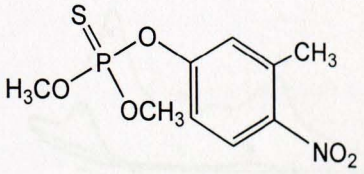

Scheme 9 Structural formula of FT

4.2.4.2 Electrochemical behavior of FT at Poly(AHNSA)/GCEs

Fig. 49A depicts cyclic voltammograms of unmodified (curve I) and poly(AHNSA) modified (curve II) glassy carbon electrodes in ABS (pH 5) containing 50 $\times 10^{-6}$ mol L^{-1} FT. As can be seen from the Figure, a pair of poorly resolved oxidative and reductive peaks (*a* and *b,* respectively), moreover diffused over a broad potential region, with peak separation ($\Delta E_{a\text{-}b}$) of 320 mV and a third reductive peak (*c*) at -713 mV appeared at the bare GCE. In a similar manner, a pair of rather well-defined oxidative and reductive peaks (*a'* and *b',* respectively) with in improved peak potential separation ($\Delta E_{a'\text{-}b'}$) of 52 mV and a reductive peak (*c'*) at -600 mV were observed at the polymer modified electrode. The peak potentials and the corresponding peak separations at the two electrodes are summarized in Table 12. The enhanced current response, the significant peak potential shift towards lower values and the improved reversibility of the redox couple (peaks *a'* and *b'*) observed at the polymer modified electrode demonstrate the electrocatalytic activity of the polymer film towards FT.

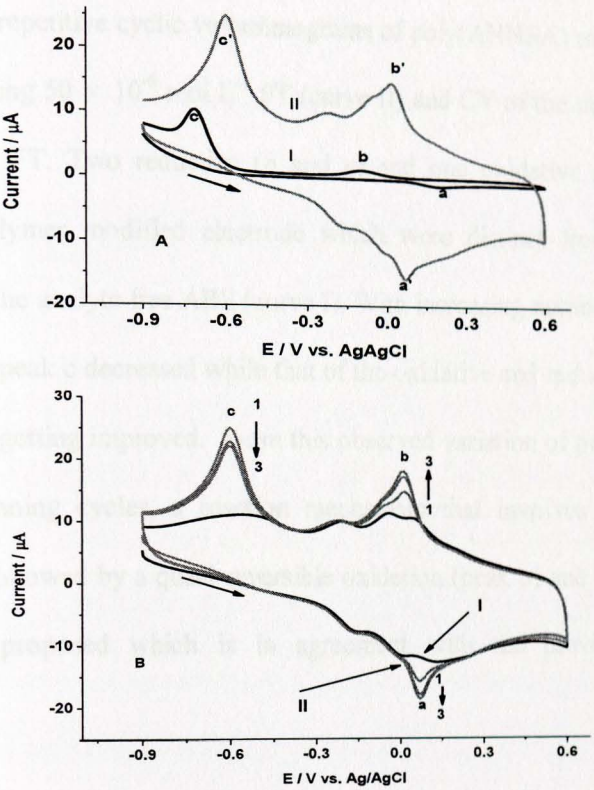

Fig. 49. (A) Cyclic voltammograms of UGCE (I) and PGCE (II) in ABS (pH 5) containing 50 × 10^{-6} mol L^{-1} FT. (B) Cyclic voltammograms of PGCE in ABS (pH 5) containing no FT (I) and 50 ×10^{-6} mol L^{-1} FT (II) at 0.1 V s^{-1}

Table 12 Summary of peak potentials of three FT peaks at PGCE and UGCE

Electrode	Peak-1	E_{pa}	Peak-2	E_{pc}	ΔE_p	Peak-3	E_{pc}
UGCE	a	+220	b	-100	$\Delta E_{a-b} = 320$	C	-713
PGCE	a'	+65	b'	+13	$\Delta E_{a'-b'} = 52$	c'	-600
ΔE_p*		155		113			113

Peaks 1 and 2 are oxidative and reductive peaks, respectively while peak-3 is an irreversible reductive peak. * potential advantage of PGCE over UGCE.

Fig. 49B shows the repetitive cyclic voltammograms of poly(AHNSA) modified GCE in ABS (pH 5) containing 50 × 10^{-6} mol L^{-1} FT (curve II) and CV of the same electrode in ABS containing no FT. Two reductive (*b* and *c*) and one oxidative (*a*) peaks were observed at the polymer modified electrode which were distinct from the polymer associated peaks in the analyte free ABS (curve I). With increasing number of cycles, the reductive current of peak c decreased while that of the oxidative and reductive couples (*a* and *b*, respectively) getting improved. From this observed variation of peak current with the number of scanning cycles, a reaction mechanism that involves an irreversible reduction (peak *c*) followed by a quasi-reversible oxidation (peak *a*) and reduction (peak *b*) processes was proposed which is in agreement with the previously reported mechanism [233].

4.2.4.3 Effect of potential scan rate

Fig. 50A presents CVs of 50 µM FT at PGCE in ABS (pH 5.0) at a scan rate range of 40-275 mV s^{-1}. The irreversible reduction peak current of FT at the polymer modified electrode (peak *c* of Fig. 49) showed linear dependence on the potential sweep rate (*a* of Fig. 50B) indicating a surface-confined kinetics of FT. In the potential range studied, the reduction peak potential shifted negatively with increasing potential scan rate confirming the irreversibility of the reduction reaction.

Since the reaction of FT at the surface of PGCE is a surface-confined process; the transfer coefficient (α), the number of electrons (*n*) participated in the rate determining step and the surface coverage (Γ) of FT at the surface of the polymer-film were

calculated using eqns. (7, 10 and 12) [105,124]. After integrating the peak area of the CV at 0.1 V s^{-1} (Fig. 50A), n and Γ were calculated to be 3.7 ($n \approx 4$) and 8×10^{-11} mole cm^{-2}, respectively.

As described by Laviron [130], the relationship between E_{pc} and scan rate for a totally irreversible surface-confined electrode process obeys eqn. (11).

Curve b of Fig. 50B depicts a linear dependence of the cathodic peak potential on the scan rate with a linear regression equation and correlation coefficient of E_{pc} (V) = -0.568 - 0.230v (V s^{-1}) and R^2 = 0.9954, respectively from which the standard reduction potential, E^0 is calculated to be -0.568 V. Moreover, the values of α and k_s were calculated to be 0.21 and 1.383 cm s^{-1}, respectively using the slope and y-intercept of the linear regression equation of the E_{pc} *vs. logv* plot (Inset of Fig. 50A).

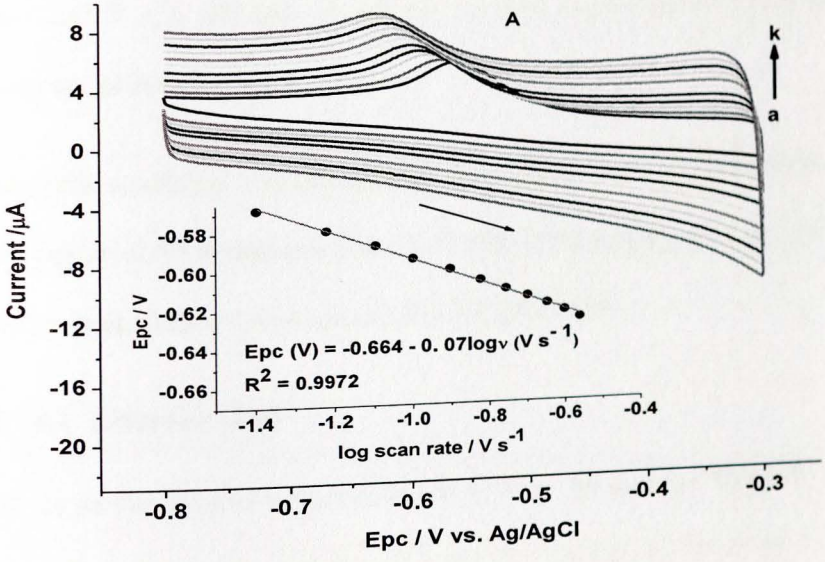

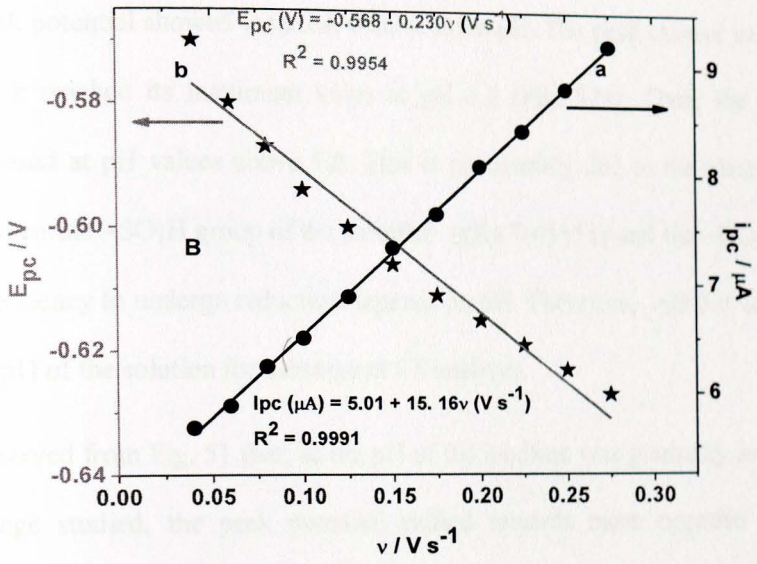

Fig. 50. (A) Cyclic voltammograms of PGCE in ABS (pH 5.0) containing 50 $\times 10^{-6}$ mol L^{-1} of FT at different scan rates (a-k: 40, 60, 80, 100, 125, 150, 175, 200, 225, 250 and 275 mV s^{-1}, respectively). Inset: plot of cathodic peak potential (V) versus log of potential scan rate (V s^{-1}). (B) plot of cathodic (a) peak current (μA) and (b) peak potential (V) versus potential scan rate

The electron transfer coefficient was also calculated according to eqn. (9) [248]. From the cyclic voltammogram of FT at scan rate of 0.1 V s^{-1} (Fig. 50A), α value was calculated to be 0.228 which is in agreement with its previously calculated value.

4.2.4.4 Influence of pH

The effect of pH on the electrochemical behavior of FT at the modified electrode was studied using cyclic voltammetry over the pH range 3.5–6.0. Fig. 51 shows the cyclic voltammograms of 50 × 10^{-6} mol L^{-1} FT in ABS of various pH values. Both the peak

current and peak potential showed variation with solution pH. The peak current increased with pH until it reached its maximum value at pH 5.0 (Fig. 52a). Then, the current response decreased at pH values above 5.0. This is presumably due to the electrostatic attraction between the $-SO_3H$ group of the modifier (pKa ≈4) [51] and the $-NO_2$ group of FT whose tendency to undergo reduction depends on pH. Therefore, pH 5.0 was used as the optimal pH of the solution for subsequent FT analyses.

It was also observed from Fig. 51 that, as the pH of the medium was gradually increased in the pH range studied, the peak potential shifted towards more negative values, suggesting the involvement of protons in the reaction. Fig. 52b shows the linear dependence of E_{pc} on pH in the range 4.5 to 6.0. A slope of 46.6 mV/pH suggests that the reduction of FT at the modified electrode obeys the Nernst equation (T = 22 ^{0}C) involving equal number of protons and electrons [222]. This could be attributed to the four-electron and four-proton transfer irreversible reduction of the nitro group (R-NO_2) to a hydroxylamine group (R-NHOH) [249].

From our observations on the cyclic voltammograms of FT at the modified GCE (Fig. 49B), the peak potential separation ($\Delta E_{a'-b'}$) (Table 12), the calculated number of electrons participated (n = 4) and the slope of the linear fit for the dependence of peak potential on scan rate ($n = m$); we proposed a reaction mechanism (scheme 10) for the overall redox reaction of FT at the poly(AHNSA)-modified GCE, which is in agreement with the previously reported mechanism [228,232,242].

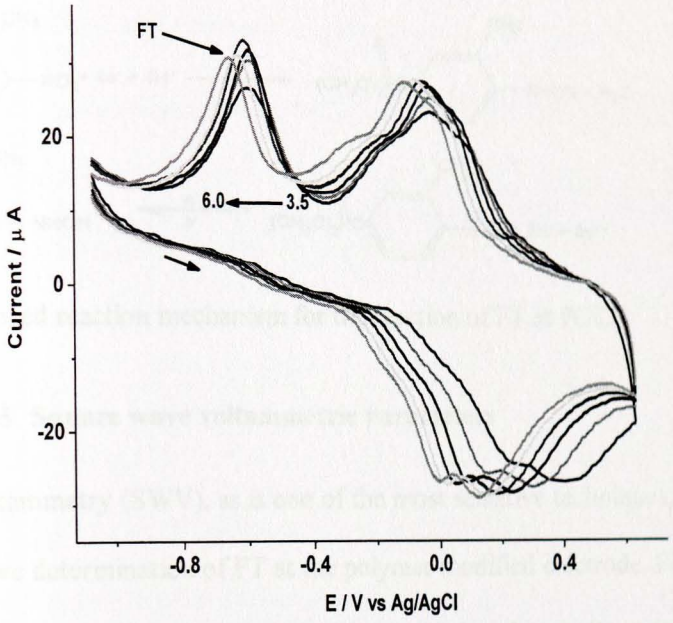

Fig. 51. Cyclic voltammograms of 50×10^{-6} mol L^{-1} FT in ABS of various pHs (3.5–6.0) at PGCE

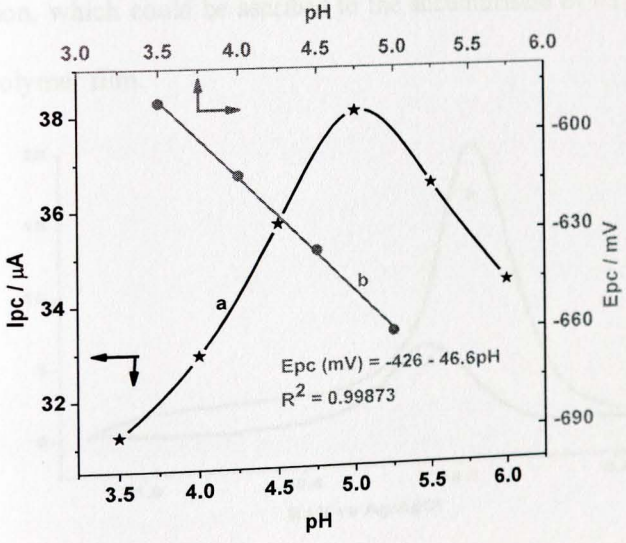

Fig. 52. Plot of cathodic (a) peak current and (b) peak potential versus pH

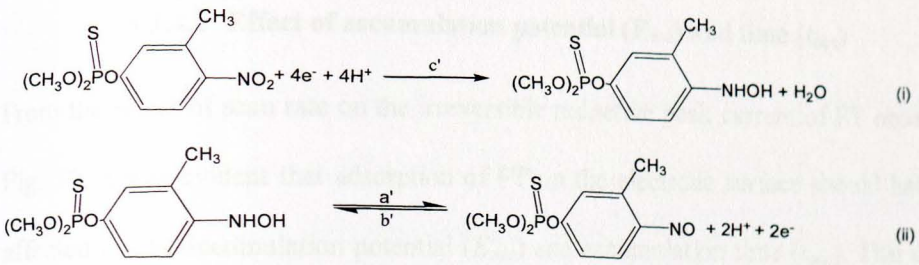

Scheme 10 Proposed reaction mechanism for the reaction of FT at PGCE

4.2.4.5 Square wave voltammetric parameters

Square wave voltammetry (SWV), as is one of the most sensitive techniques, it was used for the quantitative determination of FT at the polymer modified electrode. Fig. 53 shows the SWVs of FT at UGCE (a) and PGCE (b) recorded under similar conditions. The catalytic activity of the polymer-modified electrode towards FT reduction is confirmed by the significantly enhanced cathodic peak current response and peak potential shift in the negative direction, which could be ascribed to the accumulation of FT molecules on the surface of the polymer film.

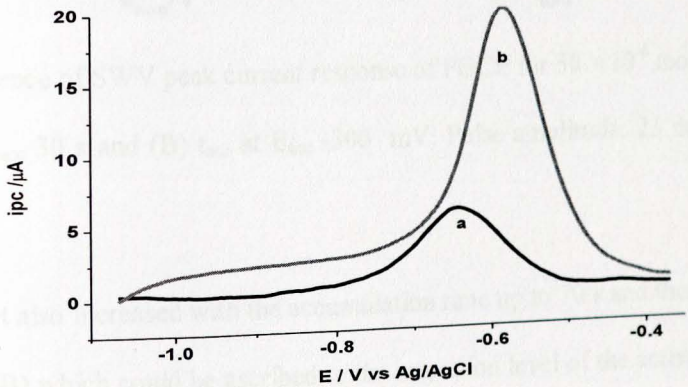

Fig. 53. Square wave voltammograms of UGCE (a) and PGCE (b) in pH 5.0 ABS containing 50 × 10^{-6} mol L^{-1} FT. Pulse amplitude: 25 mV and step potential: 4 mV

4.2.4.6 Effect of accumulation potential (E_{acc}) and time (t_{acc})

From the effect of scan rate on the irreversible reductive peak current of FT observed in Fig. 50, it was evident that adsorption of FT on the electrode surface should have been affected by the accumulation potential (E_{acc}) and accumulation time (t_{acc}). This clue has helped us to study the influence of accumulation potential and time. The peak current increased with increasing accumulation potential in the range -550 to -300 mV until it reached its maximum value at -300 mV and then decreased at potentials less negative than -300 mV (Fig. 54A). Hence, -300 mV was taken as the optimum preconcentration potential for further square wave voltammetric studies.

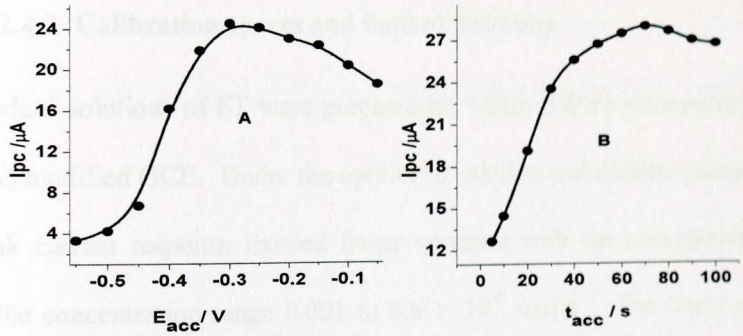

Fig. 54. Dependence of SWV peak current response of PGCE for 50 $\times 10^{-6}$ mol L^{-1} FT on: (A) the E_{acc} at t_{acc} 30 s and (B) t_{acc} at E_{acc} -300 mV. Pulse amplitude: 25 mV and step potential: 4 mV

The peak current also increased with the accumulation time up to 70 s and then decreased slightly (Fig. 54B) which could be ascribed to the saturation level of the active surface of the polymer film. Thus, 70 s was taken as the optimum preconcentration time.

Moreover, method parameters such as pulse amplitude and potential step were optimized (data not shown). It was found that the peak currents increased with increasing pulse amplitude in the range of 20 to 100 mV, accompanied by the broadening of peak width at the same time. When the pulse amplitude was higher than 80 mV, the peak width became much wider. Therefore, 80 mV was chosen as the optimum pulse amplitude. Potential step was tested in the range of 4 to 24 mV. Experimental results showed that the peak height increased with increasing potential step. When the potential step was greater than 20 mV, the peak shape became much wider as well as not smooth. Thus, 20 mV was selected as the optimal potential step.

4.2.4.7 Calibration curves and limit of detection

Aqueous standard solutions of FT were prepared for which SWVs were recorded at the poly(AHNSA) modified GCE. Under the optimized solution and method parameters, the reductive peak current response showed linear variation with the concentration of FT (Fig. 55) in the concentration range 0.001 to 6.6×10^{-6} mol L^{-1}. The linear regression equation, correlation coefficient (R^2) and detection limit (LoD = 3δ/m for n = 6) were i_{pc} (μA) = 1.616 + 13.514C (μM), 0.9994 and 7.95×10^{-10} mol L^{-1}, respectively (Inset of Fig. 55).

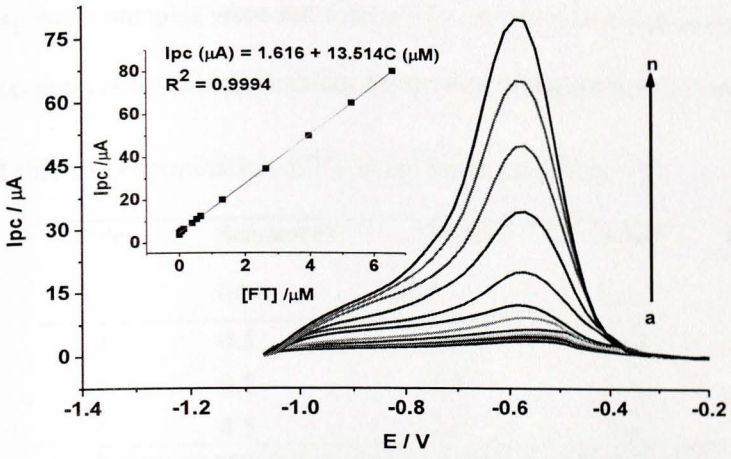

Fig. 55. SWVs of PGCE in pH 5 ABS containing variable concentrations of FT (a-n: 0.001, 0.005, 0.010, 0.053, 0.066, 0.132, 0.396, 0.528, 0.660, 1.32, 2.64, 3.96, 5.28 and 6.60 μM, respectively) under the optimized conditions (Pulse amplitude 80 mV; potential increment 20 mV; E_{acc} -300 mV and t_{acc} 70 s). Inset: Plot of cathodic peak current versus concentration of FT

4.2.4.8 Analytical application, reproducibility and interference studies

The application of the polymer modified electrode for determination of FT in tap water was studied. Three standard solutions (a, b and c) of FT each with 0.5×10^{-6} mol L^{-1} concentration were prepared using tap water without any treatment. The tap water samples (a, b and c) were then spiked with 0.5, 1.5 and 2.5×10^{-6} mol L^{-1} of standard solutions of FT, respectively. For each sample, triplicate square wave measurements were recorded under the optimized conditions. The results are summarized in Table 13. As can be seen from the Table, recoveries in the range 96–98% show that the analyses of FT in

tap water samples were not affected by sample matrix and hence the modified electrode has great potential applicability for the determination of FT in environmental samples.

Table 13 Determination of FT in tap water samples (n = 3)

Sample	Standard FT (μM)	Added (μM)	Found* (μM)	RSD** (%)	Recovery (%)
a	0.5	0.5	0.48	1.2	96
b	0.5	1.5	1.46	1.5	97.3
c	0.5	2.5	2.45	1.7	98

* Mean concentration of triplicate readings and **RSD (%) for n = 3

Regeneration of the electrode and reproducibility of the responses are two vital characteristics of an electrode for its electrochemical sensor applications. The same polymer modified GCE was used for five successive measurements of 1×10^{-5} mol L^{-1} FT. After each measurement, the surface of the poly(AHNSA)/GCE was regenerated by successively scanning four cycles between -0.1 and -1.1 V in ABS (pH 5). The electrode showed significant regeneration and reproducibility, and the relative standard deviation (RSD) of the peak current was 2.6% (n = 5).

Moreover, interference studies were performed for the analytical application of the proposed method. A 5×10^{-6} mol L^{-1} FT spiked with various amounts of methyl parathion, ascorbic acid and uric acid was evaluated under the same experimental conditions. According to the results obtained, methyl parathion showed significant interference even at concentrations as low as 1×10^{-6} mol L^{-1}. On the contrary, ascorbic acid and uric acid showed no interference effect even at concentration levels of 20×10^{-6} mol L^{-1}.

A comparison between the analytical performance of the present method and some previously reported electroanalytical methods for the determination of FT are summarized in Table 14. Among the mercury-free methods listed, the lowest limit of detection (1.6×10^{-9} M) obtained for FT determination was by carbon ceramic electrode (CCE) whose fabrication is tedious besides the problem of reproducibility. In the present work, a lower detection limit of 7.95×10^{-10} M has been achieved using an easily fabricated, stable and environmentally friendly polymer film which as to the best of our knowledge could be the first conducting polymer used as electrode modifier for the determination of FT. The lower limit of the linear range in our result also indicates the potential applicability of our method for the determination of trace level FT in real samples.

Table 14 Performance of the present method compared to previously reported methods

Electrode used	Linear range (μM)	LoD (nM)	Method used	Ref.
HMDE	0.01– 1	0.13	DPV	159
HMDE	90 – 890	5.2	SWV	226
CCE	0.005 – 0.1	1.6	SWAdSV	227
Nano-TiO_2/GCE	0.025 – 10	10	SWV	232
HMDE	0.01– 0.12	1.6	DPV	242
Poly(AHNSA)/GCE	0.001– 6.6	0.795	SWAdSV	This work

4.2.4.9 Conclusion

Compared to the unmodified GCE, the poly(AHNSA) modified electrode showed an excellent electrocatalytic effect towards the reduction of FT in 0.1 M ABS. Cyclic voltammetry was used to estimate the kinetic parameters such as n, α and k_s. SWAdSV determination of FT using the polymer-modified electrode revealed an extended linear range towards the lower concentration range. Moreover, lower LoD than the previously reported works and excellent recoveries from tap water without the need for prior treatment showed the potential application of the developed method for trace level determination of FT in real samples.

4.2.5 Methyl Parathion in tap water samples

4.2.5.1 Background

Pesticides have been of enormous benefit to developing countries attempting to produce sufficient quantities of food and protect resources such as plantations. Protection of crops from grain-eating birds, insects, weeds and herbs is crucially important to such economies. This is especially important now as many developing countries are entering phases of industrial growth and experiencing mobilities of much of the agricultural workforce to the industrial sector resulting in fewer people available to tend to crops [250]. However, reliance on chemical pesticides can be problematic as many developing countries continue to use toxic pesticides that can cause health problems and can have a serious negative impact on the environment.

After the prohibition of organochlorine pesticides due to their bioaccumulation and persistence in the environment, organophosphorous compounds became the most commonly-used class of insecticides for pest control [70]. However, these pesticides are highly toxic environmental and food chain pollutants. Due to the neurotoxic properties of organophosphorus compounds, they have even been used as chemical warfare agents [251]. Methyl parathion (scheme 11) is a toxic organophosphorous compound that is commonly used for agricultural purposes in many countries and the current EU acceptable limit in ground water is 0.1 $\mu g\ L^{-1}$ [252]. Nonetheless, it is used for a variety of crops including vegetables, fruits and cereals resulting in the accumulation of its residue and metabolites in soils, water and food commodities [253]. Traditional farmers

in developing countries are often exposed to methyl parathion as it is readily absorbed through intact skin and the lungs.

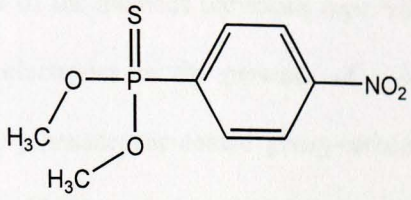

Scheme 11 Structural formula of methyl parathion

The general public in developing countries is usually exposed to organophosphorus pesticides through the ingestion of contaminated foods (such as cereals, vegetables, and fruits), which are directly treated with the pesticides or are grown in contaminated fields. Therefore, contamination of the environment and food by pesticide residues is an important topic in many areas of the world and the search for simple and sensitive methods for qualitative and quantitative determination of such species is of great interest to researchers in many parts of the world. However, expensive and time-consuming chromatographic techniques that require highly-trained operators are commonly used for pesticide analysis [254-256]. As a result, there is a growing interest in developing inexpensive, fast analytical techniques for these species. Electrochemical techniques have several attractive features for such analyses including high sensitivity, selectivity and simplicity, as well as low cost and rapid analysis times.

Generally, electrochemical methods for pesticide analysis are based on processes occurring at Hg electrode surfaces [257,258]. However, the toxicity of Hg makes it

unattractive for routine analytical procedures. Hence, our focus is on the development of new, less harmful electroanalytical techniques with high sensitivity and selectivity for pesticide detection. Some of the methods previously reported in this area include clay-modified glassy carbon electrodes in the presence of a surfactant (cetyl trimethyl ammonium bromide) [259] hexadecane-coated glassy-carbon electrodes [260], boron-doped diamond electrodes [261], molecular imprinting techniques [262-264], bismuth modified glassy carbon electrodes in the presence of a surfactant (cetyl trimethyl ammonium bromide) [265], multiwalled-carbon nanotube modified glassy carbon electrodes [266], single walled carbon nanotube modified electrodes using ionic-liquids as binders [267] and biosensors [268-270].

Coating metal electrodes with a thin film of electronically conductive polymer has proved to be a particularly simple and convenient method for the preparation of modified electrodes [271]. Polymer-modified electrodes may also exhibit preferential accumulation of analytes on bound surface functionalities, which can improve the selectivity of the electrode [221]. The use of poly(3,4-ethylenedioxythiophene) modified glassy carbon electrode for the electrochemical detection of paracetamol and paraminophenol in urine samples were recently reported [272,273]. Significantly, very few reports exist that describe the detection of parathion at polymer-modified electrodes, despite the simplicity of the method and ease by which the analysis can be performed. In one report, Liu employed a linear sweep voltammetric technique using a poly(carmine) modified glassy carbon electrode for the detection of parathion [274]

In this work we describe the SWV application of poly(4-amino-3-hydoxynaphthalene sulfonic acid)modified GCE for the analysis of methyl parathion in drinking water samples.

4.2.5.2 Voltammetry of methyl parathion at PGCE

Cyclic voltammograms of methyl parathion at a PGCE (*d*) and UGCE (*b*) are shown in Fig. 56. Also shown are voltammograms recorded at PGCE (c) and UGCE (a) in blank electrolyte containing no methyl parathion. During the first scan in the presence of methyl parathion, a single strong, irreversible reductive peak (peak 3) and weak redox couples (peaks 1 and 2) were observed at -0.560, +0.020 and +0.050 V, respectively, which were distinct from the peaks associated with the polymer (curve c of Fig. 56A). With increasing number of cycles, the peak current response for the reductive peak (peak 3) decreased while increasing for peaks 1 and 2 showing that peak 3 is due to an irreversible reduction of methyl parathion.

To further study the electrochemical behavior of methyl parathion at PGCE, the effects of solution pH and scan rate on the irreversible reductive peak current and peak potential were investigated. Fig. 57 depicts the cyclic voltammograms of the polymer modified GCE in ABS of various pHs containing methyl parathion. The peak potential shift observed with pH illustrates the participation of protons in the reduction reaction. In the pH range 4.5-6.0, a linear dependence of the peak potential on pH with a slope of 43.8 (curve a of Fig. 57B) indicated the participation of protons and electrons in a 1:1 ratio.

Moreover, the peak current response of the polymer modified GCE for methyl parathion increased with increasing pH up to pH 5 where the maximum current response is recorded (curve b of Fig. 57B). The peak current response then decreased at pHs higher than 5.0. Thus, pH 5 was taken as the optimum solution pH in the subsequent analyses. The increase in peak current with pH in the range 3.5-5.0 which then decreased at pHs higher than the *pka* of the polymer film, could be attributed to the electrostatic attractive force between the protonated polymer film and the nitro group of the analyte.

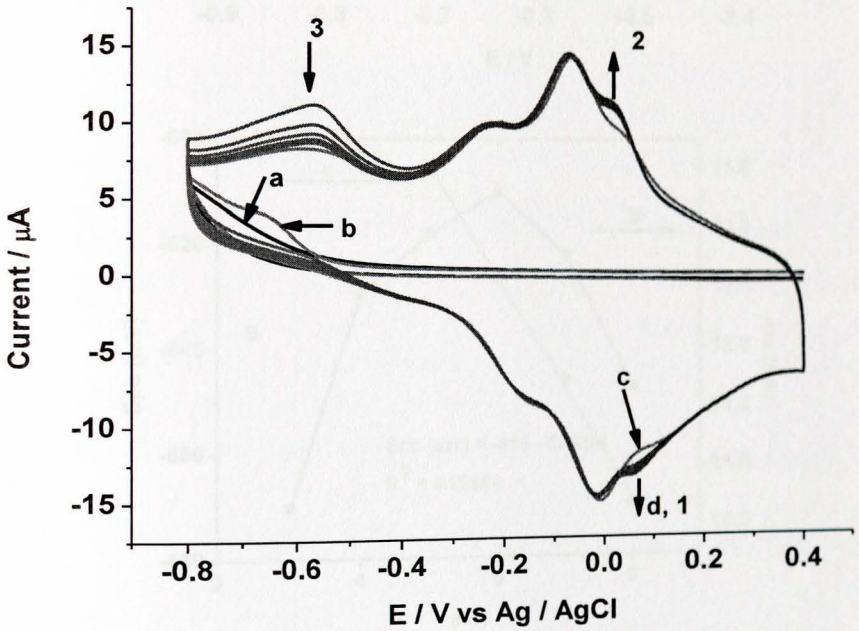

Fig. 56. Cyclic voltammograms of (a and b) UGCE, (c and d) PGCE in (a and c) the absence and (b and d) the presence of 10×10^{-6} mol L^{-1} methyl parathion (pH 5 ABS)

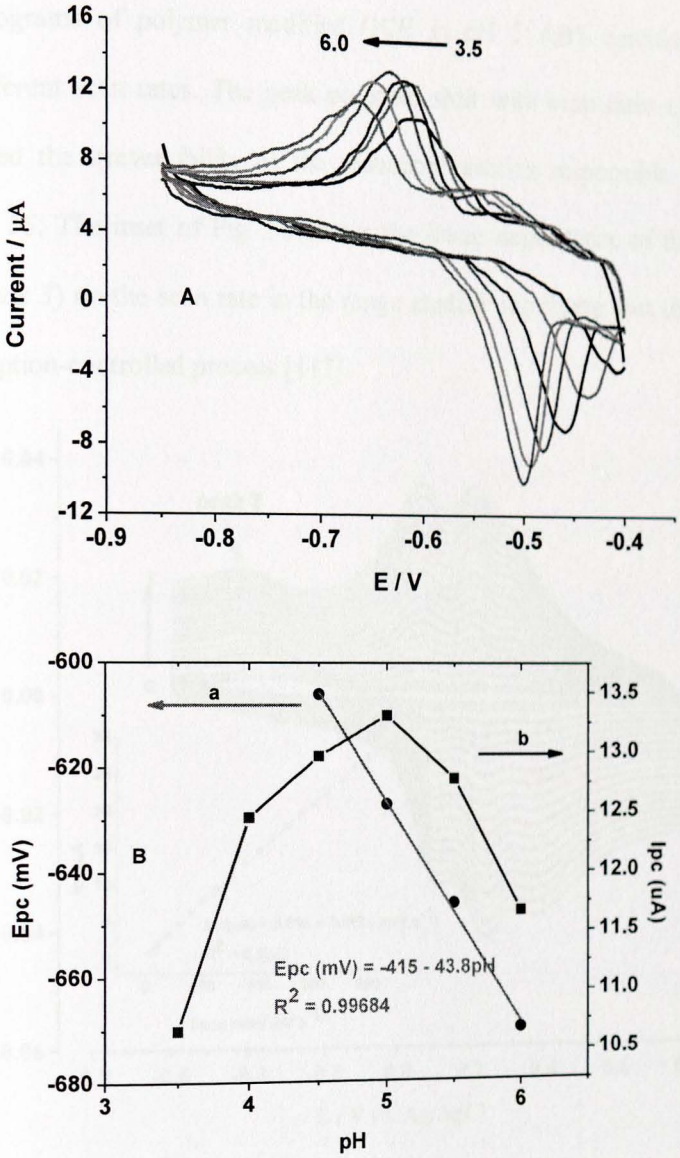

Fig. 57. (A) CVs of 10×10^{-6} mol L^{-1} methyl parathion in ABS of various pHs (3.5-6.0) at PGCE. (B) Plot of reductive peak potential (a) and peak current (b) versus pH

The effect of scan rate on the irreversible reduction peak current of methyl parathion at the polymer modified glassy carbon electrode was also investigated. Fig. 58 shows the

cyclic voltammograms of polymer modified GCE in pH 5 ABS containing methyl parathion at different scan rates. The peak potential shift with scan rates observed for *peak 3* confirmed the irreversibility of the reduction reaction responsible for *peak 3* depicted in Fig. 56. The inset of Fig. 58 shows the linear dependence of the reductive peak current (*peak 3*) on the scan rate in the range studied signifying that the reduction reaction is adsorption-controlled process [117].

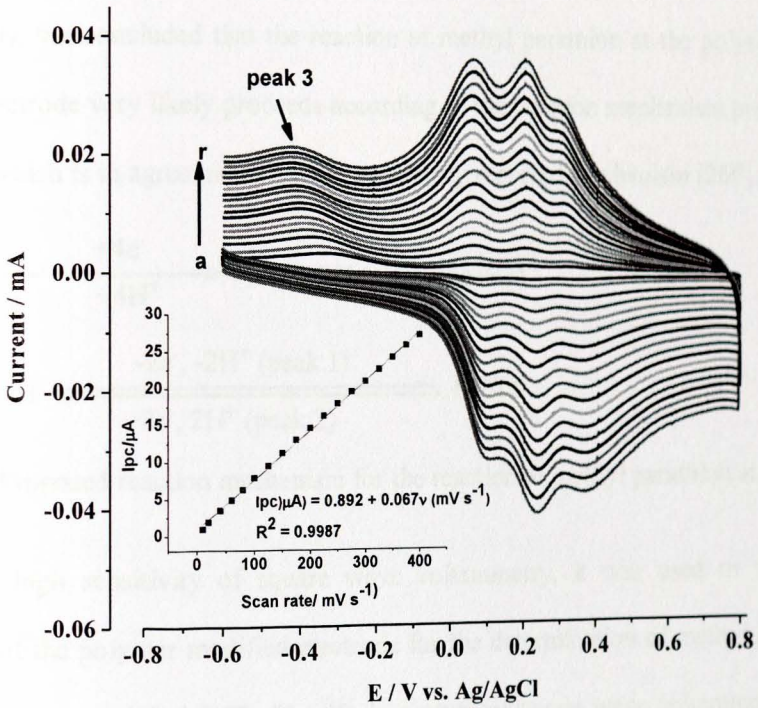

Fig. 58. Cyclic voltammograms of PGCE in 10×10^{-6} mol L^{-1} methyl parathion (pH 5 ABS) at different scan rates (a-r: 10, 20, 40, 60, 80, 100, 125, 150, 175, 200, 225, 250, 275, 300, 325, 350, 375, and 400 mV s^{-1}, respectively). Inset: plot of irreversible reduction peak current (peak 3) vs. scan rate

Since the reduction of methyl parathion at PGCE is a surface-confined irreversible reduction process, the number of electrons transferred during the process (n) and surface coverage of methyl parathion at the modified electrode, Γ, were calculated using eqns. (7 and 10) to be 3.8 and 1.7×10^{-10} mol cm^{-2}, respectively. Furthermore, the number of electrons participated in the reversible redox couple of methyl parathion (*peaks 1* and *2* in Fig. 56) was calculated using eqn. (2) to be 2.

Consequently, we concluded that the reaction of methyl parathion at the poly(AHNSA) modified electrode very likely proceeds according to the reaction mechanism proposed in scheme 12 which is in agreement with the previously reported mechanism [260].

$$\text{R-NO}_2 \xrightarrow[+4\text{H}^+]{+4\text{e}^-} \text{R-NHOH} + \text{H}_2\text{O (peak 3)}$$

$$\text{R-NHOH} \underset{+2\text{e}^-,\, 2\text{H}^+ \text{ (peak 2)}}{\overset{-2\text{e}^-,\, -2\text{H}^+ \text{ (peak 1)}}{\rightleftharpoons}} \text{R-NO}$$

Scheme 12 Proposed reaction mechanism for the reaction of methyl parathion at PGCE

Due to the high sensitivity of square wave voltammetry, it was used to study the application of the polymer modified electrode for the determination of methyl parathion using the polymer modified GCE. Fig. 59 shows typical square wave voltammograms of methyl parathion recorded at a bare glassy carbon electrode (*curve a*) and a poly(AHNSA) modified electrode (curve b).

In contrast to the bare GCE, the reduction current of methyl parathion at the polymer modified electrode was enhanced by more than one order of magnitude which most likely could be due to the pre-concentration of the analyte at the electrode surface giving rise to

the surface-confined kinetics and increased effective surface area described previously. The peak potential shift from -680 to -530 mV observed supplemented by one order of magnitude of peak current enhancement confirmed the catalytic activity of the polymer modified GCE towards the reduction of methyl parathion.

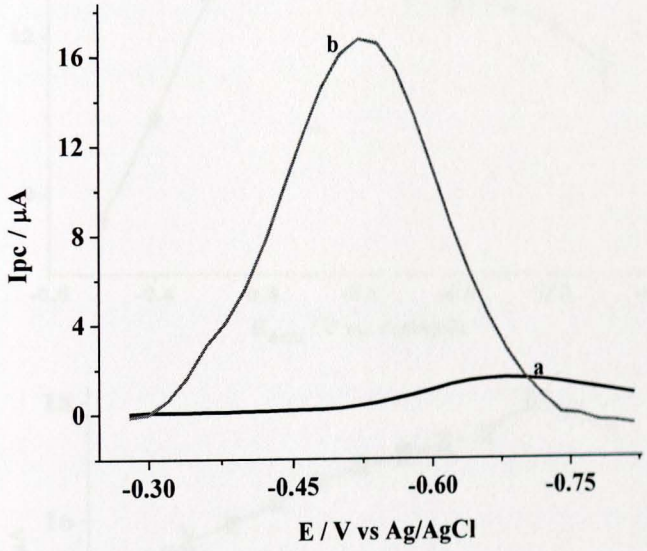

Fig. 59. SWVs of 10 × 10^{-6} mol L^{-1} of methyl parathion in pH 5.0 ABS at (a) UGCE and (b) PGCE. Pulse amplitude: 25 mV; potential step: 20 mV; frequency: 15 Hz

4.2.5.3 Effect of accumulation potential and accumulation time

The effects of accumulation potential and accumulation time on the peak current response of PGCE for methyl parathion reduction were optimized by systematically altering each parameter. Fig. 60 shows the effect of accumulation potential (E_{acc}) and accumulation time (t_{acc}) on the SWV peak current response of poly(AHNSA) modified electrode for methyl parathion. Fig. 60A shows the significant peak current drop at potentials more negative than -0.3 V. At potentials more positive than -250 mV, the current drop was not

as high as was observed for higher negative potentials. Thus, an accumulation potential of -250 mV was taken as the optimum E_{acc}.

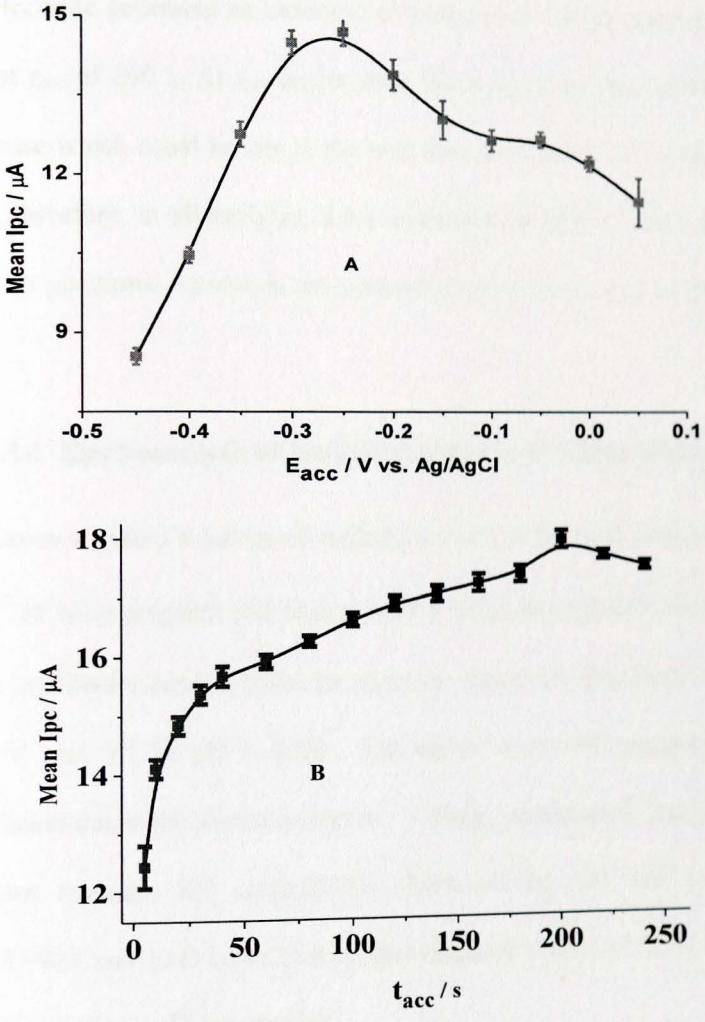

Fig. 60. Effect of (A) E_{acc} at t_{acc} 60 s and (B) $t_{acc\ at}$ E_{acc} -250 mV on the peak current

An error bar in the range of 0.461.142 signified the stability and hence reproducibility of the developed method.

The effect of the accumulation time on the peak current response was then examined and is shown in Fig. 60B. Clearly, pre-concentrating the methyl parathion at the surface of the modified electrode generated an increased reductive peak current response, reaching its maximum at t_{acc} of 200 s. At t_{acc} higher than 200 s, the reduction current response started to decrease which could be due to the saturation level of the active surface of the polymer film. Therefore, in all analyses, a pre-concentration time of 200 s at -250 mV was employed to guarantee maximum pre-concentration of the analyte at the electrode surface.

4.2.5.4 Electroanalysis of Methyl Parathion in Drinking Water Samples

A series of aqueous standard solutions of methyl parathion in the concentration range 1×10^{-8} to 2×10^{-5} M were prepared and square wave voltammograms were recorded at the poly(AHNSA) modified electrode under the optimum conditions described (t_{acc} = 200 s, E_{acc} = -0.250 V, and 0.1 M pH 5 ABS). The square wave voltammograms and the resulting calibration curve are shown in Fig. 61. Clearly, an excellent linearity between the peak current response and concentration (Inset of Fig. 61) with a correlation coefficient of 0.9991 and LoD calculated as three times the signal to noise ratio in the voltammetric signal of 1.1 nM was obtained.

To study the application of the developed method for the determination of methyl parathion in environmental samples, known concentrations of methyl parathion were spiked to two drinking water standard samples (section 3.3.2.5) and the square wave voltammograms were recorded. The recovery results of the method are summarized in

Table 15. Clearly, excellent recoveries for the spiked standard methyl parathion samples were obtained. Thus, it appears that the polymer modified electrode is very promising for the analysis of methyl parathion in drinking water samples.

Table 15 Recovery data for methyl parathion in drinking water sample

Sample	Added (μM)	Found* (μM)	Recovery (%)*
1	0.148	0.138 ± 0.009	93.24 ± 6.08
2	1.480	1.323 ± 0.019	89.39 ± 1.28

*Mean value ± standard deviation (n = 3)

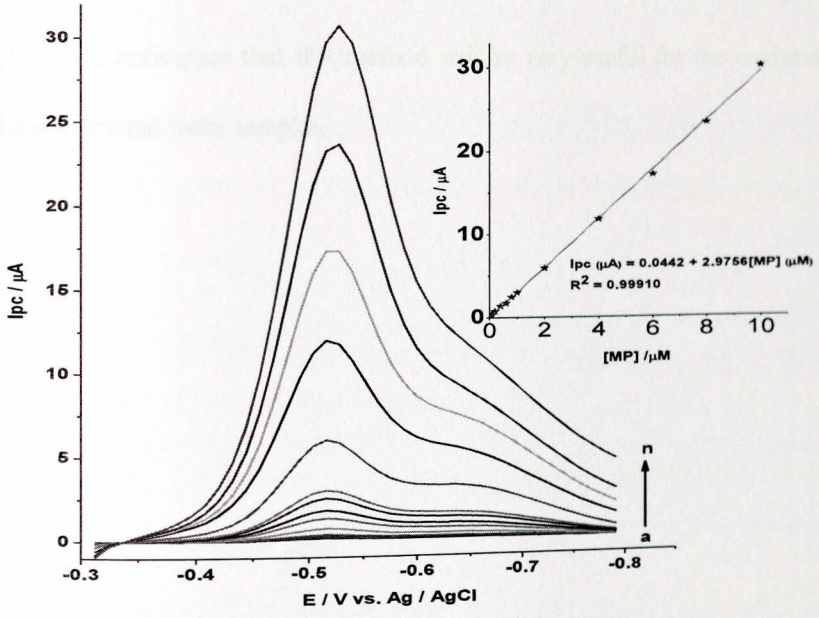

Fig. 61. SWVs of PGCE in pH 5. ABS containing various concentrations of methyl parathion (a-n: 0.01, 0.04, 0.06, 0.08, 0.2, 0.4, 0.6, 0.8, 1, 2, 4, 6, 8 and 10 × 10^{-6} M, respectively). Inset: Plot of I_{pc} as a function of concentration of methyl parathion

4.2.5.5 Conclusion

The electrochemical behavior of methyl parathion at the surface of poly(AHNSA) modified GCE was investigated using cyclic voltammetry. A reaction mechanism involving an irreversible reduction followed by a reversible redox couple was proposed. Preferential adsorption of methyl parathion at the polymer-modified electrode surface was possible and voltammetric analysis revealed that surface-confined kinetics predominated at the surface.

A linear response up to 10 nM and a low limit of detection of 1.1 nM was observed, which is well below the current acceptable limit for this pesticide in ground water. Therefore, we anticipate that this method will be very useful for the analysis of methyl parathion in ground water samples.

4.3 Electrochemically pretreated glassy carbon electrode for electrochemical determination of fenitrothion in human urine

4.3.1 Background

Due to the indiscriminate applications of fenitrothion, it finds a way into surface water bodies, through agriculture runoff and municipal waste water systems by ingestion and inhalation reaching the human system. Therefore, the presence of residues of such pesticides in natural waters and in foodstuffs is of major concern for public health reasons [225] which necessitated the development of methods that can be used to determine fenitrothion in environmental samples at trace levels.

Ontop of the conventional methods of analyses, which involve compound extraction, preconcentration and clean-up steps, making them tedious, time-consuming, expensive, not environmentally friendly and not suitable for in-field analysis, electroanalytical techniques have been of great interest due to their advantages, including high sensitivity, comparative simplicity, rapid response and low cost [104].

Although reports have been made on the application of electroanalytical methods for determination of fenitrothion [159,226-228,232,241,242], many of which used mercury as working electrode whose toxicity cannot be overlooked while the remaining used polymer modified-electrodes.

Glassy carbon electrodes are currently in widespread use in electroanalysis, primarily because of their broad potential window, low background current, rich surface chemistry,

low cost, easy surface modification, excellent mechanical and electrical properties, chemical inertness, availability in various forms and shapes and suitability for various sensing and detection applications [275-277].

Pretreatment of GCEs is an important way to improve their performance. Various kinds of pretreatment methods such as electrochemical pretreatment [157,278-282], radio frequency plasma [283] and in situ laser irradiation [284] have been reported. Among these activation methods, electrochemical pretreatment is one of the most commonly used methods to improve electrochemical responses to biological compounds due to its good reproducibility and simple operation.

The present paper deals with the development of a simple, sensitive, selective and reproducible electrochemical method based on electrochemically pretreated glassy carbon electrode applied for determination of fenitrothion in tap water and human urine samples.

4.3.2 Voltammetric behavior of fenitrothion at pretreated glassy carbon electrode

Fig. 62 depicts the cyclic voltammograms of bare glassy carbon electrode (UGCE) (curves A and B) and electrochemically pretreated glassy carbon electrode (pGCE) (curves C and D) in pH 5.0 ABS in the absence (curves A and C) and presence of 50 × 10^{-6} M FT (curves B and D). Cyclic voltammogram of FT at the UGCE (curve B) showed an irreversible weak reductive peak at about -0.71 V and diffused quasireversible reductive and oxidative peaks centered at about -0.08 and +0.21 V, respectively. At the pGCE (curve D), similar peaks but with significantly enhanced peak current and peak

potential shift were observed. Over 2 folds of peak current and a potential shift of about 140 mV was observed for the irreversibly reductive peak (peak c' of curve D) at the pGCE. These effects clearly prove the catalytic effect of the electrochemically pretreated glassy carbon electrode towards the reduction of FT. The peak current enhancement and peak potential shift at the PGCE was also observed for the quasireversible redox peaks.

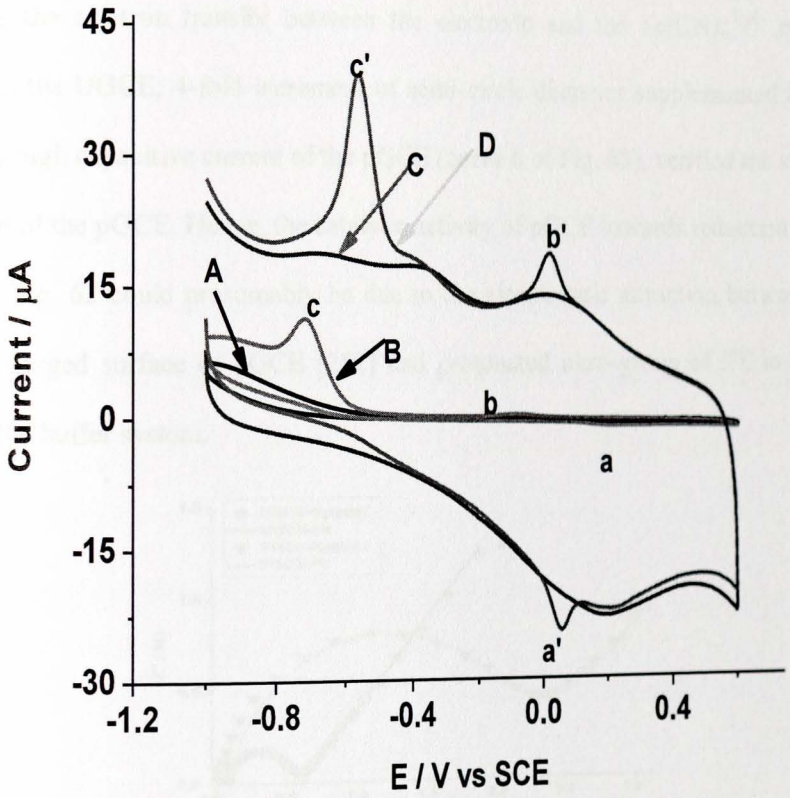

Fig. 62. CVs of pH 5.0 ABS in the presence (curves B and D) and absence of 50 µM FT (curves A and C) at UGCE (A and B) and pGCE (C and D) at100 mV s^{-1}

4.3.3 EIS characterization of pGCE

The complex-impedance plots of the untreated GCE (curve a) and the electrochemically pretreated GCE (curve b) are shown in Fig. 63. In accordance with the previous report [282], the charge transfer resistance (R_{ct}) of the pGCE, which is the diameter of the semicircle, is clearly greater than that of the UGCE indicating the formation of a layer that inhibits the electron transfer between the electrode and the $Fe(CN)_6^{3-/4-}$ system. Compared to the UGCE, 4-fold increment of semi-circle diameter supplemented by the significantly high capacitive current of the pGCE (curve b of Fig. 63), verified the surface modification of the pGCE. Hence, the catalytic activity of pGCE towards reduction of FT observed in Fig. 62 could presumably be due to the electrostatic attraction between the negatively charged surface of pGCE [282] and protonated nitro-group of FT in acidic medium of the buffer system.

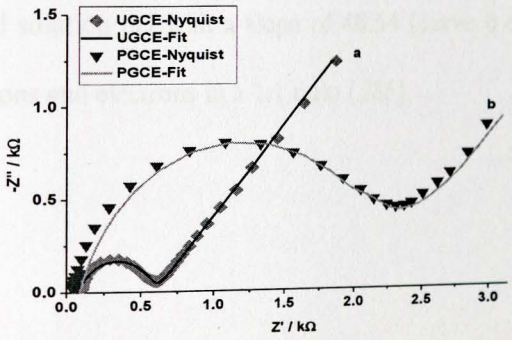

Fig. 63. Electrochemical impedance spectroscopic plots measured in 10 mM $Fe(CN)_6^{3-}/Fe(CN)_6^{4-}$ + 0.1 M KCl + PBS (pH 7.0) for UGCE (a) and pGCE (b) at an applied potential +0.23 V, amplitude 10 mV and frequency range 0.01-100000 Hz. The solid lines represent the best-fits according to the proposed EEC; Rs (Q[R_{ct}W])

4.3.4 Effect of pH

The effect of pH on the peak current and peak potential of the irreversible reduction peak of FT at the pGCE was investigated in the pH range 3.0 to 6.0. Fig. 64A represents cyclic voltammograms of 50 $\times$ 10^{-6} M FT in ABS of various pHs at pGCE. The reductive peak current increased with pH until it reached its maximum at pH 5.4 and then begun to decrease slightly (curve a of Fig. 64B). The peak current decrease observed at a pH higher than 5.4 could be ascribed to the decreasing proton concentration in the buffer system ($pKa \approx 4.75$) which is needed for the reduction of the nitro-group of FT. Therefore, pH 5.4 was taken as the optimum solution pH for further analyses.

The effect of solution pH on the reductive peak potential of FT was also investigated. A potential shift in the negative direction was observed with increasing pH indicating the participation of protons in the reduction of FT. A linear relationship between reductive peak potential (E_{pc}) and solution pH with a slope of 48.54 (curve b of Fig. 64B) shows the participation of protons and electrons in a 1:1 ratio [285].

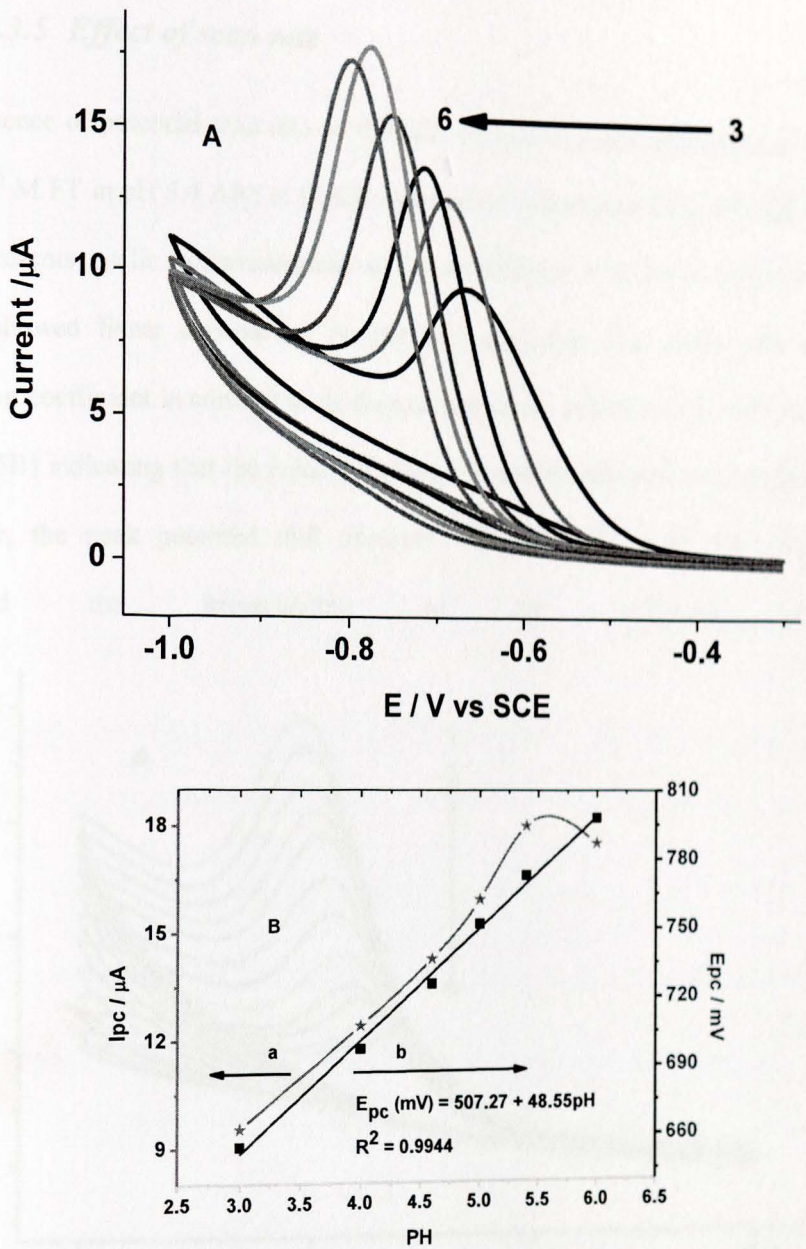

Fig. 64. (A) Cyclic voltammograms of 50 $\times 10^{-6}$ M FT in ABS of various pHs (3.0, 4.0, 4.6, 5.0, 5.4, 6) at pGCE. (B) Plot of reductive peak current (curve *a*) and reductive peak potential (curve b) versus pH of ABS containing 50 $\times$ 10^{-6} M FT at pGCE

4.3.5 Effect of scan rate

The influence of potential scan rate on the peak current (I_{pc}) and peak potential (E_{pc}) of 50×10^{-6} M FT in pH 5.4 ABS at PGCE was studied in the range 10 to 250 mV s^{-1}. Fig. 63A represents cyclic voltammograms of FT at different scan rates. Reductive peak current showed linear dependence on potential scan rate (Fig. 65B) with a better correlation coefficient in contrast to its dependence on the square root of scan rate (Inset of Fig. 65B) indicating that the reduction kinetics is surface-adsorption controlled [157]. Moreover, the peak potential shift observed with increasing scan rate (Fig. 65A) confirmed the irreversibility of the reduction reaction.

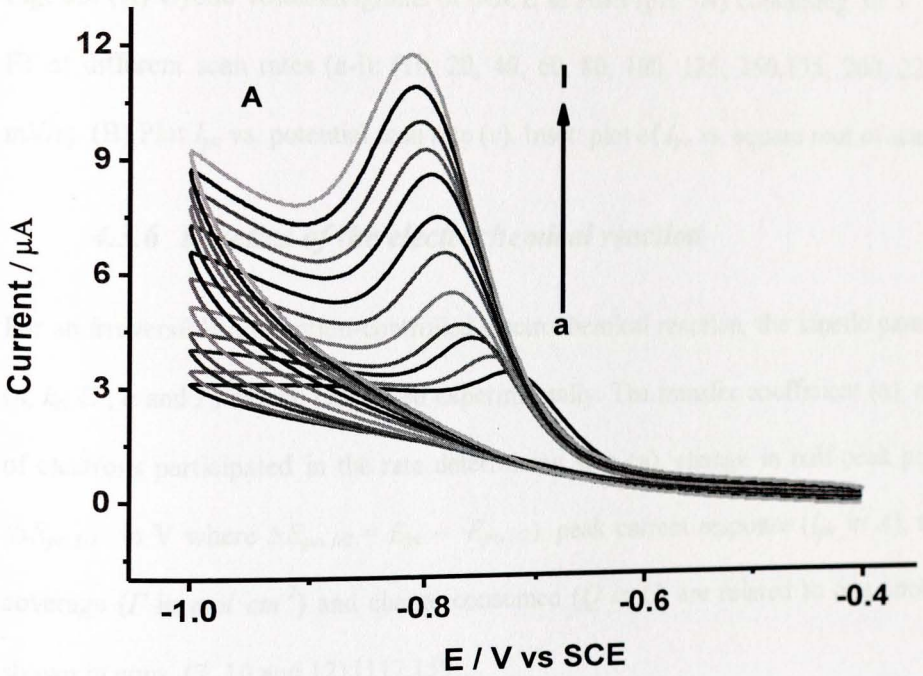

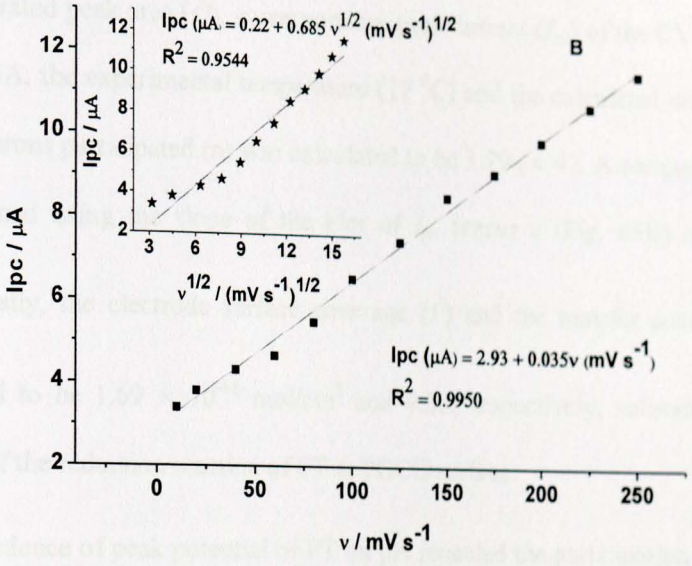

Fig. 65. (A) Cyclic voltammograms of pGCE in ABS (pH 5.4) containing 50 × 10^{-6} M FT at different scan rates (a-l): (10, 20, 40, 60, 80, 100, 125, 150,175, 200, 225, 250 mV/s). (B) Plot I_{pc} vs. potential scan rate (v). Inset: plot of I_{pc} vs. square root of scan rate

4.3.6 Kinetics of the electrochemical reaction

For an irreversible adsorption-controlled electrochemical reaction, the kinetic parameters (n, k_s, E^o, α and Γ) can be calculated experimentally. The transfer coefficient (α), number of electrons participated in the rate determining step (n), change in half-peak potential ($\Delta E_{pc,1/2}$ in V where $\Delta E_{pc,1/2} = E_{pc} - E_{pc,1/2}$), peak current response (I_{pc} in A), surface coverage (Γ in $mol\ cm^{-2}$) and charge consumed (Q in C) are related to one another as shown in eqns. (7, 10 and 12) [117,159].

Using the wave at scan rate of 0.1 V s^{-1} in Fig. 65, $\Delta E_{pc,1/2}$ and αn were calculated to be 0.046 V and 1.33, respectively.

Using the integrated peak area (Q), corresponding peak current (I_{pc}) of the CV at ν of 0.1 V s^{-1} in Fig. 65A, the experimental temperature (17 ^{0}C) and the calculated αn value, the number of electrons participated (n) was calculated to be 3.79 (≈ 4). A comparable value was also obtained using the slope of the plot of I_{pc} *versus* ν (Fig. 65B) equating to $\frac{(\alpha n)nFQ}{2.718RT}$. Finally, the electrode surface coverage (Γ) and the transfer coefficient (α) were calculated to be 1.69 × 10^{-11} mol/cm^2 and 0.33, respectively, substantiating the irreversibility of the reduction reaction of FT at PGCE surface.

Since the dependence of peak potential of FT on pH revealed the participation of protons and electrons in a 1:1 ratio and the number of electrons participated is 4, the reaction mechanism depicted in scheme 13 is proposed for the irreversible reduction reaction of FT at the pGCE, which is in agreement with the mechanism reported elsewhere [227].

$$R\text{-}NO_2 + 4e^- + 4H^+ \longrightarrow R\text{-}NHOH + H_2O$$

where R- is methyl group.

Scheme 13 Proposed reaction mechanism for the irreversibly reduction reaction of FT

The peak potential of FT at pGCE, varied linearly with scan rate in the range studied obeying the regression equation: E_{pc} (mV) = 0.2 ν + 762 mV with correlation coefficient (R^2) of 0.995 (Fig. 66). The formal potential (E^o), which is represented by the intercept of plot of E_{pc} *versus* ν [286], was found to be 0.762 V.

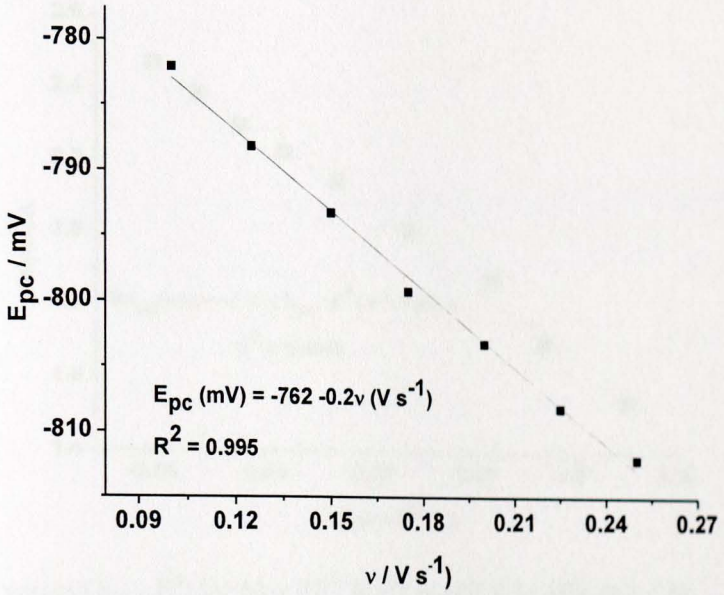

Fig. 66. Plot of E_{pc} of 50 × 10^{-6} M FT in 0.1 M ABS (pH 5.4) versus scan rate

For an adsorption-controlled totally irreversible electrode process, the peak potential (E_{pc}) is related to the scan rate (υ) by the Laviron's equation [247]. Rearrangement of eqn. (11) after the scan rate is replaced by its value in eqn. (10) gives eqn. (22), which relates peak current response with the overpotential (E_{pc}-E^0).

The intercept of the linear plot of ln(I_{pc}) *versus* overpotential (E_{pc} - E^0) (Fig. 67) was used to calculate the heterogeneous rate constant (k_s) of the reduction reaction of FT as 5.29 cm s^{-1}.

$$I_{pc} = \frac{n^2 FA\Gamma k_s}{2.178} e^{\frac{-\alpha nF}{RT}(E_{pc} - E^0)} \quad \text{.....(22)}$$

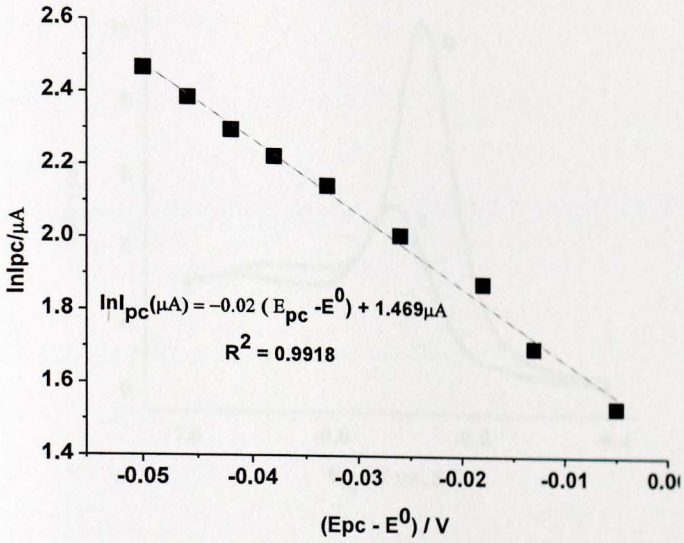

Fig. 67. ln (I_{pc}) versus (E_{pc} - E^0) for 50 × 10^{-6} M FT at pGCE in ABS (pH 5.4).

4.3.7 SWV for the quantitative analyses of FT at pGCE

Since square wave voltammetry (SWV) has a much higher sensitivity and better resolution than cyclic voltammetry, the applicability of pGCE for the quantitative determination of FT has been investigated using SWV.

Fig. 68 describes the square wave voltammograms of UGCE and pGCE in pH 5.4 ABS containing 50 × 10^{-6} M FT. The peak current response at pGCE (curve b) was two-folds when compared to the peak at the UGCE (curve a) besides the peak potential shift in the positive direction by about 40 mV. The peak current enhancement and peak potential shift are conformations for the electrocatalytic effect of the pGCE towards FT reduction.

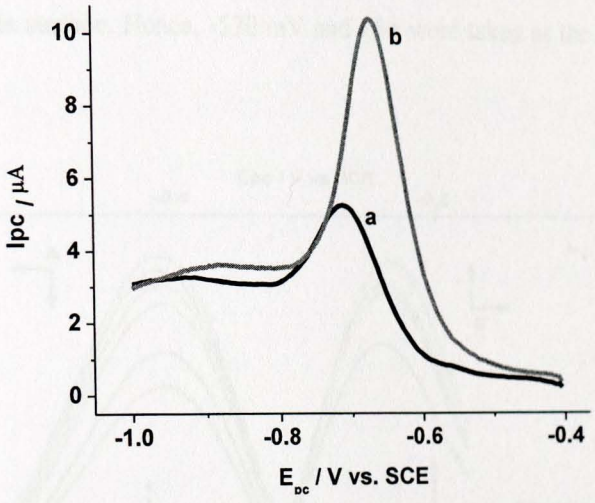

Fig. 68. SWVs of 50 × 10^{-6} M FT in ABS (pH 5.4) at UGCE (a) and pGCE (b)

Taking in to account the peak current response and peak shape, SWV parameters such as the step potential, pulse amplitude and frequency were optimized to be 12 mV, 70 mV and 30 Hz, respectively.

4.3.8 Effect of accumulation potential and time

Since the reduction of FT at the pGCE is adsorption-controlled, the effect of accumulation potential (E_{acc}) and time (t_{acc}) was investigated as depicted in Fig. 69. Inset of Fig. 69 shows the dependence of accumulation potential on the peak current response of pGCE for FT at t_{acc} 30 s. The peak current increased with increasing E_{acc} from -410 to -570 mV and then decreased at higher negative potentials showing that -570 mV is the optimum accumulation potential. Inset of Fig. 69B presents the effect of t_{acc} on the peak current response of pGCE for FT recorded at E_{acc} -570 mV. The peak current increased with t_{acc} up to 75 s beyond which is leveled off. This could be due to the saturation level

of the active electrode surface. Hence, -570 mV and 75 s were taken as the optimized E_{acc} and t_{acc}, respectively.

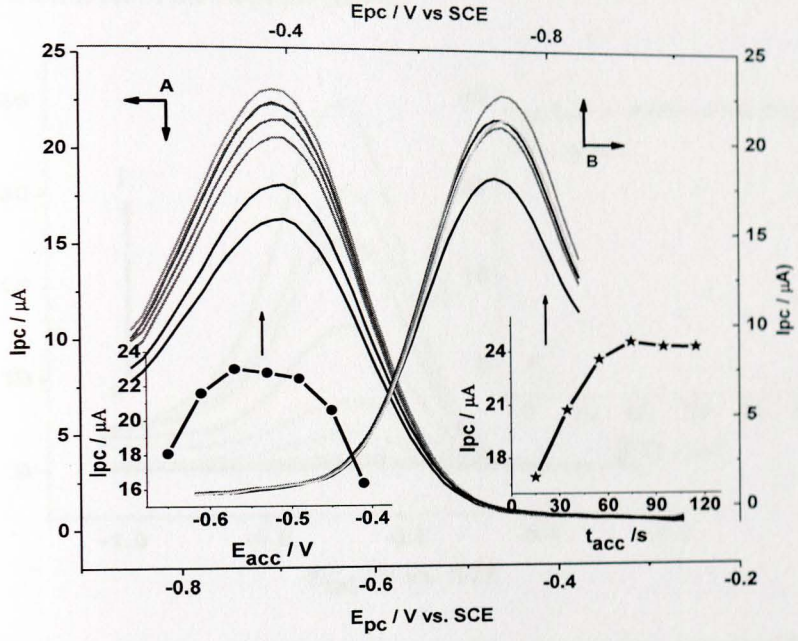

Fig. 69. SWVs of pGCE in ABS (pH 5.4) containing µM FT (A) at t_{acc} 30 s and various E_{acc}, (B) at E_{acc} -570 mV and variable t_{acc}. Step potential: 12 mV; pulse amplitude: 70; frequency: 30 Hz

4.3.9 Linear range and limit of detection

Under the optimized solution and method parameters, calibration curve was constructed by recording the SWV peak current responses of pGCE for different concentrations of standard FT (Fig. 70). The peak currents were linearly related to concentration in the range 0.4 to 50 $\times 10^{-6}$ M (Inset of Fig. 70) with a regression equation, regression coefficient (R^2) and limit of detection (LoD) of I_{pc} (µA) = 0.976C (µM) - 0.043, R^2 =

0.9972 and 7.2×10^{-8} M (S/N = 3), respectively. The observed gradual deviation from linearity of the current response for concentrations higher than 50×10^{-6} M could be due to the saturation level of the electrode surface.

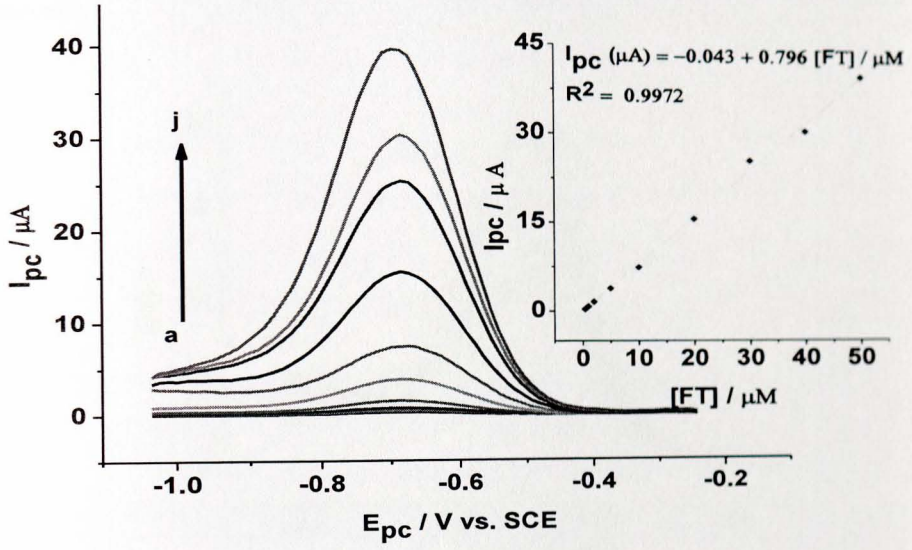

Fig. 70. SWVs of pGCE in ABS (pH 5.4) containing various concentrations of FT (a-j: 0.4, 0.6, 1, 2, 5, 10, 20, 30, 40 and 50 µM, respectively). Inset: plot of peak current vs. concentration of FT. E_{acc} -570 mV; t_{acc} 75 s; pulse amplitude (mV), step potential (mV) and frequency (Hz) of 70, 12 and 30, respectively

4.3.10 Recovery and Interference study of the developed method

The applicability of the developed method for the determination of FT in environmental samples containing potential interferents was investigated by evaluating the recovery of spiked standard FT in tap water, filtrated human urine and samples of ascorbic acid and uric acid.

4.3.10.1 Recovery study of FT from tap water

Three 10 µM standard FT samples (A, B and C) in pH 5.4 ABS were prepared using tap water. Then, the samples (A, B and C) were spiked with 5, 10 and 15 µM standard FT, respectively.

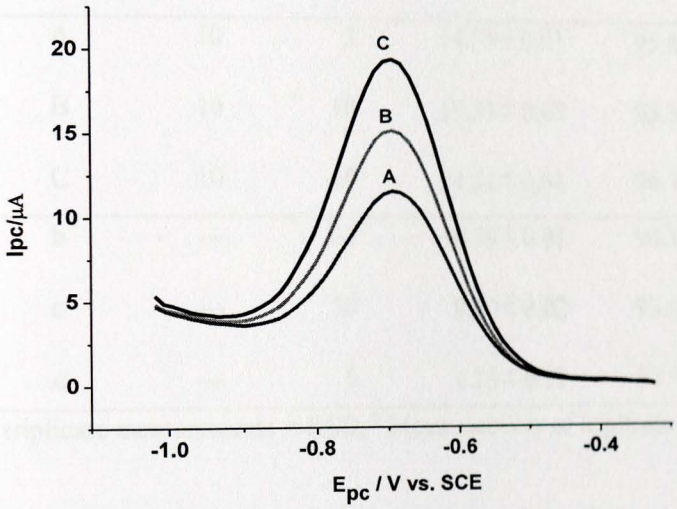

Fig. 71. SWVs of pGCE in pH 5.4 ABS (tap water) containing10 $\times 10^{-6}$ M FT spiked with (A) 5, (B) 10 and (C) 15 µM standard FT. E_{acc}: -570; t_{acc}: 75 s; pulse amplitude: 70 mV; step potential: 12 mV; frequency: 30 Hz

The SWV (Fig. 71) results recorded under the optimized conditions are summarized in Table 16. Recoveries in the range 93.3 to 96.7% showed the applicability of the developed method for quantitative determination of FT in water samples. Moreover, low RSD values indicate the reproducibility of the measurements.

Table 16 Summary of the recoveries of various concentrations of FT spiked in tap water and human urine samples using pGCE

Sample (Figure)	SWV wave	Initial (μM)	Spiked (μM)	Detected[a] (μM)	Recovery[b] (%)
Tap water	A	10	5	14.79 ± 0.01	95.8 ± 2.4
(Fig. 69)	B	10	10	19.33 ± 0.02	93.3 ± 1.4
	C	10	15	24.51 ± 0.01	96.7 ± 3.1
Human urine	b	---	20	18.79 ± 0.01	94.1 ± 0.7
(Fig. 70)	c	---	10	9.30 ± 0.02	93.0 ± 1.9
	d	---	5	4.29 ± 0.12	85.7 ± 1. 9

[a] Mean of triplicate measurements ± RSD, [b] Mean recovery of triplicate ± %error

4.3.10.2 Recovery study of FT from human urine

Three tap water and human urine samples (labeled A-C and b-d, respectively) were prepared as described in the procedure under experimental part. The three urine samples were spiked with appropriate amounts of standard FT until the final concentrations are 20, 10 and 5 μM, respectively. Recoveries in the range 85.73-93.3% from human urine (summarized in Table 16) still indicated the applicability of the method for determination FT in real samples. Moreover, lower recovery for a lower concentration of FT (curve *d* of Fig. 72) signified the influence of urine matrix in the determination of FT from human urine at low concentrations. The slight potential shift observed for the SWVs of FT in

human urine samples (curves b-d in contrast to curve a of Fig. 72) could probably be due to the effect of co-adsorption of urine matrix.

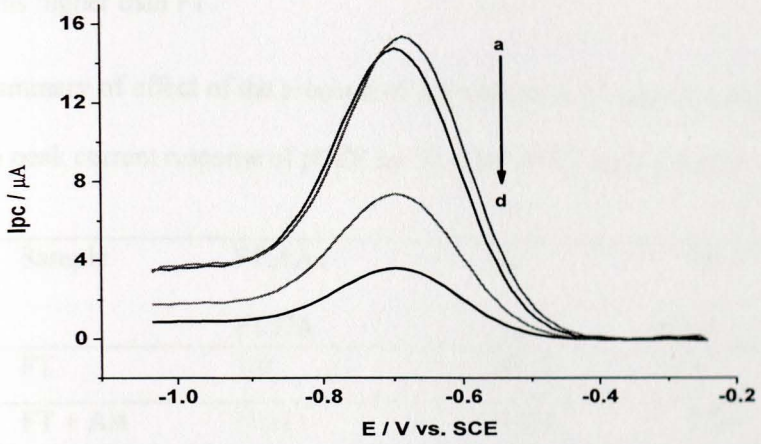

Fig. 72. SWVs of (a) 20 × 10^{-6} M FT in pH 5.4 ABS and (b-d) 20, 10 and 5 µM FT, respectively spiked to human urine diluted with pH 5.4 ABS. E_{acc}: -570; t_{acc}: 75 s; pulse amplitude: 70 mV; step potential: 12 mV; frequency: 30 Hz

4.3.10.3 Interference studies

The applicability of the developed method for determination of FT in the presence of potential interferents was studied (Fig. 73). The peak current responses of pGCE for a 50 × 10^{-6} M FT in the presence of ascorbic acid (AA) and uric acid (UA) in a 1:1 and 1:2 ratio are summarized in Table 17. In the presence of AA in a 1:1 ratio, the peak current of FT decreased by 9.1% (curve *b* of Fig. 73A). On increasing the amount of AA to 1:2 level, the peak current of FT remained the same (curve c of Fig. 73A) indicating that analyses of FT is not significantly influenced by AA. Conversely, presence of UA in a 1:1 ratio with FT showed no observable influence on the peak current of FT (*curve b* of

Fig. 73B). However, it caused a decrease in peak current of FT by 9.9% when its amount is increased to 1:2 level (*curve c* of Fig. 73B) showing the interference of UA at concentrations higher than FT.

Table 17 Summary of effect of the presence of AA and UA at 1:1 and 1:2 concentration ratios on the peak current response of pGCE for 50×10^{-6} M FT in pH 5.4 ABS

Sample	FT:AA / FT:UA	I_{pc} (μA)	% (error)
FT	1:0	48.55	-------
FT + AA	(1:1)	44.11	9.10
FT + AA	(1:2)	43.93	9.50
FT + UA	(1:1)	48.59	0.08
FT + UA	(1:2)	43.74	9.90

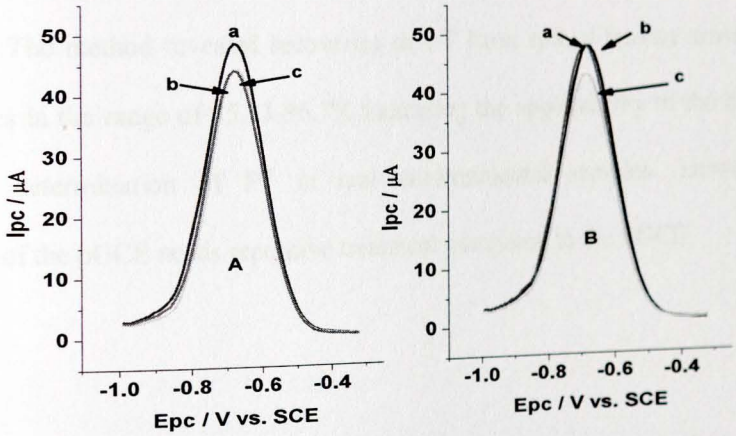

Fig. 73. SWV of pGCE in 0.1 M ABS (pH 5.4) containing 50 x 10-6 M FT with ascorbic acid (A), and uric acid (B). E_{acc}: -570; t_{acc}: 75 s; pulse amplitude: 12 mV; step potential: 12 mV; frequency: 30 Hz

4.3.11 Conclusion

The electrochemical behavior of FT both at UGCE and pGCE was studied using cyclic voltammetry. An irreversible reductive peak with a quasireversible redox couple appeared at both electrodes. In contrast to the UGCE, pGCE showed about 2-folds of peak current enhancement and potential shift to lower values signifying its catalytic activity towards FT. The effects of pH and scan rate on peak current and peak potential for the irreversible reductive peak of FT were investigated and the kinetic parameters (n, α, k_s, E^0, $\Delta E_{pc,1/2}$ and Γ) were estimated. A reaction mechanism involving 4-electron 4-proton reduction of the nitro-functional group of FT was proposed.

The SWV current response of pGCE for FT varied linearly with the concentration in the range 0.4-50 $\times$ 10^{-6} M with a linear regression equation, correlation coefficient and limit of detection of I_{pc} (μA) = 0.796 C (μM) -0.043, R^2 = 0.9972 and 7.8 $\times$ 10^{-8} M (S/N = 3), respectively. The method revealed recoveries of FT from spiked human urine and tap water samples in the range of 85.73-96.7% indicating the applicability of the developed method for determination of FT in real environmental samples. However, the regeneration of the pGCE needs repetitive treatment compared to the PGCE.

REFERENCES

[1] Shamsa, F.; Monsef, H.; Ghamooshi, R.; Verdian-rizi, M. *Thai J. Pharm. Sci.* **2008,** 32, 17.

[2] Okwu, D.E.; Okwu, M.E. J. *Sustain Agric. Environ.* **2004,** 6, 140.

[3] Okwu, D.E. *Int. J. Mol. Med. Adv. Sci.* **2005**, 1, 375.

[4] Copper, C.L.; Newman, C.I.D.; Collins, G.E. *J. Sep. Sci.* **2008**, 31, 3727.

[5] Donarski, W.J.; Dumas, D.P.; Heitmeyer, D.P.; Lewis, V.E.; Raushel, F.M. *Biochemistry* **1989**, 28, 4650.

[6] Chapalamadugu, S.; Chaudhry, G.S. *Crit. Rev. Biotechnol.* **1992**, 12, 357.

[7] Compton, J.A. *Military Chemical and Biological Agents*, Telford Press, NJ, **1988**, pp135.

[8] Food and Agricultural Organization of the United Nations, FAO Product Yearbook, Rome, **1989**, *Vol.* 43.

[9] United States Department of Agriculture, Agricultural Statistics. United States Government Printing Office, Washington, DC, **1992**, pp395.

[10] Munnecke, D.M. *J. Agric. Food Chem.* **1980**, 28, 105.

[11] Coppella, S.J.; DelaCruz, N.; Payne, G.F.; Pogell, B.M.; Speedie, M.K.; Karns, J.S.; Sybert, E.M.; Connor, M.A. *Biotechnol. Prog.* **1990**, 6, 76.

[12] Caldwell, S.R.; Raushel, F.M. *Biotechnol. Bioeng.* **1991,** 37, 103.

[13] Grice, K.J.; Payne, G.F.; Karns, J.S. *J. Agric. Food Chem.* **1996**, 44, 351.

[14] Mulbury, W.M.; Del Valle, P.L.; Karns, J.S. *Pestic. Sci.* **1996**, 48, 149.

[15] LeJeune, K.E.; Mesiano, A.J.; Bower, S.B.; Grimsley, J.K.; Wild, J.R.; Russell, A.J. *Biotechnol. Bioeng.* **1997**, 54, 105.

[16] Rainina, E.; Efremenco, E.; Varfolomeyev, S.; Simonian, A.L.; Wild, J. *Biosens. Bioelectron.* **1996**, 11, 991.

[17] Heeger, A.J.; MacDiarmid, A.G.; Shirakawa, H. "*The Nobel Prize in Chemistry, 2000: Conductive polymers*", May **2010**, Available: http://nobelprize.org/nobel_prizes/ chemistry/laureates/2000/chemadv.

[18] Angelopoulos, M. *IBM J. Res. Develop.* **2001**, 45, 57.

[19] Merz, A.; Bard, A.J. *J. Am. Chem. Soc.* **1978**, 100, 3222.

[20] Ehsani, A.; Mahjani, M.G.; Jafarian, M. *Synthetic Metals* **2012**, 162, 199.

[21] Refaey, S.A.M. *Synthetic Metals* **2004**, 40, 87.

[22] Gao, J.; Lai, Y. *Polymer* **2009,** 50, 1830.

[23] Stallinga, P. "*Electrical Characterization of Organic Electronic Materials and Devices",* John Wiley & Sons Ltd, United Kingdom, **2009**.

[24] Bower, D.I. "*An Introduction to Polymer Physics*", Cambridge University Press, Cambridge **2002**, 444.

[25] Pron, A.; Rannou, P. *Prog. Polym. Sci.* **2002**, 27, 135.

[26] Lee, J.W.; Park, D.S.; Shim, Y.B.; Park, S.M. *J. Electrochem. Soc.* **1992**, 139, 3507.

[27] Paul, E.W.; Ricco, A.J.; Wrighton, M.S. *J. Phys. Chem.* **1985**, 89, 1441.

[28] Miller, L.L.; Van de Mark, M.R. *J. Am. Chem. Soc.* **1978,** 100, 3223.

[29] Park, S.M. *Electrochemistry of p-Conjugated Polymers. In: Handbook of Organic Conductive Molecules and Polymers,* Nalwa, H. S., Ed., Chichester, Wiley, **1997**, *Vol.* 3.

[30] Guiseppi-Elie, A.; Wallace, G.G.; Matsue, T. *In: Handbook of Conducting Polymers,* 2nd ed.; Skotheim, T. A.; Elsenbaumer, R.; Reynolds, J. R., Eds.; Marcel Dekker; New York, **1998**, 963.

[31] Rahman, M.A.; Kumar, P.; Park, D.S.; Shim, Y.B. *Sensors* **2008,** 8, 118.

[32] Arbizzani, C.; Mastragostino, M.; Scrosati, B. *In: Handbook of Organic Conductive Molecules and Polymers,* Nalwa, H. S., Ed., Chichester, Wiley **1997,** 4, 595.

[33] Chaubey, A.; Malhotra, B.D. *Biosens. Bioelectron.* **2002**, 17, 441.

[34] Mulchandani, A.K.; Wang, C.L. *Electroanalysis* **1996,** 8, 414

[35] Revin, S.B.; John, S.A. *Electroanalysis* **2012**, 24, 1277.

[36] Chicharro, M.; S´anchez, A.; Zapardiel, A.; Rubianes, M.D.; Rivas, G. *Analytica Chimica Acta* **2004**, 523, 185.

[37] Gilbert, O.; Chandra, U.; Swamy, B.E.K.; Char, M.P.; Nagaraj, C.; Sherigara, B.S. *Int. J. Electrochem. Sci.* **2008**, 3, 1186.

[38] Gouveia-Caridade, C.; Brett, C.M.A. *Curr. Anal. Chem.* **2008**, 4, 206.

[39] Martins, M.; Boas, M.V.; Castro, B.; Hillman, A.R.; Freire, C. *Electrochimica Acta* **2005**, 51, 304.

[40] Yang, Z.; Hu, G.; Liu, Y.; Zhao, J.; Zhao, G. *Can. J. Anal. Sci. Spect.* **2006**, 11.

[41] Xu, X.L; Huang, F.; Zhou, G.L.; Zhang, S.; Kong, J.L. *Sensors* **2010**, 10, 8398.

[42] Ya, Y.; Luo, D.; Zhan, G.; Li, C. *Bull. Korean Chem. Soc.* **2008**, 29, 928.

[43] Cartwell, R. W. *Chemical sensors*, Oxford University Press, **1997**.

[44] Luther, J.M.; Law, M.; Song, Q.; Perkins, C.L.; Beard, M.C.; Nozik, A. *J. Am. Chem. Soc.* **2008**, 2, 271.

[45] Talapin, D.V.; Murray, C.B. *Science* **2005**, 310, 86.

[46] Juttner, K.; Schmitz, R.H.J.; Hudson, A. *Electrochimica Acta* **1999**, 44, 4177.

[47] Benyoucef, A.; Boussalem, S.; Ferrahi, M.I.; Belbachir, M. *Synthetic metals* **2010**, 160, 1591.

[48] Yang, G.J.; Qu, X.L.; Zhu, A.P.; Wang, C.Y.; Qu, Q.S. Hu, X.Y. J. Electroanal. Chem. 2007, doi:10,1016/j.jelechem.2007.02.024.

[49] Jin, G.; Zhang, Y.; Cheng, W. *Sens.Actuators B* **2005**, 107, 528.

[50] Ensafi, A.A.; Taei, M.; Khayamian, T. *J. Electroanal. Chem.* **2009**, 633, 212.

[51] Ensafi, A.A.; Taei, M.; Khayamian, T. *Colloids Surf. B* **2010**, 79, 480.

[52] Ensafi, A.A.; Rezaei, B.; Zare, S.Z.M.; Taei, M. *Sens.Actuators B* **2010**, 150, 321.

[53] Springfield, E.P.; Eagles, P.K.F.; Scott, G. *J. Ethnobotany* **2005**, 101, 75.

[54] Owolabi, M.A.; Coker, H.A.B.; Jaja, S.I. J. Nat. Med. 2007, 61, 200.

[55] Kraus, P.F.; Kutchan, T.M. *Proc. Natl. Acad. Sci. USA* **1995**, 92, 2071.

[56] Hamscher, G.; Prieâ, B.; Nau, H.; Panariti. E. *Anal. Chem.* **2005**, 77, 2421.

[57] Dehon, B.; Chagnon, J.L.; Vinner, E.; Pommery, J.; Mathieu, D.; Lhermitte, M. *Biomed.Chromatogr*. **1999**, 13, 235.

[58] Brvar, M.; Ploj, T.; Kozelj, G.; Mozina, M.; Noc, M.; Bunc, M. *Critical Care* **2004**, 8, 56.

[59] Chicharro, M.A.; Bermejo, Z.E.; Perez, J.A.; Hernandez, L. *Analytica Chimica Acta* **1993,** 273, 361.

[60] Ansell, R.J.; Wang, D.Y.; Kuah, J.K.L. *Analyst* **2008**, 133, 1673.

[61] Nikolelis, D.P.; Raftopoulou, G.; Siontorou, C.G. *Electroanalysis* **2005**, 17, 1870.

[62] Anbao, W.; Lijun, L.; Fang, Z.; Yuzhi, F. *Analytica Chimica Acta* **2000**, 419, 235.

[63] Daly, J.W. *J. Auton. Nerv. Syst.* **2000**, 81, 44.

[64] Rall, T.W. *The pharmacological basis of therapeutics*. McGraw-Hill, New York, **1993**.

[65] James, J.E. *Caffeine and health.* Academic Press Inc. San Diego, **1991**.

[66] Garrido, E.M.; Delerue-Matos, C.; Lima, J.L.F.C.; Brett, A.M.O. *Anal. Lett.* **2004,** 37, 1755.

[67] Jirnenez, A.M.; Navas, M.J. *Crit. Rev. Anal. Chem*. **1997**, 27, 291.

[68] Pimental, D.; Levitan, L. **Biosciences** 1986, 36, 86.

[69] Corbett, J.R.; Wright, K.; Baillie, A.C. *The biochemical mode of action of pesticides,* 2nd ed., Academic press, London, **1984**.

[70] Espinosa, M.; Atanasov, P.; Wilkins. E. *Electroanalysis* **1999**, 11, 1055.

[71] Lin, Y.; Lu, F.; Wang, J. *Electroanalysis* **2004**, 16, 145.

[72] Wang, J.; Gang, C.; Alexander, M.; Chatrathi, M.P.; Mulchandani, A.; Wilfred, C. *Analytica Chimica Acta* **2004**, 505, 183.

[73] Lartiges, S.B.; Garrigues, P.P. *Environ. Sci. Technol.* **1995**, 29, 1246.

[74] Diagne, R.G.; Foster, G.D.; Khan, S.U. *J. Agric. Food Chem.* **2002**, 50, 3204.

[75] Yu, L.; Priti, M.; Wilfred, C.; Ashok, M. *Sensors* **2006**, 6, 466.

[76] Yu, L.; Priti, M.; Wilfred, C.; Ashok, M. *Appl. Biochem.Biotechnol.* **2007**, 136, 243.

[77] Derbalah, A.S.; Nakatani, N.; Sakugawa, H. *Chemosphere* **2004**, 57, 635.

[78] Mulchandani, L.A.; Chen, W.; Mulchandani, P.; Wang, J.; Rogers, K.R. *Biosens. Bioelectron.* **2001**, 16, 225.

[79] Janotta, M.; Karlowatz, M.; Vogt, F.; Mizaikoff, B. *Anal. Chim. Acta* **2003**, 496, 339.

[80] Simón, B.P.; Campàs, M.; Andreescu, S.; Marty, J.L. *Sensors* **2006**, 6, 1161.

[81] Durand, G.; Abad, J.L.; Srlnchez-Baeza, F.; Messeguer, A.; Barcelo, D. *J. Agric. Food Chem.* **1994**, 42, 814.

[82] Lacorte, S.; Barcelo, D. *Environ. Sci. Technol.* **1994**, 28, 1159.

[83] Simonian, A.L.; Rainina, E.I.; Wild, J.R. *Anal. Lett.* **1997**, 30, 2453.

[84] Shi, M.; Xu, J.; Zhang, S.; Liu, B.; Kong, J. *Talanta* **2006**, 68, 1089.

[85] Arun, P.P.; Yogeswaran, U.; Shen-Ming, C. *Sensors* **2009**, 9, 4034.

[86] Namba, T.; Nolte, C.T.; Jackrel, J.; Grob, D. *Am. J. Med*, **1971**, 50, 475.

[87] Li, B.; He, Y.; Xu, C. *Talanta* **2007**, 72,223.

[88] Ansell, R.J.; Wang, D. *Analyst* **2009**, 134, 564.

[89] Spyridaki, M.H.; Tsitsimpikou, C.J.; Siskos, P.A.; Georgakopoulos, C.G. *J. Chromatogr B Biomed Sci Appl.* **2001**, 758, 311.

[90] Fernandez, P.L.; Martin, M.J.; Gonzalez, A.G.; Pablos, F. *Analyst* **2000**, 125, 421.

[91] Meyer, A.; Ngiruwonsanga, T.; Henze, G. *Fresenius' J. Anal. Chem.* **1996**, 356, 284.

[92] Holland, D.T.; Godfredsen, K.A.; Page, T.; Connor, J.D. *J. Chromatogr. B* **1998**, 707, 105.

[93] Pavlova, V.; Petrovska – Jovanović, S. *Acta Chromatographica* **2007**, 18, 157.

[94] Gebreegzi, Y.T.; Foster, G.D.; Khan, S.U. *J. Agric. Food Chem.* **2000**, 48, 5165.

[95] Fulton, M.; Key, P.; Leight, A.K.; Daugomah, J.; Bearden, D.; Sivertsen, S.; Scott, G. *Environ. Toxicol. Chem.* **2001**, 20, 37.

[96] Zuin, V.G.; Yariwake, J.H.; Bicchi, C. *J. Chromatogr. A* **2003**, 985, 159.

[97] Brito, N.M.; Navickiene, S.; Polese, L.; Jardim, E.F.G.; Abakerli, R.B.; Ribeiro, M.L. *J. Chromatogr. A* **2002**, 957, 201.

[98] Ahmadi, F.; Assadi, Y.; Hosseini, M.R.M.; Rezaee, M. *J. Chromatogra. A* **2006**, 1101, 307.

[99] Jin, Y.; Yao, J.B.; Fu, H.B.; Pan, W.; Geng, Q.H.; Ma, W. *Chinese Journal of Health Laboratory Technology* **2007**, 17, 1153.

[100] Li, S.X.; Huang, W.X.; Chen, M. *J Environ Health* **2006**, 23, 458.

[101] Ingelse, B.A.; van Dam, R.C.J.; Vreeken, R.J.; Mol, H.G.J.; Steijger, O.M. *J. Chromatogr. A* **2001**, 918, 67.

[102] Martha, P.; María, L *Food Chem.* **2009**, 114, 1510.

[103] Lu, J.Z.; Lau, C.; Lee, M.K.; Ka, M. *Anal. Lett.* **2002**, 455, 193.

[104] Zhang, H.; Zhao, J.; Liu, H.; Wang, H.; Liu, R.; Liu, J. *Int. J. Electrochem. Sci,* **2010**, 5, 295.

[105] Lane, R.F.; Blaha, C.D. *Langmuir* **1990**, 6, 56.

[106] Ewing, A.G.; Dayton, M.A.; Wightman, R.M. *Anal. Chem.* **1981**, 53, 1842.

[107] Mattson, J.S.; Jones, T.T. *Anal. Chem.* **1976**, 48, 2164.

[108] Koshets, I.A.; Kazantseva, Z.I.; Shirshov, Yu.M. *Semicond. Phys. Quantum Electron. Optoelectron.* **2003**, 6, 505.

[109] Ohnuki, Y.; Ohsaka, T.; Matsuda, H.; Oyama, N. *J. Electroanal. Chem.* **1983**, 158, 55.

[110] Volkov, A.; Tourillon, G.; Lacaze, P.C.; Dubois, J.E. *J. Electroanal. Chem.* **1980**, 115, 279.

[111] Zhao, H.; Zhang, Y.Z.; Yuan, Z.B. *Anal. Chim. Acta* **2001,** 441,117.

[112] Vinjamuri, A.; Burris, S.C.; Dahl, D. *ECS trans.* **2008**, 13, 9.

[113] Ozden, M.; Ekinci, E.; Karagozler, A.E. *Turk J Chem.* **1999**, 23, 89.

[114] Gospodinova, N.; Terlemezyan, L. *Prog. Polym. Sci.* **1998**, 23, 1443.

[115] Hui, D.; Alexandrescu, R.; Chipara, M.; Morjan, I.; Aldica, G.; Chipar, M.D.; Lau, K.T. *Journal of Optoelectronics and Advanced Materials* **2004,** 6, 817.

[116] Ansari, A.; Keivani, M.B. *E-Journal of Chemistry* **2006**, 3, 202.

[117] Bard, J.A.; Faulkner, L.R. *Electrochemical methods: Fundamentals and applications,* 2nd ed., John Wiley& Sons, **2001**.

[118] Bagotsky, V.S. *Fundamentals of Electrochemistry*, 2nd ed., Wiley, New York **2005**.

[119] Antropov, L.I.; Beknazarov, A. *Theoretical Electrochemistry*, University Press of the Pacific, **2001**.

[120] Wang, J. *Analytical Electrochemistry*. 3rd ed., John Wiley& Sons, New York, **2006.**

[121] Yilmaz, S.; Skrzypek, S.; Dilgin, Y.; Yagmur, S.; Coskun, M. *Curr. Anal. Chem.* **2007**, 3, 41.

[122] Zhang J.; Trombly N.; Mason A. *IEEE Int. Conf. on Sensors,* Vienna, Austria **2004**.

[123] Niaz, A.; Sirajuddin, N.; Shah, A.; Mahesar, S.A.; Rauf, A.; Pak. J. *Anal. Environ. Chem.* **2008**, 9, 110.

[124] Heinze, J. *Angew. Chem.* **1984**, 23, 831.

[125] Kounaves, S.P. *Voltammetric techniques, in Handbook of Instrumental Techniques for Analytical Chemistry*, Settle, F. (Ed.), Prentice Hall PTR, **1997**, 37.

[126] Yilmaz, N.; Ozkan, S.A.; Uslu, B.; Senturk, Z.; Biryol, I. *Turk. J. Chem.* **1998**, 22, 175.

[127] Nicholson, R.S. *Anal. Chem.* **1966**, 38, 1406.

[128] Lovric, M. *Square-wave voltammetry, in Electroanalytical Methods*, Scholz, F. (Ed.), Springer, Berlin, Heidelberg, New York, **2001**.

[129] Pocard, N.L.; Aismeyer, D.C.; McCreery, R.L.; Neenan, T.X.; Callstrom, M.R. *J. Mater. Chem.* **1992**, 2, 771.

[130] Laviron, E. *J. Electroanal. Chem.* **1979**, 101, 19.

[131] Stojek, Z. *Pulse voltammetry, in Electroanalytical Methods*, Scholz, F. (Ed.), Springer, Berlin, Heidelberg, New York, **2001**.

[132] Macdonald, J.R. *Impedance Spectroscopy: Emphasizing Solid Materials and Systems*, John Wiley & Sons, New York **1987.**

[133] Suni, I.I. *Trends Anal. Chem.* **2008**, 27, 604.

[134] Sluyters-Rehbach, M. *Pure & Appl. Chem.* **1994**, 66, 1831.

[135] Nahir, T.M.; Bowden, E.F. *Electrochim. Acta* **1994**, 39, 2347.

[136] Boubour, E.; Lennox, R.B. *J. Phys. Chem. B* **2000**, 104, 9004.

[137] Boubour, E.; Lennox, R.B. *Langmuir* **2000**, 16, 7464.

[138] Janek, R.P.; Fawcett, W.R. *Langmuir* **1998**, 14, 3011.

[139] Barsoukov, E.; Macdonald, J.R. *Impedance spectroscopy: theory, experiment, and applications*, 2nd edn. Wiley, NewJersey, **2005**.

[140] Horvat-Radosevic, V.K.; Kraljic-Rokovic, M. *Electrochim. Acta* **2006**, 51, 3417.

[141] Mulder, W.H.; Sluyters, J.H. *J. Electroanal. Chem.* **1990**, 285, 103.

[142] Tribollet, B. *J. Electroanal.Chem.* **1989**, 37, 264.

[143] DeVooys, D.A.; Pieper, J.H.A. *J. Elecrroanal. Chem.* **1976**, 72, 147.

[144] Epelboin, I.; Keddam, M. J. *Electrochem. Sot.* **1970**, 117, 1052.

[145] Hladky, K.; Callow, L.M.; Dawson, J.L. *Br. Corros. J.* **1980**, 15, 20.

[146] Rammelt, U.; Reinhard, G.; Rammelt, K. *J. Elecrroanal. Chem.* **1984**, 180, 327.

[147] Silverman, D.C.; Carrico, J.E. *Corrosion* **1988**, 44, 280.

[148] Walter, G.W. *Corros. Sci.* **1991**, 32, 1059.

[149] Thompson, I.; Campbell, D. *Corros. Sci.* **1994**, 36, 187.

[150] Adrian, W.B. *Electrochemical Techniques for the Characterization of Redox Polymers.* **(2001).** West Lafayette; Bioanalytical Systems [on-line]. Available: http://www.Currentseparations. Com..

[151] Hunter, T.B.; Tyler, P.S.; Smyrl, W.H.; White, H.S. *J. Electrochem. Soc.* **1987**, 134, 2198.

[152] Kouloumbi, N.; Tsangaris, G.M.; Kyvelidis, S.T. J. *Coat. Technol.* **1994**, 66, 83.

[153] Ross, G.J.; Watts, J.F.; Hill, M.P.; Morrissey, P. *Polymer* **2000,** 41, 1685.

[154] Barr, T. *Crit. Rev. Anal. Chem.* **1991**, *Vol.* 115.

[155] Laskin, A.; Cowin, J.P.; Iedema, M.J. *Journal of Electron Spectroscopy and Related Phenomena* **2006**, 150, 260.

[156] Bragadeeswaran, S.; Balasubramanian, S.T.; Raffi, S.M.; Sophia, S. *World Appl. Sci. J.* **2010**, 10, 169.

[157] Acosta, A.; Aineto, M.; Iglesias, I.; Romero, M.; Rincon, J.M. *Materials Letters* **2001**, 50, 246.

[158] Li, F.; Song, J.; Gao, D.; Zhang, Q.; Han, D.; Niu, L. *Talanta* **2009**, 79, 845.

[159] Mazloum-Ardakani, M.; Rajabi, H.; Beitollahi, H.; Mirjalili, B.B.; Akbari, A.; Taghavinia, N. *Int. J. Electrochem. Sci.* **2010**, 5, 147.

[160] Pawlak, M. K. *Pol. J. Environ. Stud.* **2004**, 13, 411.

[161] Wylie, F.M.; Torrance, H.; Seymour, A.; Buttress, S.; Oliver, J.S. *Forensic Sci. Int.* **2005,** 150, 199.

[162] Joseph, Y.; Besnard, I.; Rosenberger, M.; Guse, B.; Nothofer, H.; Wessels, J.M.; Wild, U.; Knop-Gericke, A.; Su, D.; Schlo1gl, R.; Yasuda, A.; Vossmeyer, T. *J. Phys. Chem. B* **2003**, 107, 7406.

[163] Cavallieri, O.; Oliveri, L.; Dacca, A.; Parodi, R.; Rolandi, R. *Appl. Surf. Sci.* **2001**, 175, 357.

[164] Cookeas, E.G.; Efstathiou, C.E. *Analyst* **2000**, 125, 1147.

[165] Hernandez, L.; Zapardie, A.; Bermejo, E.; Perez, J.A.; Chicharro, M.; Garijo, M.J. *Electroanalysis* **1997**, 9, 1214.

[166] Platts, M.; Smith, R.B.; Mould, N.; Davis, J. *Electrochem. Commun.* **2006**, 8, 633.

[167] Couper, F.J.; Pemberton, M.; Jarvis, A.; Hughes, M.; Logan, B.K. *J. Forensic Sci.* **2002**, 47, 562.

[168] Haller, C.A.; Jacob, P.; Benowitz, N.L. *Clin. Pharmacol. Ther.* **2004,** 75, 259.

[169] *List of Prohibited Classes of Substances and Prohibited Methods*, International Olympic Committee, Lausanne, **2001**.

[170] Aymard, G.; Labarthe, B.; Warot, D.; Berlin, I.; Diquet, B. *J. Chromatogr. B* **2000**, 744, 25.

[171] Wang, Y.; Fice, D.S.; Pollen K.F. *Yeung, J. Pharma. Biomed. Anal.* **1999**, 21,519.

[172] Van der Merwe, P.J.; Hendrikz, S.E. *J. Chromatogr. B* **1995**, 663, 160.

[173] Imaz, C.; Navajas, R.; Carreras, D.; Rodr´ıguez, C.; Rodr´ıguez, A.F. *J. Chromatogr. A* **2000**, 870, 23.

[174] Al-Dirbashi, O.; Kuroda, N.; Akiyama, S.; Nakashima, K. *J. Chromatogr. B* **1997**, 695, 251.

[175] Van Eenoo, P.; Delbeke, F.T.; Roels, K; De Backer, P. *J. Chromatogr. B* **2001,** 760, 255.

[176] Averrin, G.M; Isiah, M.W. *Anal. Chim. Acta* **1995**, 306, 49.

[177] Turnball, A. *J. Br. Nutr. Found-Nutr. Bull.* **1981**, 6, 153.

[178] Hideko, K.; Ryoko, A.; Yoshikazu, M.; Junko, K. *J. Chromatogr. A* **2000**, 870, 87.

[179] Yuan-Hai, Z.; Zhi-Ling, Z.; Dai-Wen, P. *J. Electroanal. Chem.* **2005**, 581, 303.

[180] Llobat-Estelles, M.J.; Marin-Saez, R.M.; San-Martin, M.D. *Talanta* **1996**, 43, 1589.

[181] Miroslav, S.; Andrea, P.; Stanislav, M.; Jozef, S. *Anal. Biochem.* **2000,** 285, 225.

[182] Susanto, F.; Humfeld, S.; Niederau, C.M.; Reinauer, H. *Fresenius J. Anal. Chem.* **1992,** 344, 549.

[183] Axel, M.; Tharcisse, N.; Günter, H. *Fresenius J. Anal. Chem.* **1996**, 356, 284.

[184] Kazoka, H. *J. Chromatogr. A* **1999**, 836, 235.

[185] Petr, S.; Alexandr, J.; Frantisek, D. *J. Chromatogr. A* **1994**, 679, 195.

[186] Mohamed, H.A.; Mustafa, A.A.; Mohie, S. *Analyst* **1992**, 117, 157.

[187] Quan-xun, D.; Ling-xiao, Y. *J. Chromatogr.* **1993**, 630, 363.

[188] Gang, C.; Qingcui, C.; Luyan, Z.; Jiannong, Y. *Anal. Chim. Acta* **2002,** 457, 225.

[189] Hector, C.G.; Alejandro, C.O.; Arsenio, M.P. *Anal. Chim. Acta* **1999**, 384, 95.

[190] Nevin, E. *J. Pharm. and Biomed. Analysis* **2000**, 23, 255.

[191] Nicolae, S.; Bulusu, V.S.; Donald, A.T.; Akira, F. *Electroanalysis* **2002**, 14, 271.

[192] Yogesh, K.; Om Prakash, M.; Mahipat, S.; Rajayashree, P. *Int.J. ChemTech Res.* **2010**, 2, 1907.

[193] Jyh-Myng, Z.; Tung-yue, Y.; Ying, S. *Talanta* **1999**, 50, 635.

[194] Gong-Jun, Y.; Kun, W.; Jing-Juan, X.; Hong-Yuan, C. *Anal. Letters* **2005,** 37, 629.

[195] Xiao-Li, X.; Fei, H.; Guo-Liang, Z.; Song, Z.; Ji-Lie, K. *Sensors* **2010**, 10, 8398.

[196] Kangbing, W.; Junjie, F.; Shengshui, H. *Anal. Biochem.* **2003**, 318, 100.

[197] Ewa, K.; Borys, K.; David, S. *Acta Biochimica Polonica* **2004**, 51, 493.

[198] Cauli, O.; Morelli, M. *Behav. Pharmacol.* **2005**, 16, 63.

[199] Frary, C.D.; Johnson, R.K.; Wang, M.Q. *J. Am. Diet. Assoc.* **2005**, 105, 110.

[200] Barone, J.J.; Roberts, H.R. *Food Chem. Toxicol.* **1996**, 34, 119.

[201] Christian. M.S.; Brent, R.L. *Teratology* **2001**, 64, 51.

[202] Knight, C.A.; Knight, I.; Mitchell, D.C.; Zepp, J.E. *Food Chem. Toxicol.* **2004**, 42, 1923.

[203] Dhar, R.; Stout, C.W.; Link, M.S.; Homoud, M.K.; Weinstock, J.; Mark Estes III, N.A. *Mayo Clinic Proceedings* **2005**, 80, 1307.

[204] Garrett, B.E.; Griffiths, R.R. *Pharmacol. Biochem. Behav.* **1997**, 57, 533.

[205] McMullen, M.K.; Whitehouse, J.M.W.; Shine, G.; Towel, A. *Food Funct.* **2011**, 2, 197.

[206] Sharma, V.; Gulati, A.; Ravindranath, S.D.; Kumar, V. *J. Food Compos. Anal.* **2005**, 18, 583.

[207] Wang, A.; Li, L.; Zang, F.; Fang, Y. *Anal. Chim. Acta.* **2000**, 419, 235.

[208] Regan, F.; Shakalisava, Y. *Anal. Chim. Acta.* **2005**, 540, 103.

[209] López-Martinez, L.; López-de-Alba, P.L.; Garcia-Campos, R.; De León-Rodriguez, L.M. *Anal. Chim. Acta.* **2003**, 493, 83.

[210] Khanchi, A.R.; Mahani, M.K.; Hajihosseini, M.; Maragheh, M.G.; Chaloosi, M.; Bani, F. *Food Chem.* **2007**, 103, 1062.

[211] Jones, J.; Magri, R.; Rios, R.; Jones, M.; Platea, C.; Lewisa, D. *Anal. Methods* **2011**, 3, 1310.

[212] Rawat, A.; Chandra, S.; Sarkar, A. *Anal. Bioanal. Electroch.* **2010**, 2, 212.

[213] Sanghavi, B.J.; Srivastava, A.K. *Electrochim. Acta* **2010,** 55, 8638.

[214] Câmpean, A.; Tertiş, M.; Săndulescu, R. *Cent. Eur. J. Chem.* **2011**, 9, 688.

[215] Brunetti, B.; Desimoni, E.; Casati, P. *Electroanalysis* **2007**, 19, 385.

[216] Yang, S.; Yang, R.; Li, G.; Qua, L.; Li, J.; Yu, L. *J. Electroanal. Chem.* **2010**, 639, 77.

[217] Zhang, J.; Wang, L.P.; Guo, W.; Peng, X.D.; Li, Z.M.; Yuan, B. *Int. J. Electrochem. Sci.* **2011**, 6, 997.

[218] Alizadeha, T.; Ganjalib, M.R.; Zareb, M.; Norouzib, P. *Electrochim. Acta.* **2010**, 55, 1568.

[219] Martínez-Huitle, C.A.; Fernandes, N.S.; Ferro, S.; De Battisti, A.; Quiroz, M.A. *Diamond Relat. Mater.* **2010**, 19, 1188.

[220] Lourencao, B.C.; Medeiros, R.A.; Rocha-Filho, R.C.; Fatibello-Filhoa, O. *Electroanalysis* **2010**, 22, 1717.

[221] Guo, S.; Zhu, Q.; Yang, B.; Wang, J.; Ye, B. *Food Chem.* **2011,** 129, 1311.

[222] Zhang, L.; Li, W.; Shi, M.; Kong, J. *Talanta* **2006**, 70, 432.

[223] Xiao, P.; Zhou, Q.; Xiao, F.; Zhao, F.; Zeng, B. *Int. J. Electrochem. Sci.* **2006**, 1, 228.

[224] Aoki, K.; Osteryoung, J. *J. Electroanal. Chem.* **1988**, 240, 45.

[225] Fei, S.; Chen, J.; Yao, S.; Deng, G.; He, D.; Kuang, Y. *Anal. Biochem.* **2005**, 339, 29.

[226] Subrahmanyam, P.; Krishnapriya, B.; Suvardhan, K.; Rekha, D.; Suneeta, Y.; Jayaraj, B.; Chiranjeevi, P. *J. Hazard. Mater.* **2007**, 146, 51.

[227] Melgar, L.Z.; Machado, S.A.S. *J. Braz. Chem. Soc.* **2005**, 16, 743.

[228] Sreedhar, N.Y.; Prasad, P.R.; Reddy, C.N.; Prasad, K.S. *Int. J. Nanosci. Nanotech.* **2011**, 1, 6.

[229] Galeano-Diaz, T.; Guiberteau-Cabanillas, A.; Espinosa-Mansilla, A.; Lopez-Soto, M.D. *Anal. Chim. Acta* **2008**, 618, 131.

[230] Jenner, P. *Trends Neurosci.* **2011**, 24, 245.

[231] Fildes, K.; Astheimer, L.B.; Buttemer, W.A. *Environ. Toxicol. Chem.* **2009**, 28, 388.

[232] Al-Sarari, A.S.; Hafiz, A.M.; Bayoumi, A.E.; Hussein, H.I.; Baker, Y.A. *Int. J. Agric. Biol.* **2011**, 13, 560.

[233] Li, C.; Wang, C.; Ma, Y.; Hu, S. *Microchim. Acta* **2004**, 148, 27.

[234] Galeano-Dıaz, T.; Guiberteau-Cabanillas, A.; Mora-Diez, N.; Parrilla-Vazquez, P.; Salinas-Lopez, F. *J. Agric. Food Chem.* **2000**, 48, 4508.

[235] Watanabe, E.; Kanzaki, Y.; Tokumoto, H.; Hoshino, R.; Kubo, H.; Nakazawa, H. *J. Agric. Food Chem.* **2002**, 50, 53.

[236] Choi, J.; Caquet, T.; Roche, H. *Environ. Toxicol. Chem.* **2002**, 21, 2725.

[237] Karamfilov, V.K.; Fileman, T.W.; Evans, K.M.; Mantoura, R.F.C. *Anal. Chim. Acta* **1996**, 335, 51

[238] Pitarch, E.; Serrano, R.; López, F.J.; Hernández, F. *Anal. Bioanal. Chem.* **2003**, 376, 189.

[239] Lei, Y.; Mulchandani, P.; Chen, W.; Mulchandani, A. *Sensors* **2006**, 6, 466.

[240] Lei, Y.; Mulchandani, P.; Chen, W.; Mulchandani, A. *Appl. Biochem. Biotechnol.* **2007**, 136, 243.

[241] Chough, S.H.; Mulchandani, A.; Mulchandani, P.; Chen, W.; Wang, J.; Rogers, K.R. *Electroanalysis* **2002**, 14, 273.

[242] Ly, S.Y. *J. Korean Chem. Soc.* **2006**, 50, 208.

[243] Ni, Y.; Qiu, P.; Kokot, S. *Anal. Chim. Acta* **2004**, 516, 7.

[244] Amare, M.; Assefa, W.; Admassie, S. *Anal. Bioanal. Electrochem.* **2011**, 3, 365.

[245] Amare, M.; Admassie, S. *Bull. Chem. Soc. Ethiop.* **2012**, 26, 73.

[246] Amare, M.; Admassie, S. *Talanta* **2012**, 93, 122.

[247] Geto, A.; Amare, M.; Tesema, M.; Admassie, S. *Electranalysis* **2012**, 24, 1.

[248] Ghoneim, M.M.; El-Hallag, I.S. *J. Braz. Chem. Soc.* **2010**, 21, 7.

[249] Zen, J.M.; Jou, J.J.; Kumar, A.S. *Anal. Chim. Acta* **1999**, 396, 39.

[250] Ecobichon, D.J. *Toxicology* **2001**, 160, 27.

[251] Lei, Y.; Mulchandani, P.; Chen, W.; Mulchandani, A. *J. Agric. Food Chem.* **2005**, 53, 524.

[252] Arapoglou, D.; Vlyssides, A.; Israilides, C.; Zorpas, A.; Karlis, P. *J. Haz. Mat.* **2003**, 98, 191.

[253] Amaya-Chavez, A.; Martınez-Tabche, L.; Lopez-Lopez, E.; Galar-Martınez, M. *Chemosphere* **2006**, 63, 1124.

[254] Hogendoorn, E.; van Zoonen, P. *J. Chromatogr. A* **2000**, 892, 435.

[255] Futagami, K.; Narazaki, C.; Kataoka, Y.; Shuto, H.; Oishi, R. *J. Chromatogr. B* **1997**, 704, 369.

[256] Hiskia, A.E.; Atmajidou, M.E.; Tsipi, D.F. *J. Agric. Food Chem.* **1998**, 46, 570.

[257] Ignjatovi, L.M.; Markovi, D.A.; Veselinovik, D.S.; Beiik, B.R. *Electroanalysis* **1993**, 5, 529.

[258] Bowen, C.V.; Edwards, F.I. *Anal. Chem.* **1950**, 22, 702.

[259] Manisankar, P.; Selvanathan, G.; Vedhi, C. *Talanta* **2006**, 68, 686.

[260] Xu, C.; Wu, K.; Hu, S.; Cui, D. *Anal. Bioanal. Chem.* **2002,** 373, 284.

[261] Pedrosa, V.A.; Miwa, D.; Machado, S.A.; Avaca, L.A. *Electroanalysis* **2006**, 18, 1590.

[262] Marx, S.; tsman, A.; Turyan, Zall.; Mandler, D. *Anal. Chem.* **2004**, 76, 120.

[263] Yamazaki, T.; Yilmaz, E.; Mosbach, K.; Sode, K. *Anal. Chim. Acta* **2001**, 435, 209.

[264] Jenkins, A.L.; Yin, R.; Jensen, J.L. *Analyst* **2001**, 126, 798.

[265] Dua, D.; Ye, X.; Zhang, J.; Liu, D. *Electrochim. Acta* **2008**, 53, 4478.

[266] Du, D.; Wang, M.; Zhang, J.; Cai, J.; Tu, H.; Zhang, A. *Electrochem. Comm.* **2008**, 10, 85.

[267] Fan, S.; Xiao, F.; Liu, L.; Zhao, F.; Zeng, B. *Sens. Actuators B* **2008**, 132, 34.

[268] Palchetti, I.; Cagninia, A.; Del Carlo, M.; Coppi, C.; Mascini, M.; Tumer, A.P.F. *Anal. Chim. Acta.* **1997**, 337, 315.

[269] Schöning, M.J.; Krause, R.; Block, K.; Musahmeh, M.; Mulchandani, A.; Wang, J. *Sens. Actuators B* **2003**, 95, 291.

[270] Du, D.; Chen, S.; Cai, J.; Zhang, A. *Talanta* **2008**, 74, 766.

[271] Edwards, G.A.; Bergen, A.J.; Porter, M.D. *Handbook of Electrochemistry*, (Ed. C. G. Zoski), Elsevier, The Netherlands, **2007**.

[272] Mehretie, S.; Admassie, S.; Hundie, T.; Tessema, M.; Solomon, T. *Talanta* **2011**, 85, 1376.

[273] Mehretie, S.; Admassie, S.; Tessema, M.; Solomon, T. *Anal. Bioanal. Electrochem.* **2011**, 3, 38.

[274] Liu, X.Y.; Li, C.Y.; Hu, S. *Microchim. Acta.* **2006**, 154, 275.

[275] Uslu, B.; Ozkan, S.A. *Comb. Chem. High Throughput Screening* **2007**, 10, 495.

[276] Ranganathan, S.; Kuo, T.; McCreery, R.L. *Anal. Chem.* **1999,** 71, 3574.

[277] McCreery, R.L. *Chem. Rev.* **2008**, 108, 2646.

[278] Alliata, D.; Häring, P.; Haas, O.; Kötz, R.; Siegenthaler, H. *Electrochem. Solid-state Lett.* **1999**, 2, 33.

[279] Alemu, H.; Hlalele, L. *Bull. Chem. Soc. Ethiop.* **2007**, 21, 1.

[280] Thiago, R.L.C.; Kosminsky, L.; Bertotti, M. *Sens. Actuators, B* **2002**, 87, 41.

[281] Wang, H.; Ju, H.; Chen, H. *Electroanalysis* **2001**, 13, 1105.

[282] Qiao, J.X.; Luo, H.Q.; Li, N.B. *Colloids Surf. B* **2008**, 62, 31.

[283] Sentürk, Z.; Ozkan, S.A.; Ozkan, Y. *J. Pharm. Biomed. Anal.* **1998**, 16, 801.

[284] Poon, M.; McCreery, R.L. *Anal. Chem.* **1986**, 58, 2745.

[285] Shahrokhiana, S.; Ghalkhania, M.; Adeli, M.; Amini, M.K. *Biosens. Bioelectron.* **2009**, 24, 3235.

[286] Zhou, C.; Liu, Z.; Dong, Y.; Li, D. *Electroanalysis* **2009**, 21, 853.